

30438. cyl

AL-TR-89-016



Final Report
for the period
August 1986 to
December 1988

BURN RATE MECHANISMS
Vol. II - A Model for Ammonium
Nitrate Propellant Combustion

February 1990

Author:
M.W. Beckstead

Brigham Young University
Department of Chemical Engineering
Provo UT 84602

Subcontract to Hercules for
F04611-86-C-0029

Approved for Public Release

Distribution is unlimited. The AL Technical Services Office has reviewed this report, and it is releasable to the National Technical Information Service, where it will be available to the general public, including foreign nationals.

Prepared for the:

Astronautics Laboratory (AFSC)
Air Force Space Technology Center
Space Systems Division
Air Force Systems Command
Edwards AFB CA 93523-5000

20040210 130

REPORT DOCUMENTATION PAGE

Form Approved
OMB No. 0704-0188

1a. REPORT SECURITY CLASSIFICATION UNCLASSIFIED			1b. RESTRICTIVE MARKINGS	
2a. SECURITY CLASSIFICATION AUTHORITY			3. DISTRIBUTION/AVAILABILITY OF REPORT Approved for Public Release; Distribution is Unlimited	
2b. DECLASSIFICATION/DOWNGRADING SCHEDULE				
4. PERFORMING ORGANIZATION REPORT NUMBER(S)			5. MONITORING ORGANIZATION REPORT NUMBER(S) AL-TR-89-016	
6a. NAME OF PERFORMING ORGANIZATION Brigham Young University		6b. OFFICE SYMBOL (If applicable)	7a. NAME OF MONITORING ORGANIZATION Astronautics Laboratory (AFSC)	
6c. ADDRESS (City, State, and ZIP Code) Department of Chemical Engineering Provo UT 84602			7b. ADDRESS (City, State, and ZIP Code) AL/LSCF Edwards AFB CA 93523-5000	
8a. NAME OF FUNDING/SPONSORING ORGANIZATION		8b. OFFICE SYMBOL (If applicable)	9. PROCUREMENT INSTRUMENT IDENTIFICATION NUMBER F04611-86-C-0029	
8c. ADDRESS (City, State, and ZIP Code)			10. SOURCE OF FUNDING NUMBERS	
			PROGRAM ELEMENT NO. 62302F	PROJECT NO. 5730
11. TITLE (Include Security Classification) Burn Rate Mechanisms (U) Volume 2. A Model for Ammonium Nitrate Propellant Combustion (U)				
12. PERSONAL AUTHOR(S) Beckstead, M.W.				
13a. TYPE OF REPORT Final		13b. TIME COVERED FROM 8608 TO 8812		14. DATE OF REPORT (Year, Month, Day) 9002
15. PAGE COUNT 130				
16. SUPPLEMENTARY NOTATION This is volume 2 of a two volume report. Only the second volume is cleared for public release.				
17. COSATI CODES			18. SUBJECT TERMS (Continue on reverse if necessary and identify by block number) burn rate, combustion modeling, solid propellants, temperature sensitivity, Ammonium Nitrate	
FIELD	GROUP	SUB-GROUP		
21	02			
21	08			
19. ABSTRACT (Continue on reverse if necessary and identify by block number) A model describing the combustion of ammonium nitrate (AN) containing propellants has been developed based on the Beckstead SST model for composite propellants. Calculations for an monopropellant have been made and compared to available data showing good agreement for burn rate and predicting a σ_p of $\sim 0.3\%/K$. The SST model for composite propellants has been modified for application to HTPB propellants containing various combinations of AN, ammonium perchlorate, and sodium nitrate. Burn rate calculations for mixed oxidizer propellants compare well with available experimental data covering a range of pressures, oxidizer particle size and concentration. The model shows that the low burn rates of AN propellants is due to their low flame temperature, and that the kinetic aspects of the primary flame dominate the diffusion aspects, virtually eliminating the possibility of using AN particle size to tailor propellant burn rate. The calculated σ_p values of 0.2 to 0.3%/K are quite high compared to conventional AP propellants, and the addition of AP and SN to the propellants has little effect on the calculated σ_p values.				
20. DISTRIBUTION/AVAILABILITY OF ABSTRACT <input checked="" type="checkbox"/> UNCLASSIFIED/UNLIMITED <input type="checkbox"/> SAME AS RPT. <input type="checkbox"/> DTIC USERS			21. ABSTRACT SECURITY CLASSIFICATION UNCLASSIFIED	
22a. NAME OF RESPONSIBLE INDIVIDUAL JESSE K. CRUMP, CAPT, USAF			22b. TELEPHONE (Include Area Code) (805) 275-5442	
			22c. OFFICE SYMBOL LSCF	

PREFACE

This is Volume 2 of a two volume report documenting the results achieved in an experimental and theoretical program designed to determine the effect of propellant composition. The overall program objective is to identify, evaluate, and develop ammonium nitrate propellant tailoring techniques. The objective of this subtask of the program has been to develop a model to describe the combustion of ammonium nitrate based propellants, including auxiliary oxidizers such as ammonium perchlorate and sodium nitrate.

This volume of the report describes the separate surface temperature model for predicting combustion characteristics of ammonium nitrate solid propellants. This volume contains a description of the theoretical development of the model, and a description of the results. A description of the corresponding computer program has been published and is contained in AFAL-TR-88-109, Temperature Sensitivity Study, Volume III, Computer Users Manual. The test cases corresponding to ammonium nitrate propellants are contained in Appendix A of this report.

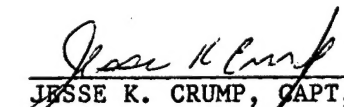
NOTICE

When U.S. Government drawings, specifications, or other data are used for any purpose other than a definitely related Government procurement operation, the fact that the Government may have formulated, furnished, or in any way supplied the said drawings, specifications, or other data, is not to be regarded by implication or otherwise, or in any way licensing the holder or any other person or corporation, or conveying any rights or permission to manufacture, use, or sell any patented invention that may be related thereto.

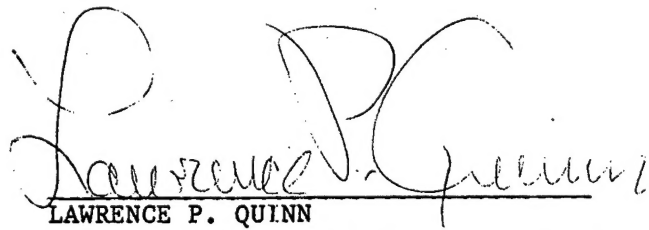
FOREWORD

This subcontractor's final report was submitted by Brigham Young University on completion of Hercules, Inc., Magna UT's Contract F04611-86-C-0029 with the Astronautics Laboratory (AFSC), Edwards Air Force Base CA. AL Project Managers were Capt Marlow D. Moser and Capt Jesse K. Crump.

This report has been reviewed and is approved for release and distribution in accordance with the distribution statement on the cover and on the DD Form 1473.

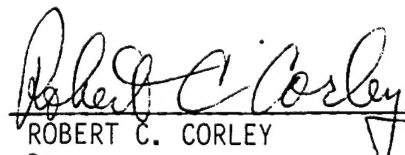


JESSE K. CRUMP, CAPT, USAF
Project Manager



LAWRENCE P. QUINN
Chief, Aerothermochemistry Branch

FOR THE DIRECTOR



ROBERT C. CORLEY
Deputy Director, Astronautical
Sciences Division

TABLE OF CONTENTS

INTRODUCTION	1
THERMOCHEMICAL CALCULATIONS	4
General Performance Calculations	4
Ammonium Nitrate Monopropellant Flame	12
Primary Flame Temperatures	13
Other Primary Flame Temperatures	15
Performance Characteristics of AN/Silicone Rubber Propellants	16
COMBUSTION MECHANISM OF SOLID PROPELLANTS	19
The Condensed Phase	19
Surface Temperature	20
Condensed Phase Heat Release	23
Oxidizer Burning Characteristics	23
Composite Propellant Flame Structure	25
Allocation of Binder to Oxidizer	27
AN MONOPROPELLANT MODELING	29
Basic Model Equations	29
Pressure Exponent and Temperature Sensitivity	30
Comparison of Monopropellant Model with AP Data	31
AN Monopropellant Calculations	35
MODEL EQUATIONS FOR AP AND AN COMPOSITE PROPELLANTS	40
Surface Temperature Calculation	40
Rate Averaging Basis	42
Multimodal and Mixed Oxidizer Propellants	44
Oxidizer Ignition Delay Time	45
Binder Burnthrough Time	46
Calculated Diffusion Flame Heights	46
Competing Flames	47
Heat Transfer From the Primary Flame	50
Effect of Catalysts	50
AP COMPOSITE PROPELLANT RESULTS	52
AN COMPOSITE PROPELLANT RESULTS	56
AN/HTPB Propellant	56
Effect of Catalysts	59
Effect of AP on AN Propellants	64
Effect of SN on AN Propellants	68
Propellants Containing AN/AP/SN	68

SUMMARY AND CONCLUSIONS	74
NOMENCLATURE	80
REFERENCES	82
APPENDIX A - Computer Program for AN Propellant Test Cases	87
APPENDIX B - Composite Propellant Modeling Bibliography	107
APPENDIX C - Aluminum Combustion References	113

LIST OF FIGURES

<u>Figure</u>	<u>Caption</u>	<u>Page</u>
1.	Calculated Isp, adiabatic flame temperature and product molecular weight for propellants containing lithium nitrate (LN), sodium nitrate (SN), potassium nitrate (KN), and ammonium nitrate (AN) with 10% HTPB binder, all at 1000 psi.	6
2.	Comparison of Isp values for mixed oxidizer systems containing ammonium nitrate plus stoichiometric amounts of alkali metal nitrates needed to scavenge chloride ion from different levels of AP.	7
3.	Comparison of HCl exhaust concentrations for mixed oxidizer systems containing ammonium nitrate plus stoichiometric amounts of alkali metal nitrates needed to scavenge chloride ion from AP.	7
4.	A comparison of calculated Isp values versus the concentration of HCl in the exhaust of propellants containing AN, AP and SN.	8
5.	A comparison of calculated Isp-density values versus the concentration of HCl in the exhaust of propellants containing AN, AP and SN.	9
6.	A comparison of Isp-density values versus the concentration of HCl in the exhaust of propellants containing ANPN, AP and SN.	10
7.	A comparison of calculated Isp-density values versus the concentration of AP for propellants containing ANPN, AP and SN.	11
8.	A comparison of the HCl exhaust concentration versus the concentration of SN for propellants containing ANPN, AP and SN.	11
9.	Calculated flame temperatures for three different postulated flame structures.	13
10.	Calculated primary flame temperatures for the CO equilibrium flame for AN/HTPB propellants for use in the model.	14
11.	Exhaust gas composition for AN/HTPB propellants varying percent AN.	15
12.	Comparison of calculated flame temperatures for primary flames in AP, AN, and SN/HTPB propellants.	16
13.	Comparison of calculated flame temperatures for primary flames in AP, AN, and SN propellants with HTPB and Sylgard binders.	17
14.	Comparison of calculated Isp for AP and AN propellants with HTPB and Sylgard binders varying binder level.	18
15.	Comparison of calculated Isp for AP and AN propellants with HTPB and Sylgard binders varying aluminum level.	18

16.	Surface temperature data for pressed pellets of AN. The hot plate data are from Anderson and the combustion data from Whittaker.	21
17.	Surface temperature data by Frolov, et al for a composite mixture containing SN and aluminum.	21
18.	A comparison of surface temperature data for AP, AN, SN, and HTPB, the principal ingredients of interest in this study.	22
19.	A comparison of the burning rates of AN, AP, and HMX monopropellants and composite propellants.	24
20.	Flame structure for AP, AN, and SN composite propellants.	26
21.	Comparison of AP burning rate data and model calculations for varying pressure.	32
22.	Calculated temperature sensitivity for AP monopropellant for varying flame activation energy.	32
23.	Comparison of AP surface temperature data and model calculations.	33
24.	Calculated condensed phase heat release (values are exothermic).	34
25.	Calculated flame stand-off distance for AP monopropellant.	35
26.	Comparison of AN burning rate data and model calculations for varying pressure.	36
27.	Calculated temperature sensitivity for AN monopropellant varying the flame activation energy.	36
28.	Comparison of AN burning rate data and model calculations for varying surface temperature.	37
29.	Calculated condensed phase heat release (values are exothermic).	38
30.	Calculated flame stand-off distance and melt thickness for AN monopropellant.	39
31.	Different flame configurations that can occur during the burning time of an individual particle. Approximate values of β_F and β_P that correspond to the flame structure are noted.	49
32.	A comparison of calculated and experimental burning rates for Miller's Series III propellants at 1000 psi (6.8 MPa). Datum points lying outside of +10% have been labeled with their identification number.	53
33.	A comparison of calculated and experimental pressure exponents for Miller's Series III propellants at 1000 psi (6.8 MPa). Datum points lying outside of +20% have been labeled with their identification number.	54

34.	A comparison of calculated and experimental temperature sensitivity for Miller's Series III propellants at 1000 psi (6.8 MPa). Datum points lying outside of +20% have been labeled with their identification number.	55
35.	Calculated temperature sensitivity for Miller's Series III propellants at 1000 psi (6.8 MPa), compared with experimental data as a function of fine AP fraction size.	55
36.	Calculated burn rates of AN/HTPB propellants with varying amounts of AN.	57
37.	Burn rate and pressure exponent of AN/HTPB propellants for varying AN content.	57
38.	The effect of the primary flame activation energy on burn rate for varying AN content.	58
39.	The effect of the primary flame activation energy on temperature sensitivity for varying AN content.	59
40.	Burn rate calculations for AN/AD/HTPB propellants, varying the catalyst concentration and the percentage solids. Two experimental datum points are included for reference.	60
41.	Calculated pressure exponent for AN/AD/HTPB propellants, varying the catalyst concentration and the percentage solids.	61
42.	Calculated temperature sensitivity for AN/AD/HTPB propellants, varying the catalyst concentration and the percentage solids.	62
43.	Calculated temperature sensitivity for AN/HTPB propellants, comparing the catalyzed and uncatalyzed temperature sensitivities for varying solids percentage.	62
44.	Burn rate calculations for AN/AD/HTPB propellants, varying the concentration and size of the AN fine fraction at 86% solids.	63
45.	Temperature sensitivity calculations for AN/AD/HTPB propellants, varying the concentration and size of the AN fine fraction at 86% solids.	64
46.	Burn rate calculations for 86% solids AN/AP/HTPB propellants, varying the concentration and size of the AP.	65
47.	Calculated pressure exponents for 86% solids AN/AP/HTPB propellants, varying the concentration and size of the AP.	65
48.	Comparison of calculated and experimental burn rates for 86% solids AN/AP/HTPB propellants, varying the concentration and size of the AP.	66

49.	Temperature sensitivity calculations for 86% solids AN/AP/HTPB propellants, varying the concentration and size of the AP.	67
50.	AP particle size effect on the temperature sensitivity calculations for 86% solids AN/AP/HTPB propellants.	67
51.	Burn rate calculations for 86% solids AN/SN/HTPB propellants, varying the concentration and size of the SN.	68
52.	Calculated burning rates of AN/HTPB propellants with varying amounts of AN, AP, and SN compared to experimental data.	69
53.	Calculated temperature sensitivity for AN/AP/SN propellants, varying the oxidizer concentrations and the percentage solids.	70
54.	A comparison of calculated and experimental burning rates for the six propellants BRM-270, 271, 272, 275, 277 and 278 at varying pressure.	71
55.	Burn rate calculations for AN/AP/SN/HTPB propellants, varying the concentration and size of the AN fine fraction at 86% solids. Data from propellants BRM-270, 271, 272 are included for reference.	72
56.	Temperature sensitivity calculations for AN/AP/SN/HTPB propellants, varying the concentration and size of the AN fine fraction at 86% solids.	72

INTRODUCTION

When the space shuttle is launched, each Solid Rocket Motor (SRM) booster generates approximately 100 tons of HCl in the exhaust¹. Thus, with the two boosters, over 200 tons of HCl is generated from each space shuttle launch. The HCl presents several potential problems. The HCl provides nucleation sites for moisture in the air with the result being the condensed, hydrated form of hydrochloric acid ($\text{HCl} \cdot \text{H}_2\text{O}$). The resultant acid cloud results in a very visible cloud which through further condensation can result in acid rain. The acid rain is obviously detrimental to both plant and animal life dependent on the concentration levels it achieves as it reaches the ground. In addition, at higher elevations, the HCl can react with the protective layer of ozone causing a degradation of some of the ozone. The HCl comes from the AP (ammonium perchlorate) which is the oxidizer in the solid propellant for the SRM boosters. The SRM propellant contains approximately 70% AP¹ which generates slightly more than 21 weight percent HCl in the exhaust gases. For these reasons it is desirable to find a replacement for the AP to eliminate the HCl in the rocket exhaust.

The two oxidizers used most often in modern solid propellants are AP, and cyclotetramethylene tetranitramine, HMX. Although HMX does not contain chlorine and generates "clean" exhaust, it is relatively expensive and sensitive which makes it undesirable for a potential replacement for AP. To develop an alternate oxidizer for AP that would be cheaper and would be "clean", i.e. would not produce HCl in the exhaust, ammonium nitrate, AN, and sodium nitrate, SN, are being considered. Neither contain chlorine and both are potentially less expensive than AP. However, neither are as energetic as AP and the burning characteristics are not well known.

The objective of this study has been to develop a model to describe the combustion of AN based propellants, including auxiliary oxidizers such as AP and SN.

No burn rate modeling research for AN propellants has been conducted during the last 20 years. In the late 1950s, AN propellant studies were performed by researchers at Aerojet²⁻⁴ that postulated a two-temperature model similar in concept to the Beckstead SST (Separate Surface Temperature) model^{5,6}. Since that time, the lack of interest in AN propellants has precluded any serious modeling attempts specifically related to AN.

The status of combustion modeling of composite propellants was reviewed by Cohen in 1980⁷ which resulted from a 1978 JANNAF Workshop. In 1982 Cohen⁸ revised his model to incorporate most of the recommendations that were made during the JANNAF workshop. More recently, 1986, Gusachenko and Zarko⁹ have reviewed the status of combustion modeling of composite propellants including a perspective from the Russian literature. Appendix A consists of an annotated bibliography of papers relevant to modeling monopropellants and composite propellants (double base propellant modeling papers were excluded).

In Cohen's review article, he compared the four models of Cohen¹⁰⁻¹², Beckstead^{6,13}, King¹⁴⁻¹⁶, and the PEM model of Glick, Condon, Renie, etc.¹⁷⁻²⁵. The review concentrated on these four models as being the most representative of the state of the art and as having the most widely accepted physical basis. Each of these

models is based on the BDP multiple flame concept^{26,27} that is most representative of the physical mechanisms that control propellant combustion. Table 1 is a brief summary of the contents and physical basis of the various models that have been reviewed and considered for application to the present study.

In the development of the various models there has been considerable discussion relative to the proper method of averaging the burn rate of the various ingredients in that make up the propellant. Cohen, the original BDP approach, and the PEM models all use an area or surface averaging approach that nominally appears to work well for AP propellants. Beckstead's SST model and King's model both use a time averaging technique that appears to work better with HMX propellants, and thus, might be better with mixed oxidizers having widely varying burn rates.

All of the models are based on the BDP multiple flame concept, considering a premixed monopropellant flame, an initial diffusion flame between the oxidizer and binder decomposition products, and a final diffusion flame between the products of the oxidizer monopropellant flame and the binder decomposition products. In each the analysis of the diffusion flame is based on the Burke-Schumann²⁸ approach with minor modifications. All are based on global kinetics. None of the models consider an explicit interaction of flames between adjacent particles of differing sizes. Most of the models have been applied to aluminized propellants, but only in a superficial manner.

The Beckstead SST model was selected as the basis for development because of its flexibility and its apparent potential for handling mixed oxidizers with significantly varying surface temperatures. Therefore, the current work is an extension of the Beckstead SST model with some modifications taken from Cohen's model⁸.

Table 1 Comparison of Models

Physical Mechanisms	Beckstead (BDP)	Cohen (old)	PEM	Cohen(new)	KIng	SST (Beckstead)
Publication Year	'72,'76	'72,'75,'77	'73,'79	'82	'78,'79,'80	'77,'81
Reference Number	13	10,11,12	17-25	8	14-16	5,6
Monopropellant flame	yes	yes	yes	yes	yes	yes
Primary diffusion flame	yes	yes	yes	yes	yes - distributed	yes
Final diffusion flame	yes	yes	yes	yes	yes	yes
Burn rate averaging (type)	area	area	area	area	time	time
# of oxidizer modes	3	2	3	3	1	3
size distribution	unimodal	bi-modal	log normal	distribution	unimodal	unimodal
Handle mixed oxidizers?	no	no	no	yes	no	yes
Binder to oxidizer distribution	by weight	by weight	arbitrary	by weight	by weight	by surface area
Interaction effects	none	none	ox/binder dist	through flames	none	ox/binder dist
Oxidizer ignition delay	little effect	little effect	little effect	little effect	little effect	Important
Binder ignition delay	no	no	no	no	no	yes
Binder surface temperature	no	no	no	yes	no	yes
Active binder capability	no	no	no	yes	no	yes
Nitramine capability	marginal	marginal	no	yes	no	yes
Global Arrhenius kinetics	yes	yes	yes	yes	yes	yes
Catalyst effects						
change activation energy	yes	yes	yes	yes	yes	yes
specific area term?	yes	no	no	no	no	yes
Aluminum capability						
agglomeration model	no	no	no	pocket model	no	data correlation
ignition model	yes	no	comprehensive	yes	no	yes
combustion model	D-squared	D-squared	comprehensive	D-squared	no	D-squared

THERMOCHEMICAL CALCULATIONS

General Performance Calculations

A general investigation was conducted evaluating the performance of several alkali metal nitrates as potential combustion/scavenger additives for low cost, clean propellants. Lithium nitrate (LN), sodium nitrate (SN), and potassium nitrate (KN) all have the potential to scavenge the undesirable chloride from AP, yielding the corresponding alkali metal chloride. In addition, KNO_3 acts as a phase stabilizer for AN, and NaNO_3 has been studied extensively by the Soviets²⁹⁻³¹ in conjunction with aluminum agglomeration. Both of these ingredients seem to show potential within the context of a clean propellant. Some of the thermochemical and physical properties of these oxidizers have been tabulated in Table 2. Although AP, AN and HMX all burn as monopropellants, none of the alkali metal nitrates burn as monopropellants and thermochemical calculations do not give flame temperatures, Isp values, etc. Both AP and AN burn as monopropellants providing excess oxygen in their products, 29 mole % for AP and 14% for AN. HMX on the other hand is actually fuel rich with CO being the dominant carbon product with virtually no CO_2 . All of the alkali metal nitrates have relatively high densities which is desirable, and AN has the lowest density which is undesirable. AN also has a relatively low melting point and AP has the highest.

Table 2 Oxidizer Thermochemical and Physical Properties

	<u>AP</u>	<u>AN</u>	<u>HMX</u>	<u>LN</u>	<u>SN</u>	<u>KN</u>
Density (gm/cc)	1.95	1.73	1.91	2.38	2.26	2.11
Melting Point (K)	865	443	553	534	580	607
" " (C)	592	170	280	261	307	334
Enthalpy (Kcal/mole)	-70.7	-87.4	18.06	-115.3	-111.8	-118.2
MW (gm/mole)	117.5	80	256	69	85	101
Flame Temperature (K)	1,405	1,247	3,277	DNR	DNR	DNR
Isp (sec)	157	152	265			
Products (mole fraction):						
H ₂ O	0.376	0.571	0.227			
N ₂	0.119	0.286	0.326			
O ₂	0.287	0.143				
HCl	0.197					
Cl ₂	0.019					
CO			0.246			
CO ₂			0.082			
H ₂			0.088			
OH			0.013			
H			0.012			

Figure 1 shows the calculated performance, adiabatic flame temperature and molecular weight of each of the three alkali metal nitrates (compared to an AN propellant as a reference condition). The calculations were performed assuming a 10% HTPB binder and the percentage of aluminum was varied with the percentage of the nitrate.

Calculated values of Isp for the corresponding AP propellant were included in the Isp plot. The Isp values are very low (as expected) with the Isp values in the order $LN > SN > KN$. The Isp of the AN propellant is significantly higher than that of the three alkali metal nitrates due to the much lower molecular weight of its products. The ammonium ion provides a source of hydrogen atoms which results in 20 to 30% hydrogen in the exhaust products, and the very low molecular weight. The large fraction of hydrogen in the AN propellant exhaust is part of the attractiveness of AN propellants. By contrast the alkali metals form their corresponding carbonates as exhaust products, which have very high molecular weights and contribute to their low Isp values.

The comparison between AN and AP propellants is interesting. The AP propellant has a maximum Isp at 22% aluminum but the curve is a very broad curve. On the other hand, the AN propellant has a maximum Isp at 28% aluminum and the curve has a much sharper peak. The two have equivalent Isp values at 26% aluminum. Unfortunately, it is difficult to get good combustion efficiency above about 20% aluminum, which reduces the potential practical usage of AN propellants.

It is significant that the LN flame temperature is significantly higher than the other flame temperatures. It could provide a source of high temperature near the surface to help as an ignition aid. However, it is very hygroscopic as are most of these compounds, which would probably preclude its practical usage.

It is anticipated that AP will be required for a practical AN containing propellant in order to achieve the desired combustion efficiency and burn rate control (in the same way that AP is used in double base propellants). With this in mind, a series of calculations were made examining the performance of propellants containing a mixture of AP, AN and an alkali metal nitrate. The percent alkali metal nitrate was added in a stoichiometric ratio of AP to nitrate, calculated to scavenge all of the chloride ion. For example,



Thus, the mole ratios of 0.59, 0.72, and 0.86 were used for AP to $LiNO_3$, $NaNO_3$, and KNO_3 , respectively. The results for a 10% HTPB propellant having 10 or 20% AP with varying amounts of aluminum are shown in Figure 2. As expected the AP/LN propellant family shows the best performance, with the AP/KN propellant family having the worst performance. Many of the propellants have calculated Isp values in the 250 to 260 range which are not unreasonable. The calculated percentage of HCl in the exhaust for all of the propellants was below 2% and is shown in Figure 3. The dramatic decrease in HCl concentration at 27% aluminum is due to the preferential formation of $AlCl$ at the very high aluminum concentrations.

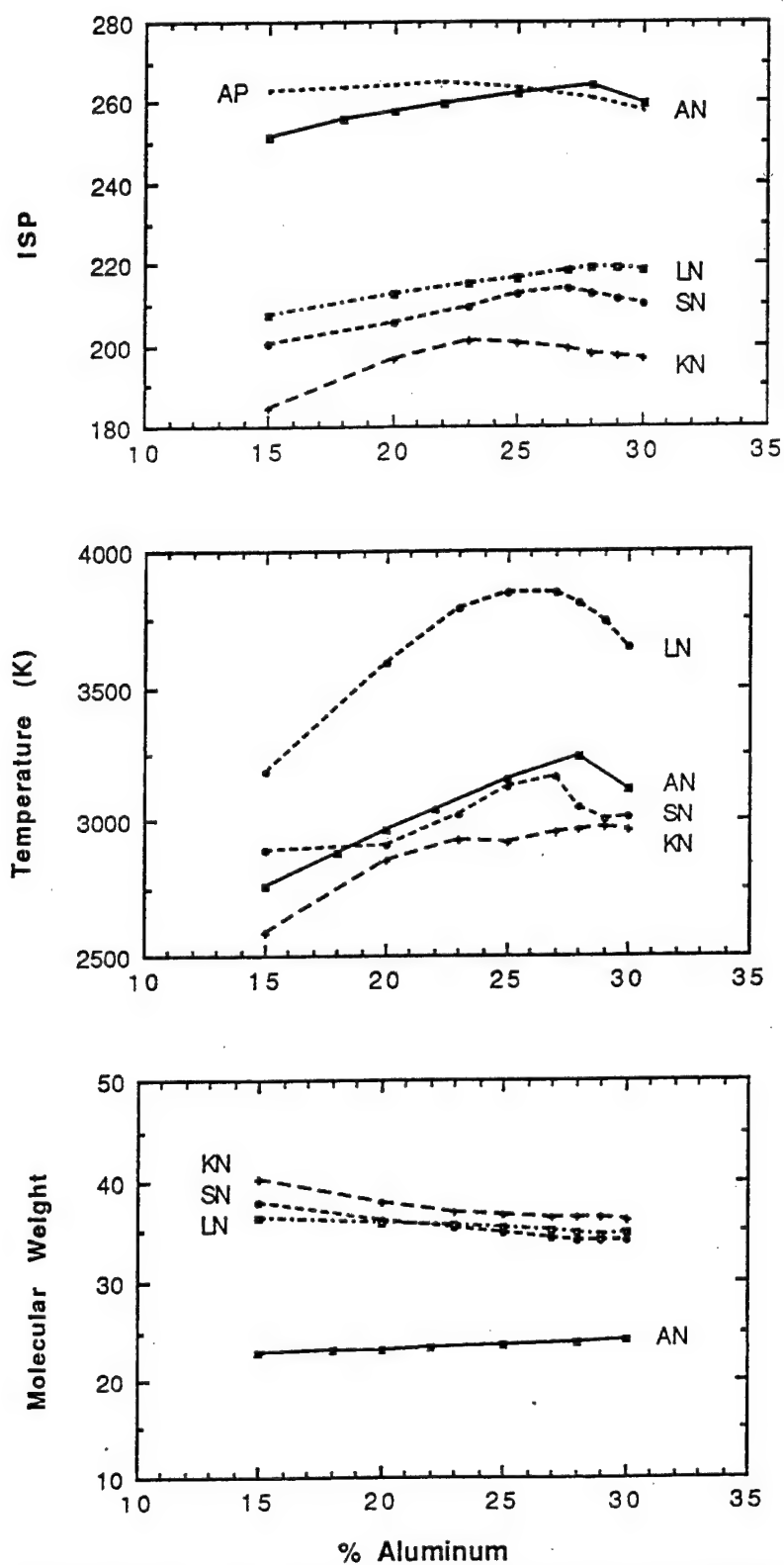


Figure 1. Calculated Isp, adiabatic flame temperature and product molecular weight for propellants containing lithium nitrate (LN), sodium nitrate (SN), potassium nitrate (KN), and ammonium nitrate (AN) with 10% HTPB binder, all at 1000 psi.

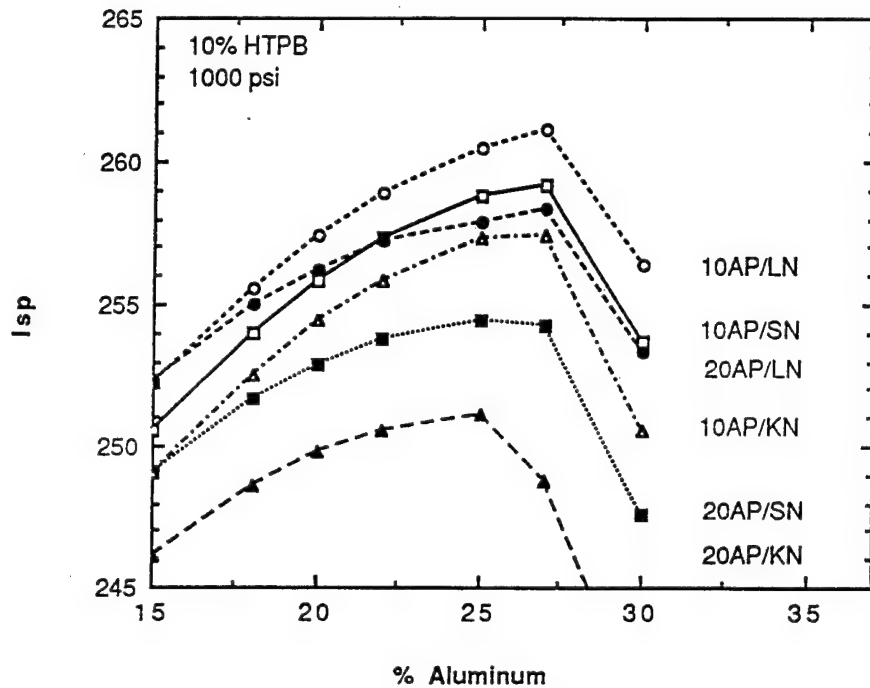


Figure 2. Comparison of Isp values for mixed oxidizer systems containing ammonium nitrate plus stoichiometric amounts of alkali metal nitrates needed to scavenge chloride ion from different levels of AP.

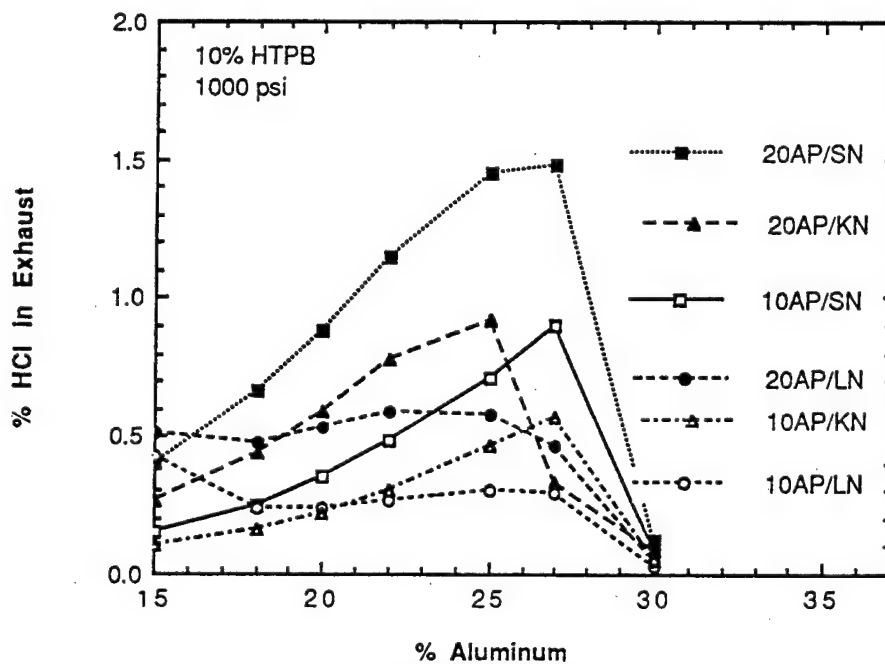


Figure 3. Comparison of HCl exhaust concentrations for mixed oxidizer systems containing ammonium nitrate plus stoichiometric amounts of alkali metal nitrates needed to scavenge chloride ion from AP.

Although SN did not appear to be as effective as lithium nitrate, it is less hygroscopic and more compatible with the other composite propellant ingredients than the LN. Therefore, it appeared to be the most desirable of the scavenging nitrates, and ultimately became the additive of choice for the study. In addition to these properties the SN also made a significant, positive impact on the agglomeration tendencies of the propellants.

Additional calculations were made to examine the effects of SN on propellants of interest. The calculations were made for a 12% HTPB binder with 20% aluminum and 10 or 20% AP. The amount of SN was varied from 0 to 10% with the remainder of the formulation being AN. The calculations show that both the Isp and the percentage HCl decrease with increasing SN content. The results are summarized in Figure 4 where the Isp has been plotted versus the percent HCl in the exhaust. Although the SN is a very effective scavenger, it also reduces the Isp significantly.

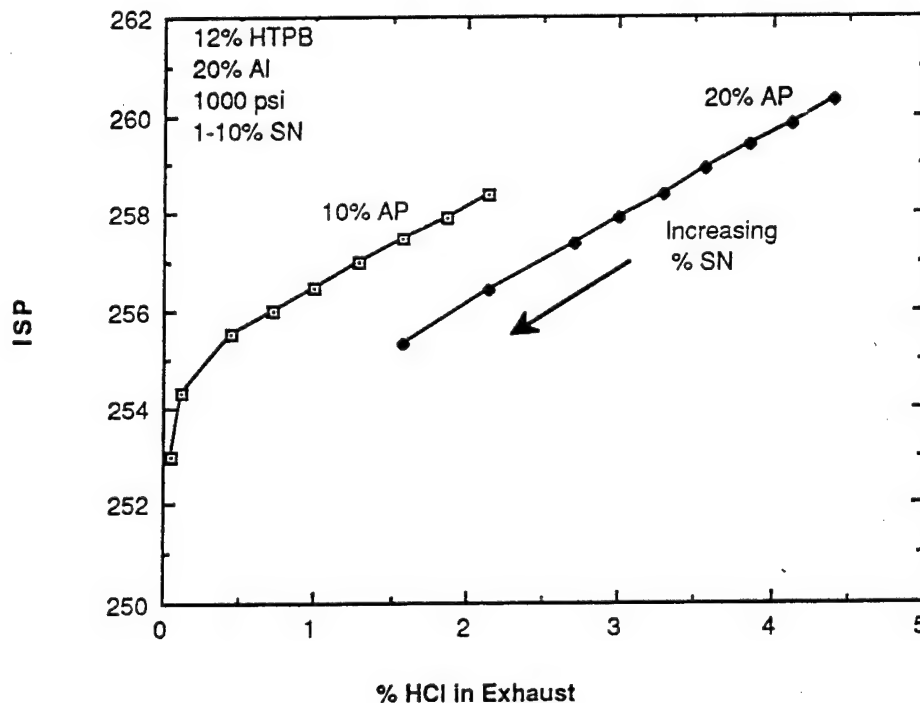


Figure 4. A comparison of calculated Isp values versus the concentration of HCl in the exhaust of propellants containing AN, AP and SN.

The calculated Isp values are on a per unit mass basis and the figure of merit for a large space booster is more logically based on the volume of the booster, which corresponds to the product of the Isp and the density. Therefore, the Isp-density has been examined to evaluate the performance of SN in an AN propellant on this basis. Figure 5 shows the calculations from Figure 4 replotted as Isp-density versus percent HCl in the exhaust. Sodium nitrate has a much higher density (see Table 2) than either AN or AP (2.26 versus 1.73 and 1.95, respectively), and the increase in propellant density due to the trade-off between SN and the lower density AN makes the SN look much more attractive on the Isp-density basis. However, it is also

apparent that the increased amount of AP also improves the performance due to its higher density and inherently higher performance.

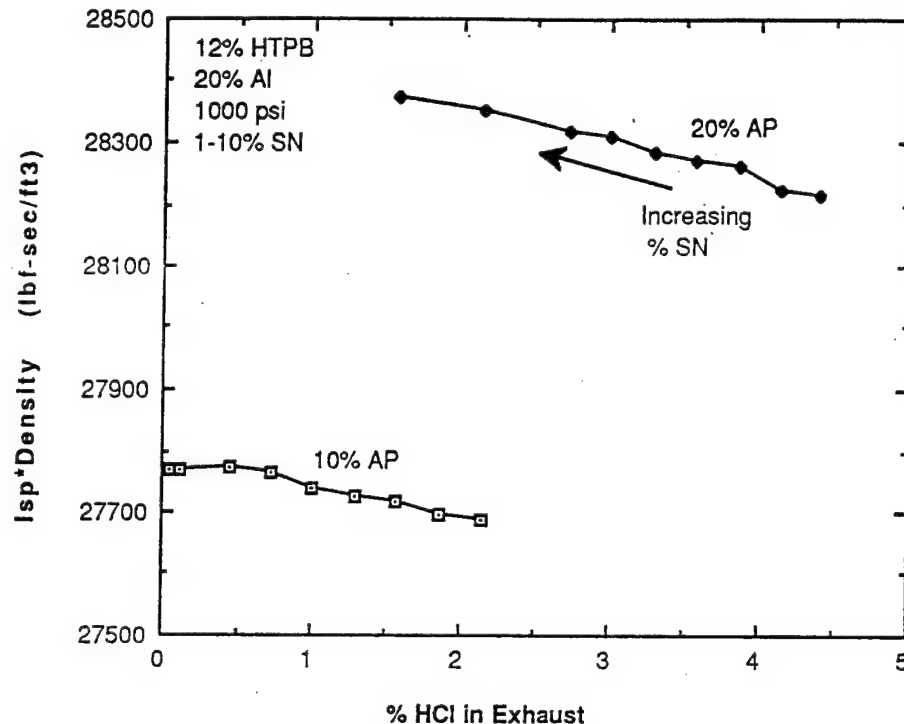


Figure 5. A comparison of calculated Isp-density values versus the concentration of HCl in the exhaust of propellants containing AN, AP and SN.

During the course of the contract³² curing problems were encountered with the nickel oxide phase stabilized AN. Ultimately a potassium nitrate phase stabilized AN (ANPN) was selected as the standard AN to be used throughout the contract. The ANPN contains approximately 11% KNO_3 (KN), added for phase stabilization, but which obviously will provide some scavenging capability for hydrogen chloride.

A series of calculations were made to evaluate the performance of what might be candidate type propellants using the ANPN material. The baseline propellant formulation was assumed to be 10% HTPB with 20% aluminum. AP content was varied with SN and with the ANPN. Figure 6 is a plot similar to Figure 5 where Isp-density has been plotted versus percent HCl in the exhaust. Different levels of AP were assumed and the amount of SN was traded off versus the amount of ANPN. For all levels of AP up to 40%, it was possible to add sufficient SN to scavenge the HCl to less than 2% of the exhaust gases. The 40% AP calculation required 30% SN as a scavenger, thus precluding any ANPN at all. It would not be possible to keep the HCl content below 2% for AP levels above 40%.

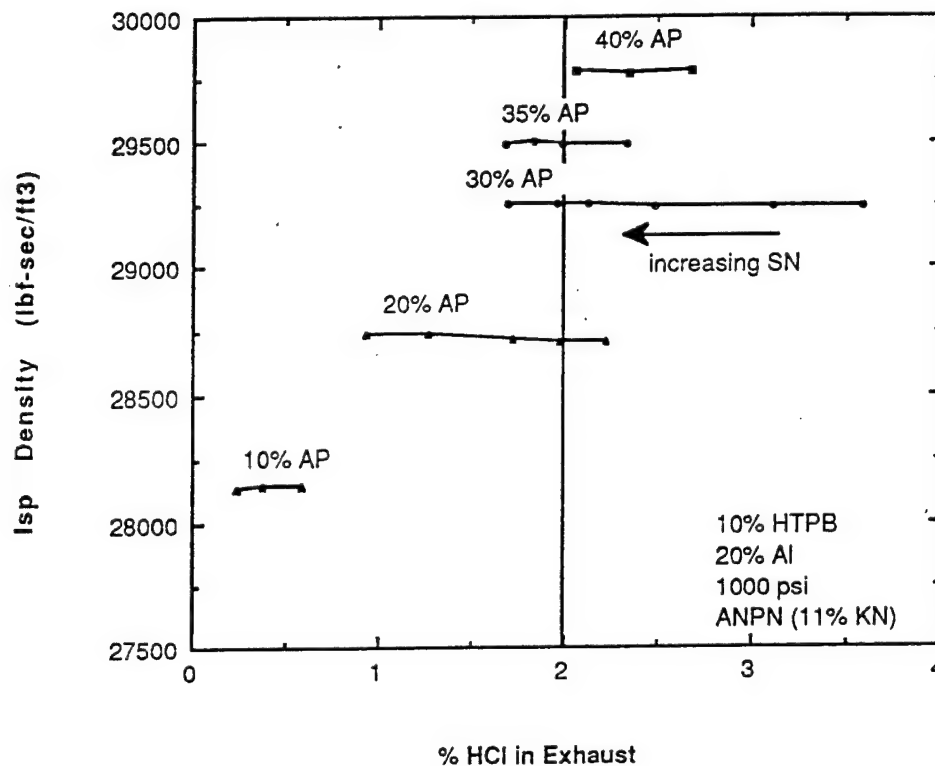


Figure 6. A comparison of calculated Isp-density values versus the concentration of HCl in the exhaust of propellants containing ANPN, AP and SN.

The same calculations were used to identify the amount of SN necessary to keep the HCl at or below 2% and the results are plotted in Figure 7 as Isp-density versus percent AP. Increasing AP requires increasing SN up to the 40% AP level where all of the ANPN is eliminated. The performance is impressive in that the elimination of the ANPN dramatically improves the performance. The low inherent performance of AN plus its low density result in very unimpressive performance numbers for the propellant. The efficiency of the SN as a scavenger is shown in Figure 8, where the data from Figure 6 have been replotted as percent HCl versus SN content for increasing levels of AP. The ratio of SN to AP needed to scavenge the HCl increases as the AP content increases due to the decreasing amount of KN present as the ANPN content is reduced. From a practical point of view, AN does not appear to be a very good candidate for space booster applications. The combination of AP and SN appears to be much better.

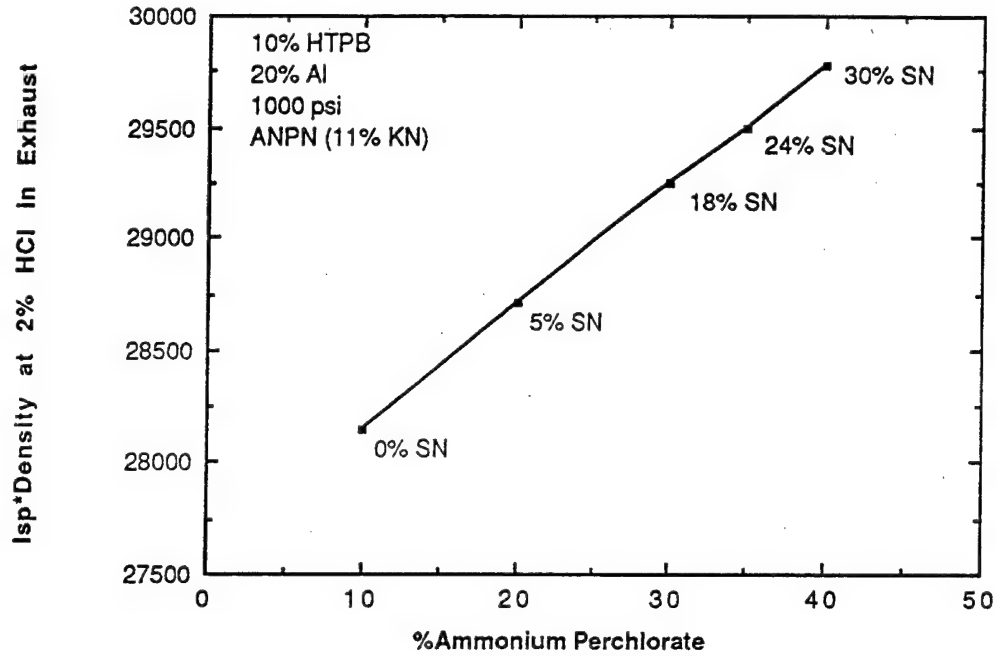


Figure 7. A comparison of calculated Isp-density values versus the concentration of AP for propellants containing ANPN, AP and SN.

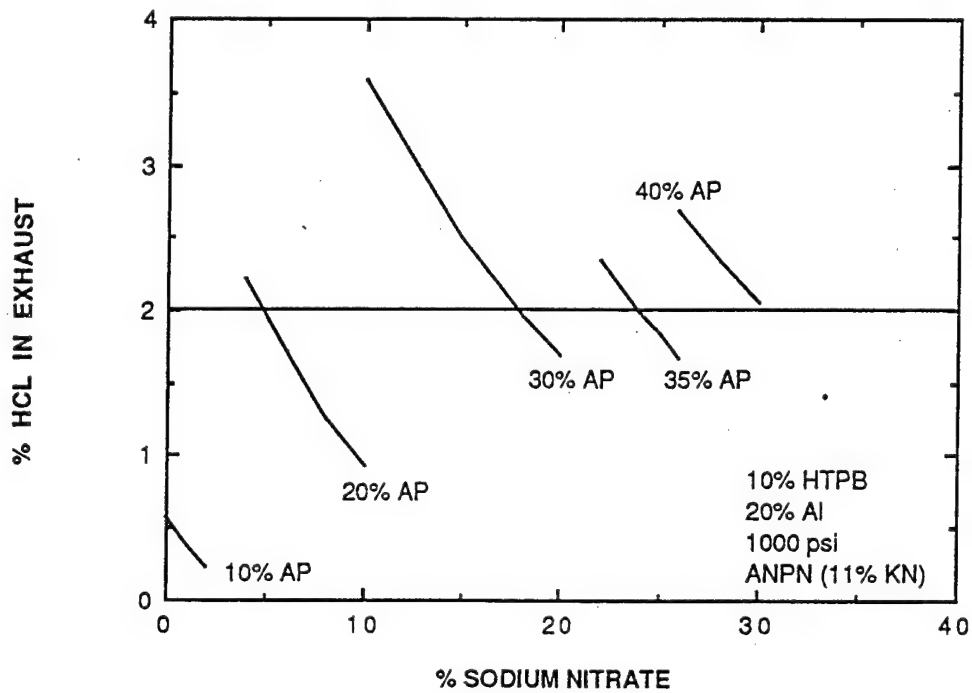


Figure 8. A comparison of the HCl exhaust concentration versus the concentration of SN for propellants containing ANPN, AP and SN.

Ammonium Nitrate Monopropellant Flame

Due to the nitrate in AN, it had been speculated that the AN flame structure might be similar to double base propellants or HMX, where a dual stage flame exists. In an attempt to determine what the flame structure might be, a series of thermochemical calculations were made that correspond to different potential products in the flame. The results are summarized in Table 3 where the heat of reaction and adiabatic reaction temperature are recorded for five possible sets of products. The key molecule that characterizes the energy release is nitrogen, as it is reduced from the nitrate ion through the various nitrogen oxides to N_2 .

Table 3 AN Monopropellant Reactions

	<u>ΔH (Kcal)</u>	<u>cal/gm</u>	<u>T (K)</u>
(1) $NH_4NO_3 = HNO_3 + NH_3$	44.5	556	-
(2) $NH_4NO_3 = NO_2 + H_2O + H_2 + 1/2 N_2$	37.6	470	-
(3) $NH_4NO_3 = NO + 2 H_2O + 1/2 N_2$	-6.6	-83	550
(4) $NH_4NO_3 = N_2O + 2 H_2O$	-8.7	-109	625
(5) $NH_4NO_3 = N_2 + 2 H_2O + 1/2 O_2$	-28.2	-352	1247

The initial decomposition of AN to HNO_3 and NH_3 and the reaction leading to NO_2 are both very endothermic and unlikely to occur in a flame but are more likely to occur in the condensed phase. The other three reactions were considered as potential flame reactions. The most obvious would be to assume that the flame is in complete equilibrium with final products of N_2 , H_2O , and O_2 . Initially, this was not considered to be very likely because of the dark zone flame structure in double base flames, where NO forms in a pseudo equilibrium condition. The third reaction would be similar to double base propellants with a dark zone flame where the principal nitrogen product would be NO . This leads to final products of NO and H_2O . However, this possibility has been rejected for two reasons. First, experimental decomposition data³² indicate that N_2O appears to be the principal nitrogen product coming off the propellant surface. Apparently the melting and subsequent condensed phase reactions reduce the nitrogen past the NO step to N_2O . Secondly, the resultant flame temperature calculated for NO as a product is less than 600 K, which is the nominally measured surface temperature of burning AN. The fourth reaction has been rejected for the same two reasons. Therefore, it would appear that the nitrate is reduced at least to NO in the condensed phase and probable some of the reaction proceeds to N_2O , which is the predominant nitrogen product leaving the surface. Thus it seems unlikely that there is an inner flame for AN combustion where either NO or N_2O is in equilibrium. Based on these various reasons it has been assumed that the flame is in complete equilibrium with final products of N_2 , H_2O , and O_2 and at a monopropellant flame temperature of 1247 K. The need for flame temperature measurements is readily apparent. It would be of great benefit to have at least one thermocouple

measurement, or a concentration measurement to determine the flame temperature or the species present in the AN monopropellant flame.

Primary Flame Temperatures

A critically important part of the model is the primary diffusion flame that occurs between the decomposition products of the binder and the oxidizer. For AP composite propellants the primary diffusion flame is the dominant combustion mechanism in determining the burning rate of the propellant³³. Understanding the characteristics of the diffusion flame in AN propellants is prerequisite to the development of a realistic propellant combustion model. Flame temperature calculations have been made for HTPB/AN propellants to aid in identifying the flame structure and for incorporation into the computer program. As it has been discussed in the previous section, it had been speculated that the AN flame structure may be similar to double base propellants due to the nitrate in AN. In an attempt to determine what the flame structure might be, a series of thermochemical calculations were made corresponding to different potential flames. The calculations were made varying the percent AN in an HTPB binder over a range of pressures from 100 to 10,000 psi. Typical results are shown in Figure 9.

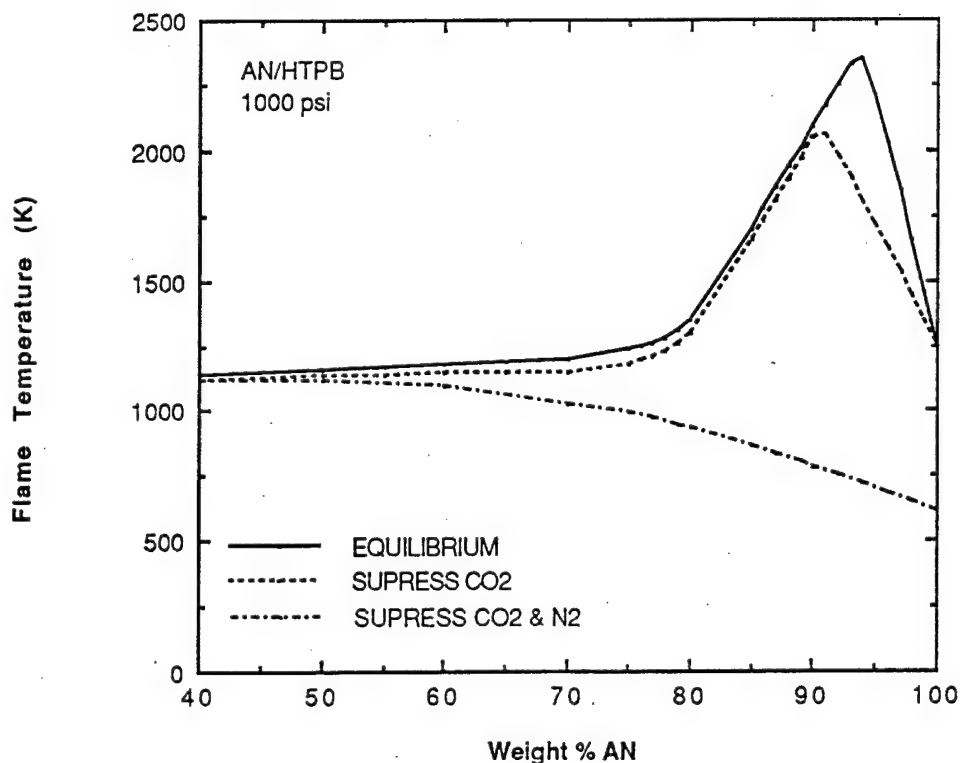


Figure 9. Calculated flame temperatures for three different postulated flame structures.

Initially four separate flame structures were postulated. The most obvious is to assume that the flame is in complete equilibrium (the solid curve in the figure). This was not considered to be very likely. The other extreme was assumed to be similar to

double base propellants with a dark zone flame where the principal nitrogen product would be NO. However, this possibility has been rejected for the reasons discussed above pertinent to the AN monopropellant flame. Therefore, it was anticipated that if there were an inner flame for AN combustion it would correspond to the case where the N_2O is in equilibrium (this is represented by the curve marked 'suppress CO_2 and N_2 ' in the figure), and corresponds to a calculated monopropellant flame temperature of 650 K. As discussed above this possibility of an inner monopropellant flame reacting to N_2O seems highly unlikely. The corresponding flame between AN and HTPB seems equally unlikely due to the very low temperatures that are calculated (i.e. the temperatures are consistently below 1000 K). The final alternative to be considered would be the case where it is assumed that the nitrogen reacts completely to N_2 and there is no inner flame except for the delayed reaction of CO to CO_2 . This is shown in the figure as the curve marked 'suppress CO_2 '. It was finally concluded that the primary flame between AN and the binder occurs with N_2 , CO and H_2O as the final products. Previous work on AP^{6,33} and other systems³⁴ leads to the conclusion that the formation of CO_2 is relatively slow and that CO is the product of importance near the burning surface.

The flame temperatures were calculated as a function of pressure and concentration with the CO_2 suppressed. The results are presented in Figure 10. The peak temperature occurs at 91 percent AN or at an oxidizer to fuel ratio of 10.1. The effect of pressure is to cause the temperature to increase with pressure at low oxidizer concentrations, but virtually no effect of pressure is observed above 82 percent AN. These are the data that have been programmed into the computer program to provide the primary flame temperature as a function of pressure and oxidizer to fuel ratio.

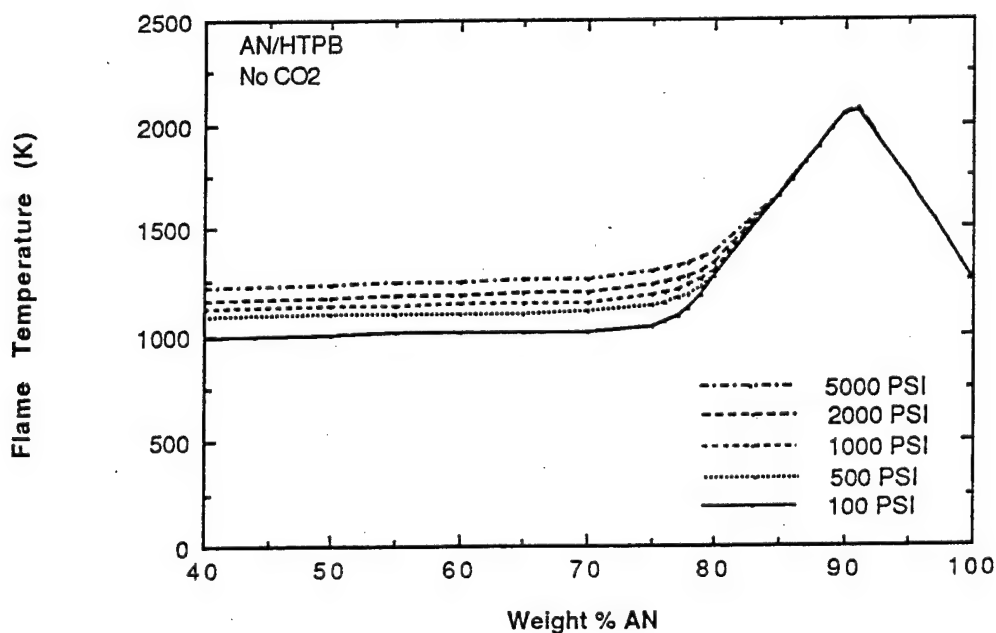


Figure 10. Calculated primary flame temperatures for the CO equilibrium flame for AN/HTPB propellants for use in the model.

It is also informative to look at the composition of the gas for the same conditions. Figure 11 shows the variation of gas composition at 1000 psi. Below about 70 percent AN a significant amount of solid carbon is predicted to form, and the numbers in the figure do not reflect the free carbon in the products. At 50 percent AN 29 percent of the exhaust products are predicted to be solid carbon. Above 70 percent AN no free carbon is predicted. The very high percentage of H_2 in the products contributes to a very low molecular weight of the gases which makes the Isp reasonable for AN propellants.

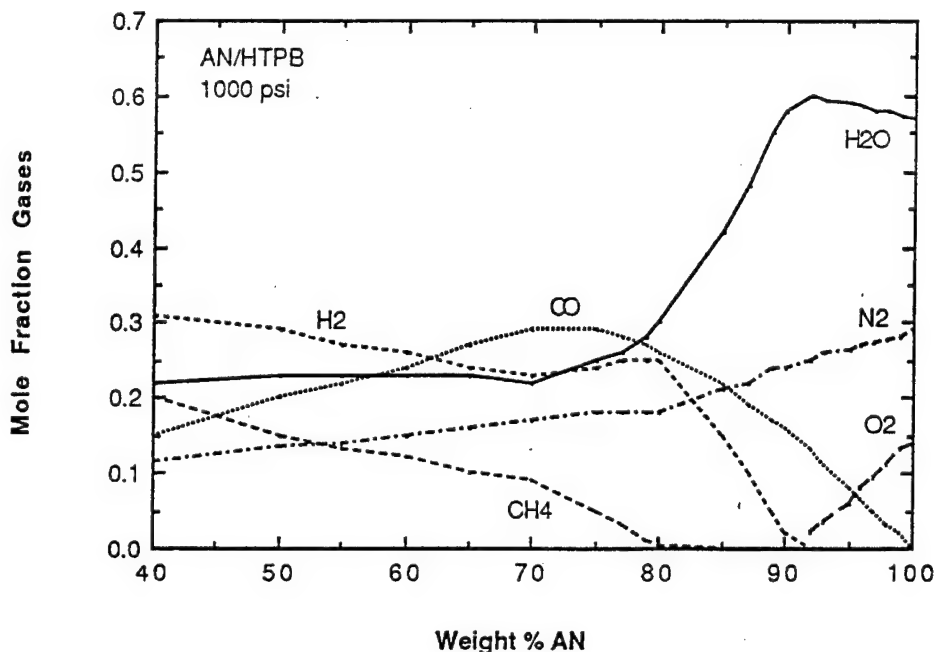


Figure 11. Exhaust gas composition for AN/HTPB propellants varying percent AN.

Other Primary Flame Temperatures

Because the propellants to be considered were to have multiple oxidizers, flame temperature calculations were also made for AP and SN propellants. The same approach was taken as described above, i.e. the formation of CO_2 was suppressed and the calculations were made as a function of oxidizer fraction and pressure. Typical results are shown graphically in Figure 12. The peak of the curves for AP and SN are nearly the same weight fraction of oxidizer while the AN peak occurs at a higher oxidizer fraction. The AP system has a peak temperature of 2750 K and SN has a peak temperature slightly greater than 2300 K while the peak temperature for AN is barely 2000 K. It is apparent from this very low temperature that an AN propellant would have a much lower burn rate and its propensity to ignite and burn aluminum would be very low.

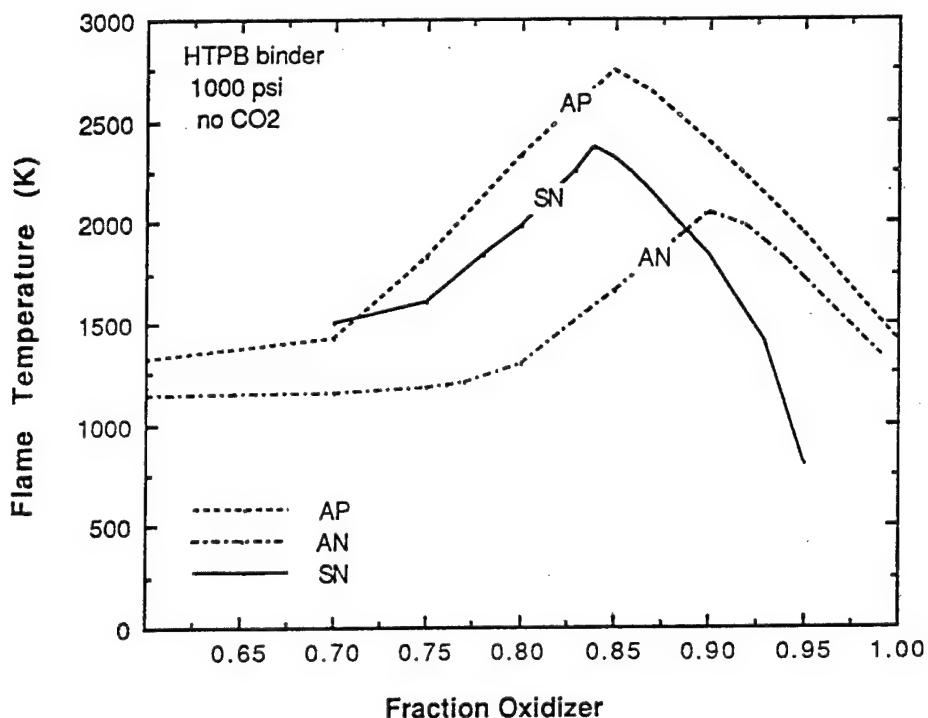


Figure 12. Comparison of calculated flame temperatures for primary flames in AP, AN, and SN/HTPB propellants.

Performance Characteristics of AN/Silicone Rubber Propellants

In a parallel contract at Hercules (the Aluminum-Water Rocket Program)³⁵, propellant evaluation work was performed developing a highly metallized AN based propellant. Under that contract it was decided to use a silicone rubber binder (Sylgard 182) due to the improved combustion characteristics that were obtained using that binder within a highly metallized propellant.

For comparative purposes calculations were performed for a series of propellants identical to those in Figure 12, but with the silicone rubber binder in place of HTPB. The silicone rubber has a nominal formulation of SiCH_2O with a heat of formation* of -24.9 Kcal/mole. The results are displayed in Figure 13. The flame temperatures of the silicone based propellants are dramatically different for each of the three oxidizers, giving higher flame temperatures and much broader peaks in the curves than the corresponding HTPB propellants. The extra oxygen in the silicone rubber broadens the curve and causes the peak to shift to a much lower oxidizer fraction. The increase in temperature is apparently due to the different exothermicity of the products from the two binders. The Sylgard binder forms SiO_2 in addition to the CO and CO_2 formed by the HTPB binder. The higher heat of formation of SiO_2 relative to CO and CO_2 apparently accounts for the increased temperature. The net result being the observed shift in both the flame temperature and the stoichiometric ratio of oxidizer to binder.

The propellants used in the Aluminum-Water Rocket Program³⁵ were formulated with approximately 18 percent binder. From the figure it is apparent that at 18 percent binder loading the silicone propellant flame temperature is significantly higher than a corresponding HTPB binder propellant and one would expect the silicone propellant to burn better, both faster and more efficiently, which was observed experimentally.

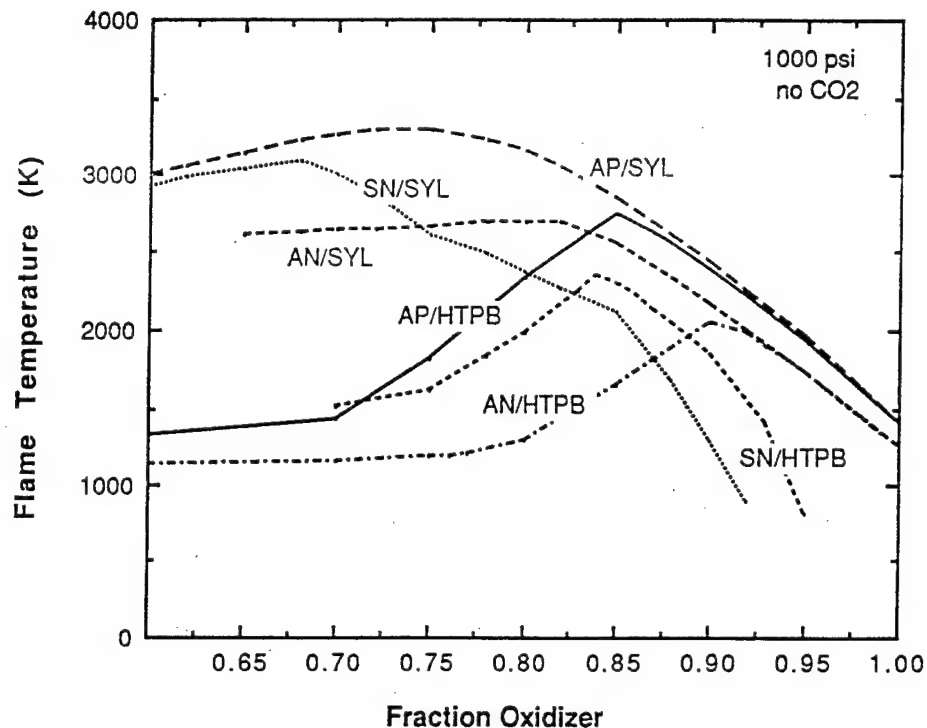


Figure 13. Comparison of calculated flame temperatures for primary flames in AP, AN, and SN propellants with HTPB and Sylgard binders.

Performance calculations were also made comparing the different binder systems, and are presented in Figures 14 and 15. Figure 14 displays the calculated Isp values for AP and AN systems with both the Sylgard binder as well as an HTPB binder for reference. Although the Sylgard binder produces SiO₂ which gives the Sylgard propellants an increased molecular weight, the flame temperature is sufficiently higher than the HTPB propellants that the AN/Sylgard propellant has a much superior Isp than the AN/HTPB propellant. The AP based calculations reach comparable Isp values but at very different binder loadings. Figure 15 compares the four different cases plotted versus the aluminum content. The additional oxygen in the silicone binder apparently reduces the overall performance slightly, so that the calculated Isp values for the AP propellant are about 10 sec below the HTPB values. However, the AN silicone system is very comparable to the HTPB system (they are equal at ~17% binder), and considering combustion efficiency, the silicone binder would appear to be a better choice than the HTPB binder. Above 20% aluminum the HTPB binder gives significantly improved performance, but obtaining good combustion efficiency in that range of propellant formulations could be very difficult.

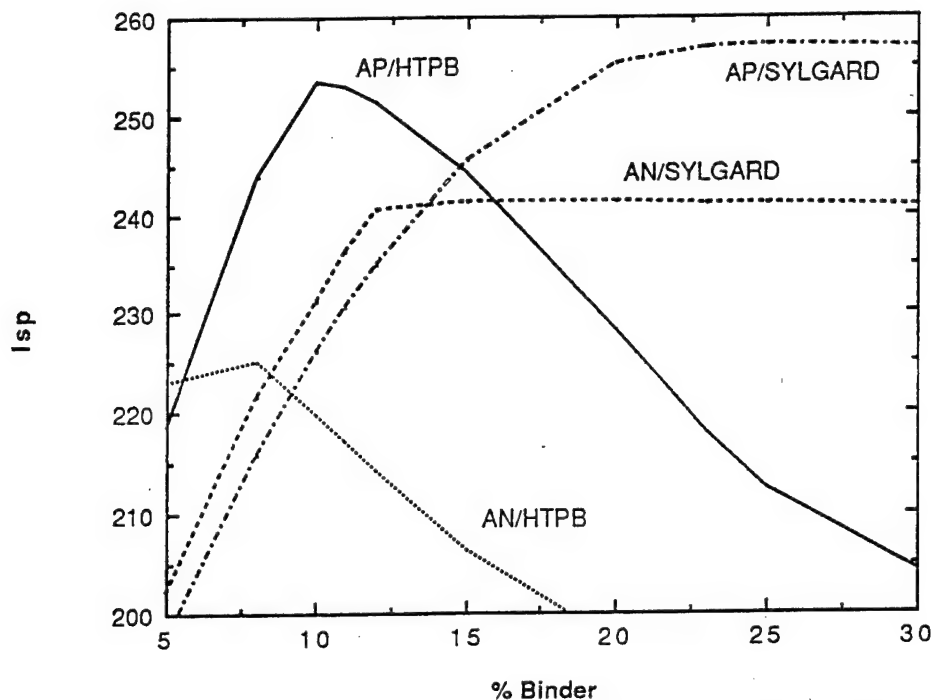


Figure 14. Comparison of calculated Isp for AP and AN propellants with HTPB and Sylgard binders varying binder level.

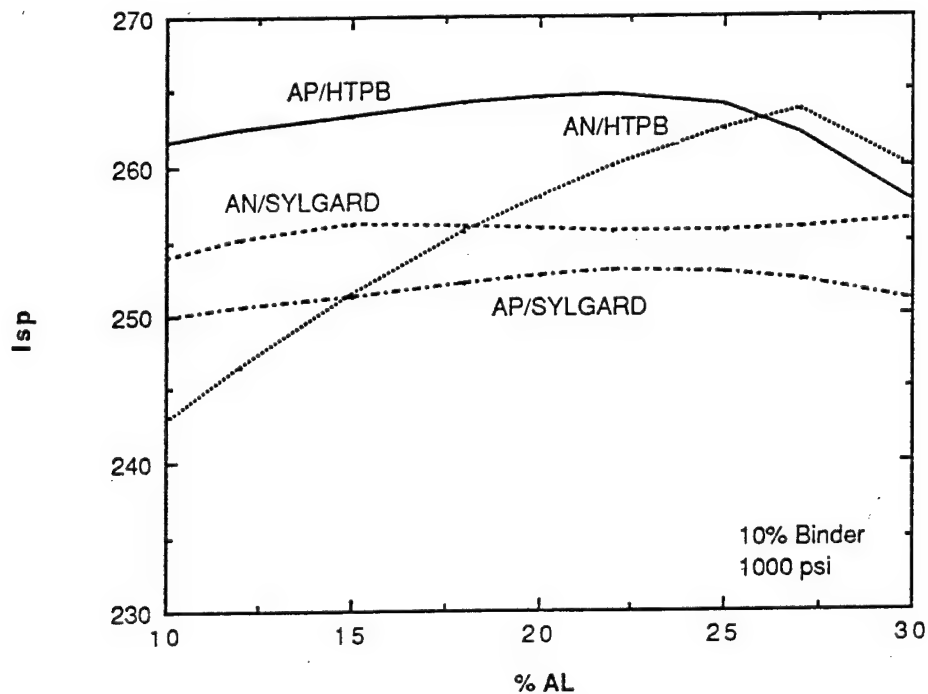


Figure 15. Comparison of calculated Isp for AP and AN propellants with HTPB and Sylgard binders varying aluminum level.

COMBUSTION MECHANISMS OF SOLID PROPELLANTS

The Condensed Phase

The two oxidizers used most often in modern solid propellants are ammonium perchlorate, AP, and cyclotetramethylene tetranitramine, HMX. In this study two additional oxidizers have been considered. These are ammonium nitrate, AN, and sodium nitrate, SN. The motivation for studying them is to develop an alternate oxidizer for AP that would be cheaper and would be "clean", i.e. would not produce HCl in the exhaust. The two most common binder systems consist of either an inert binder system based on a polybutadiene polymer (almost always HTPB), with various plasticizers, additives and cross linking agents or an active binder system based on energetic components such as nitroglycerin, NG, and nitrocellulose, NC. As referenced in the previous chapter, a silicone based binder has also been used rather successfully in a program using AN as the propellant oxidizer. However, the current study is limited to the more common HTPB binder propellants.

As a propellant burns, both oxidizer and binder are preheated by conduction as they approach the surface. The initial step in the overall process is probably melting which results in a thin liquid layer on the oxidizer surface (probably on the binder surface also). AP and HMX melting points are approximately 865 K and 553 K, respectively (see Table 1). AN melts at 443 K and SN melts at 580 K, both of which are much lower than the melting point of AP. The very low melting point of AN will result in a relatively long residence time for the molten material, a thicker melt layer, and could allow for some lateral mixing at the propellant surface. In the liquid layer and immediately below the propellant surface the initial decomposition step is apparently the endothermic dissociation of the oxidizer. Ammonia and perchloric acid are the initial products for AP, while AN yields ammonia and nitric acid. While still near the surface in the liquid layer, these decomposition products apparently undergo further exothermic condensed phase reactions before passing through the surface into the gas phase (see Table 3 in the previous chapter). These additional reactions are exothermic, to the extent that the overall condensed phase decomposition is exothermic. The possibility of similar exothermic reactions occurring at the binder surface must also be considered. These could occur by reaction with oxygenated species coming from within the binder itself or by diffusion of reactive species to the binder from the adjacent oxidizer.

The products observed from the low pressure, high heating rate decomposition of ammonium perchlorate include chlorine, nitrogen oxides, water, hydrogen chloride as well as ammonia and perchloric acid. The corresponding tests for AN yield a mixture of NO, N₂O, N₂ and water. As was discussed in the previous section, the gases coming from the oxidizer surface are a mixture of partially decomposed products. A significant amount of the available energy is apparently released in the condensed phase. During combustion it is anticipated that the gases coming from the oxidizer surface contain little or none of the initial decomposition products but are almost exclusively, the partially decomposed products.

A question to be addressed is, how important or relevant are these initial reactions to the ultimate burning rate of the propellant. Boggs, et.al.³⁶ in a recent

paper on AP(ammonium perchlorate), concludes that low temperature decomposition studies can and do lead to conflicting predictions relative to actual deflagration. The authors quote many instances showing that low temperature decomposition tests do not correlate with actual combustion conditions. The initial decomposition reactions apparently only provide a boundary condition of gaseous products and temperature for the energy feedback from the flame. As the energy feedback varies, the reactions at the surface apparently adjust to provide a different, compatible composition and temperature for the given energy feedback.

Surface Temperature

The surface temperature is related to the burning rate in most models as a one-step, zero-order Arrhenius pyrolysis law

$$r = A_S e^{(-E_S/RT_S)} \quad (1)$$

Based on Equation (1) the surface temperature is directly dependent on the burning rate but only indirectly dependent on the pressure (due to the fact that the burning rate is dependent on pressure).

Only two sources of surface temperature data for AN were found in the literature. Anderson, et al³⁷ reported hot plate data for pellets of AN in 1958. In 1964 Whittaker and Barham³⁸ measured temperature profiles using thermocouples in burning pressed pellets of AN containing up to 2.5% Cr₂O₃. Their data were taken over a range of pressures from 1000 to 4800 psi. It is curious that they concluded that the Anderson data were incorrect. Figure 16 shows the combined data plotted as rate versus 1/K. The Whittaker/Barham combustion data are much more scattered than the hot plate data. Within the data scatter, the data are actually in very reasonable agreement, with an apparent activation energy of 10.4 Kcal/mole. It is significant that the burn rate catalyst did not appear to have a significant influence on the surface decomposition characteristics.

Two sources of data were found for the surface temperature of SN. Frolov, et al³⁰ report three datum points for composite mixtures of SN, aluminum and an additive, but do not say what method was used to measure the surface temperature. Girdhar and Arora³⁹ report surface temperatures for SN composite propellants, but they infer the surface temperatures from temperature sensitivity data and an empirical relationship between the rate, the surface temperature and the temperature sensitivity. Their data indicate an activation energy less than zero which is considered to be inconsistent and unreliable. Therefore, their data were not used. Frolov's data are plotted in Figure 17. The data indicate a very high surface temperature for SN, in the neighborhood of 1000 K, and a relatively low activation energy, 4.5 Kcal/mole.

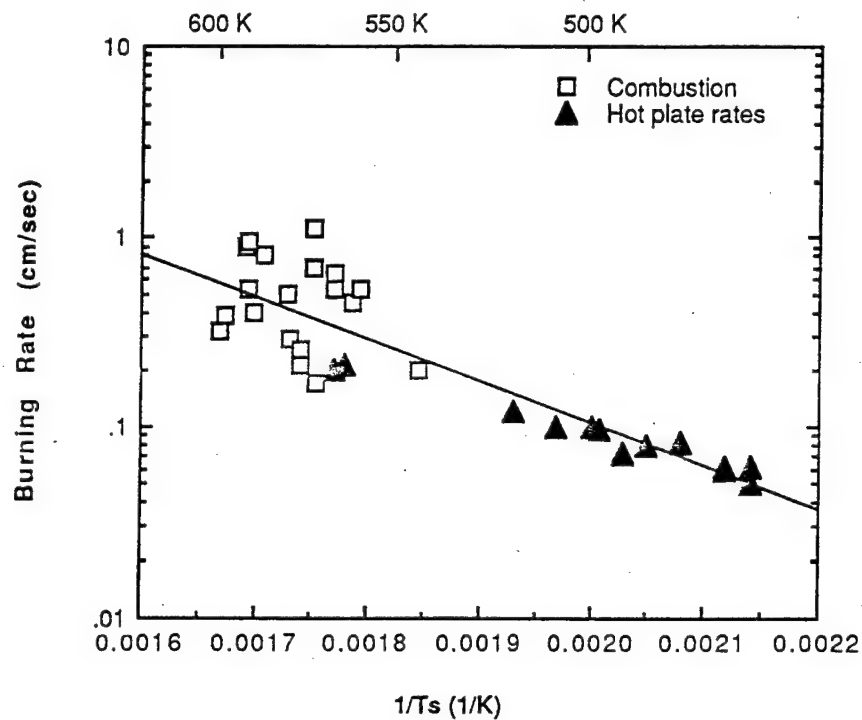


Figure 16. Surface temperature data for pressed pellets of AN. The hot plate data are from Anderson and the combustion data from Whittaker.

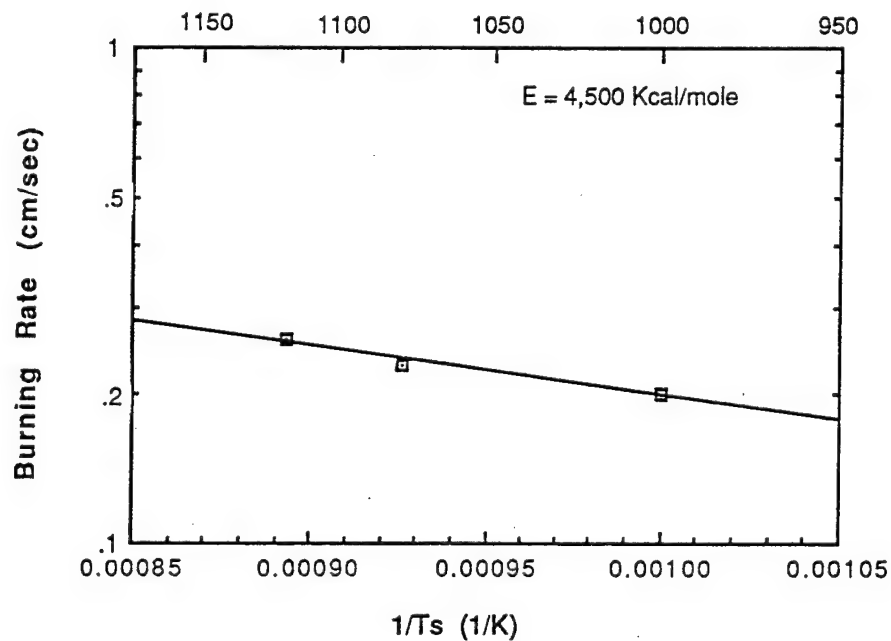


Figure 17. Surface temperature data by Frolov, et al for a composite mixture containing SN and aluminum.

AN and SN are to be used in composite propellants with AP as a co-oxidizer. For comparative purposes the data from Figures 16 and 17 have been combined with data for AP^{40,41,42} and are plotted in Figure 18. In addition the calculated values that are used for HTPB binder in the model are also included in the figure. The wide diversity in surface temperatures poses some interesting possibilities. For example, if a propellant were burning at a rate of one cm/sec, for all of the components to be in equilibrium, the surface temperatures would have to be 700 K for AN, 1000 K for AP, 1400 K for HTPB, and much higher for SN. Obviously this is not realistic. However, there must be a wide diversity of surface temperatures and individual rates occurring simultaneously on a propellant surface. To model such a situation, one must allow for separate surface temperatures of each ingredient and individual rates for each ingredient. An ingredient such as SN should burn very rapidly once it ignites, possibly leaving an empty pocket of binder or possibly disrupting the adjacent surface regions with an explosive type of flow due to the very high relative rate. AN on the other extreme could possibly puddle and flow along a surface due to its high residence time and low combustion rate. The physical picture for such an environment is obviously very complicated.

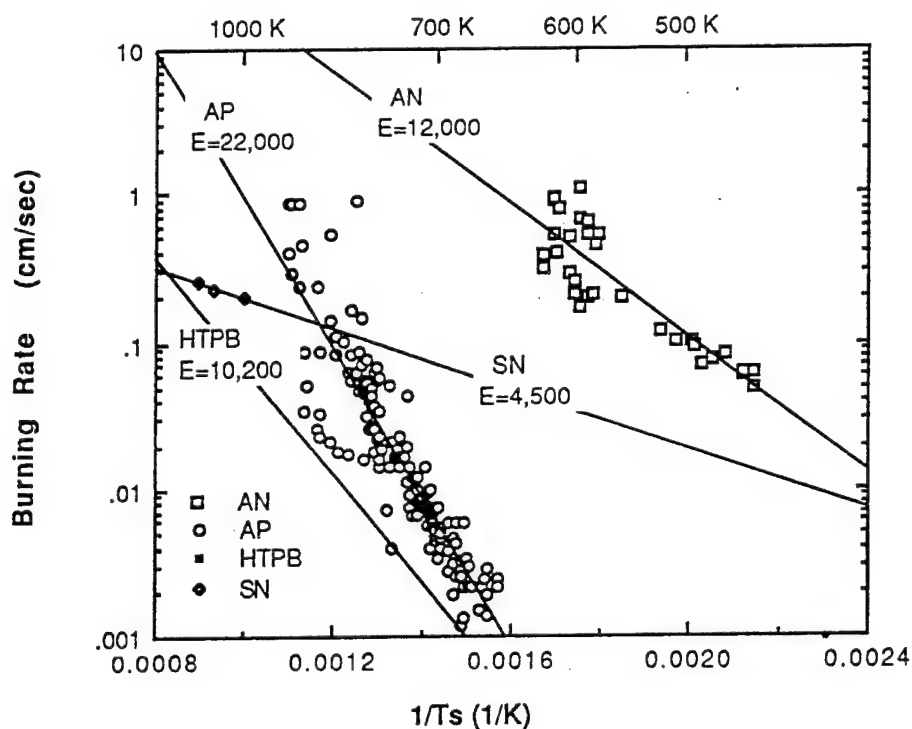


Figure 18. A comparison of surface temperature data for AP, AN, SN and HTPB, the principal ingredients of interest in this study.

Condensed Phase Heat Release

A critical step in the combustion process is the energy release in the condensed phase. Attempts have been made during this contract to calculate this condensed phase heat release, but there isn't sufficient information about the condensed phase reactions to allow a general calculation. To calculate a heat of reaction, the enthalpies of the reactants, and products must be known at the initial temperature and the reaction temperature. Based on the calculations reported in Table 3 of the previous chapter, the heat release in the condensed phase should be on the order of 80 to 110 cal/gm exothermic. In a parallel contract studying double base propellants⁴³, it was determined from an examination of experimental data that the heat of reaction will be proportional to the reaction temperature and decreases with increasing initial temperature. The data were correlated by plotting the surface heat release versus the difference of $T_s - T_o$, which provided an excellent correlation of the data. In the model the condensed phase heat release was assumed to be

$$Q_L = Q_C(T_s - T_o) \quad (2)$$

where Q_C is a proportionality constant. The reader is referred to Reference 43 for a complete presentation of the data and logic supporting this equation.

Oxidizer Burning Characteristics

The relative burning rates of HMX, AP, and AN as monopropellants and in composite propellant mixtures are shown in Figure 19. As monopropellants the rate of HMX is slightly higher than that of AP and they both have similar burn rate exponents for typical solid propellant rocket pressures. The burning rate of AN is approximately a factor of five lower than the other two monopropellants. Although the difference between the linear burning rates of AP and HMX does not appear to be significant, but when the two oxidizers are mixed into a composite propellant, the resultant burn rates vary by as much as an order of magnitude. AP composite propellants typically have a rate higher than the monopropellant, while HMX propellants typically have a rate lower than the monopropellant. When AN is added to a binder, the propellant rate is comparable to that of the monopropellant. Thus, it would appear that AN composite propellants burn by a mechanism similar to AP propellants. Also, because of the very dramatic effects observed with each different oxidizer, it must be assumed that the primary diffusion flame between the oxidizer and binder decomposition products is the dominant mechanism controlling the burning rate.

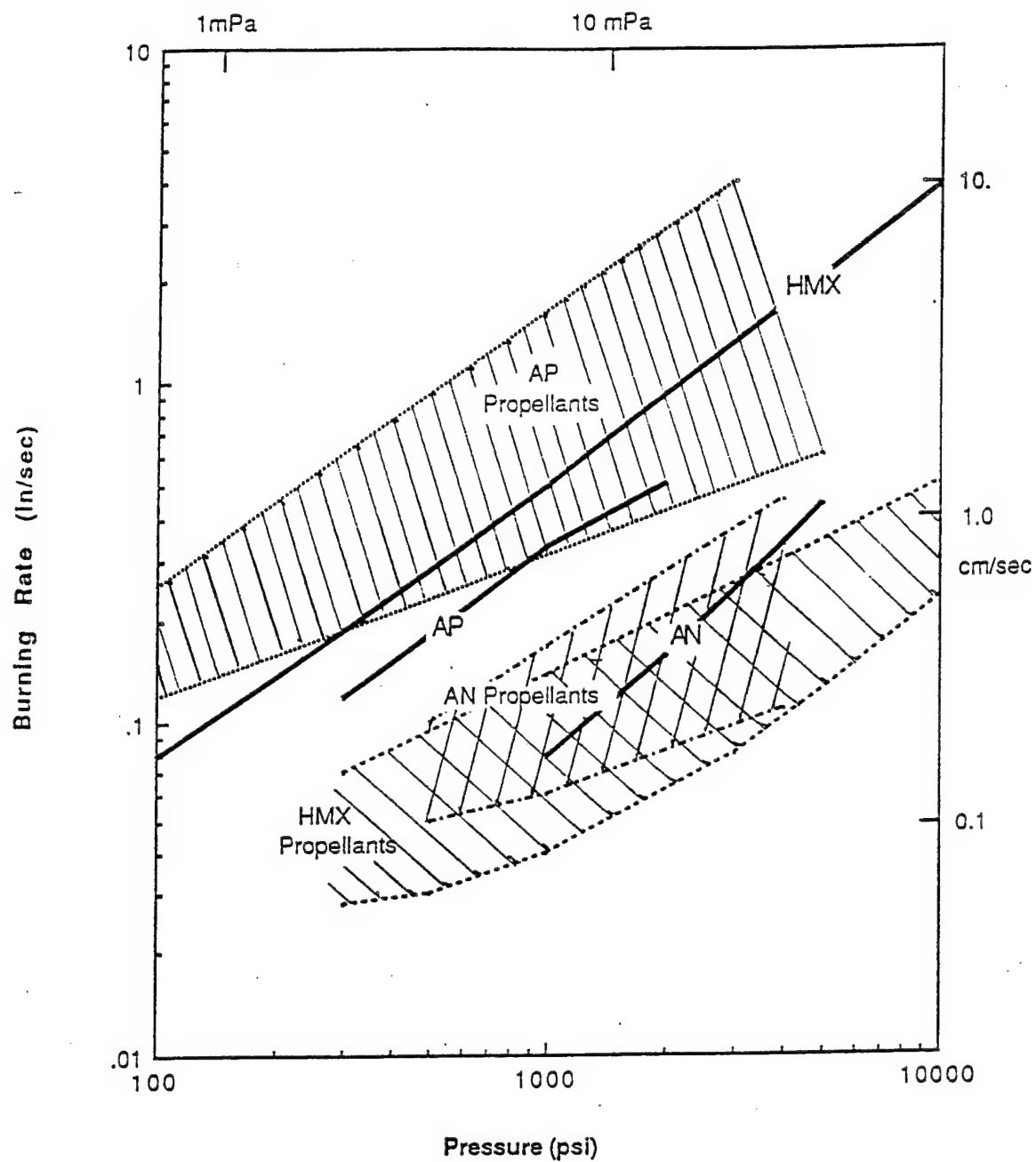


Figure 19. A comparison of the burning rates of AN, AP, and HMX monopropellants and composite propellants.

Composite Propellant Flame Structure

As has been discussed above, when an oxidizer decomposes during combustion, a mixture of partially oxidized products are formed in the thin liquid layer on the propellant surface. In a propellant this mixture of partially decomposed products coming from the oxidizer surface is available to either react and form the monopropellant flame, or react with the fuel decomposition products and form the primary diffusion flame. In an AP propellant the reactive gases leaving the surface are apparently a mixture of chlorine oxides probably ClO and ClO_2 . These species are very reactive and react readily with fuel species from the binder to form a very powerful primary diffusion flame. When HMX decomposes formaldehyde, hydrogen cyanide, and nitrogen oxides are formed which are actually fuel rich (relative to CO_2). None of these products is a very strong oxidizer. They can react to form a monopropellant flame, or when combined with fuel decomposition products they form a low temperature diffusion flame (due to their fuel rich nature). When AN decomposes nitrogen oxides (somewhat similar to HMX or double base propellants) are formed which are not very strong oxidizers compared to the chlorine oxides. They can react to form a monopropellant flame, or when combined with fuel decomposition products they also form a low temperature diffusion flame due to their low inherent energy. SN is somewhat unique in that it does not form a monopropellant flame. Only the diffusion flame is formed.

Figure 20 shows the postulated flame structure for AP, AN, and SN within a composite propellant with the various flame and surface temperatures indicated.

The relative surface temperatures for each oxidizer are significantly different and have been discussed previously. SN has the highest apparent surface temperature, with AP in between and AN has a very low value. Each apparently burns with a thin liquid layer on the surface. The characteristics of the liquid layer have not been determined experimentally, but have been inferred from calculations, quench samples and microcinematography. The liquid layer is inferred to be on the order of a few microns thick for AP, but should be much thicker for AN perhaps as thick as 100 microns due to the lower melting point and lower rate. Because the rate increases with increasing pressure, the liquid layer thickness will decrease with increasing pressure. Reactions in the liquid layer are probably relatively unimportant at pressures of interest and only become significant at low pressures where the flame heights become large.

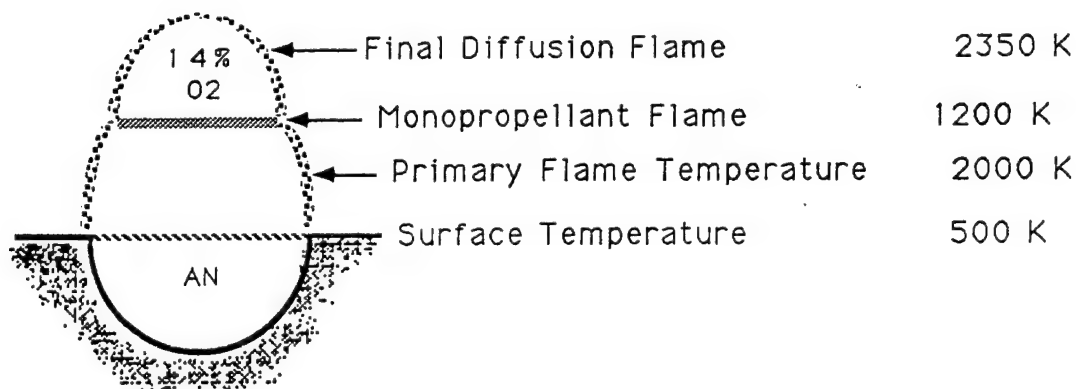
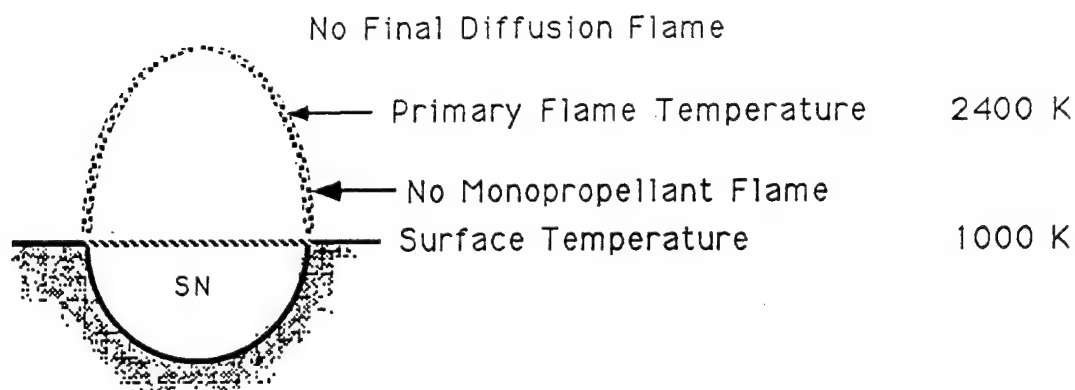
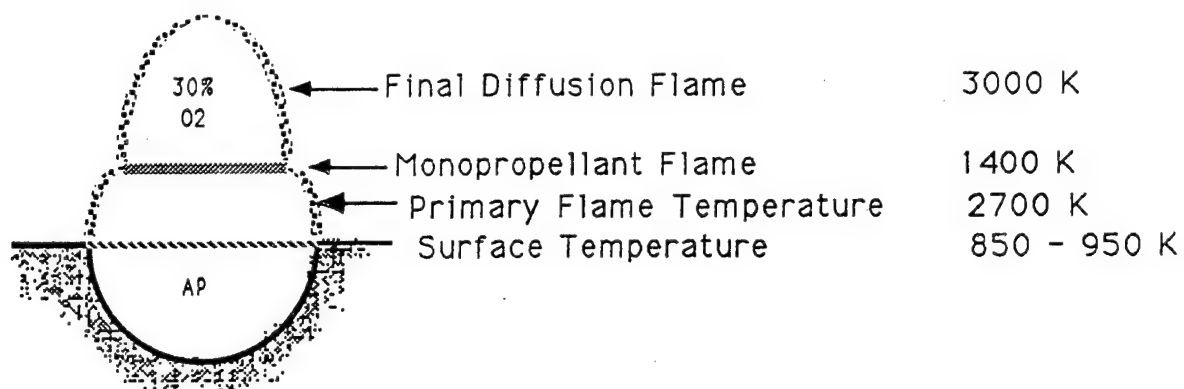


Figure 20. Flame structure for AP, AN, and SN composite propellants

At low pressures (ambient to ~100 psi) composite propellants probably burn as a premixed flame with the oxidizer and binder decomposition products mixing completely before reaction occurs. This would especially be true for small oxidizer particles. With increasing pressure, it becomes more difficult for the fuel products to diffuse into the stream above the oxidizer (and vice versa) and the two reaction paths (i.e. the monopropellant flame versus the primary diffusion flame) become competitive. At higher pressures where reactions occur more rapidly, the oxidizer products react preferentially to yield the normal monopropellant flame before the binder products can diffuse into the oxidizer stream and react. However, near the binder-oxidizer interface, a fraction of the oxidizing products will always react with the binder products. To properly describe the trade-off between these two flames and the relative heat transfer from them, is a major challenge in modeling solid propellants.

In addition to the monopropellant flame and the primary diffusion flame there is also a final diffusion flame for AP and AN propellants. As indicated in Table 2 in the preceding chapter, the AP and AN monopropellant products are approximately 30% and 14% O_2 , respectively. When either the AP or AN monopropellant flame occurs, it is followed by a diffusion flame (a 2-stage flame) where the oxygen-rich products of the flame can react with the binder pyrolysis products. This reaction should depend on mixing only, as the oxygen is heated to the temperature of the monopropellant flame, 1400 K or 1250 K, and at this temperature oxygen would be expected to be very reactive. All the characteristics of a typical diffusion flame can be expected for this final flame. In Figure 20 a higher temperature is indicated for the final diffusion flame than for the primary diffusion flame. This is based on the assumption that the preheated oxygen will react completely to CO_2 , while the primary diffusion flame is only expected to react to CO.

Allocation of Binder to Oxidizer

A critical assumption in developing the SST model relates to how the binder is proportioned to the various oxidizer fractions. Two approaches have been considered in the past. In the SST approach, it is assumed that the primary flame temperature is the adiabatic flame temperature for the stoichiometric mixture ratio of binder and oxidizer. However, some relationship between the decomposing binder and the amount of these decomposition products that react in the primary flame must be obtained, which amounts to estimating how much binder reacts in the primary flame and how much does not react. To accomplish this, a term accounting for the fraction of binder that reacts must be introduced into the equations. In the approach used in both the original BDP model and the PEM type models, all the binder associated with a given crystal is considered to react with the available oxidizer in the diffusion flames. This assumption leads to a variable flame temperature per oxidizer size fraction.

The theoretical concept of a diffusion flame as well as experimental data dictate that the flame burns at "stoichiometric" conditions. In other words, when sufficient fuel and oxidizer have diffused together, they will react, independent of the overall O/F ratio. However, if there is excess fuel or oxidizer present, the excess material will ultimately reduce the temperature in the rocket. This final mixing and equilibration probably occurs far enough from the surface that it does not effect the burn rate significantly.

It must also be noted that the stoichiometric condition within the SST model was not assumed to be that corresponding to final production of CO_2 . Because the CO to CO_2 reaction is a relatively slow reaction, an intermediate "stoichiometric" condition was assumed for CO products. Further reaction and formation of CO_2 undoubtedly occurs, and the final temperature of the gases far from the surface will be the flame temperature corresponding to the overall propellant formulation. However, it is most likely that this equilibration and 'after burning' also occurs too far from the surface to have an effect on the burning rate.

The assumption of a variable flame temperature is the common assumption used in most models, but it is not necessarily on a sound mechanistic basis. Furthermore, it leads to peculiar results due to the fact that the AP/HTPB flame temperature has a maximum with respect to AP concentration. The PEM models assume an unrealistic distribution of binder per oxidizer distribution (and corresponding flame temperature) in order to match experimental data. The crux of the problem is really in how the binder is assumed to be distributed in the propellant.

Cohen⁸ has proposed and used a compromise position which appears to be quite realistic on a mechanistic basis. He assumes that the fuel left over from the fine particle size is available to be burned in the diffusion flame of the next larger size fraction. This makes sense. Typical binder thicknesses associated with the intermediate and coarse oxidizer fractions are on the order of 0.2μ for 20μ particles and 2μ for 200μ particles (i.e. 1% of the particle diameter)⁴⁴. This is smaller than the roughness and non-sphericity of typical crystals. Thus, it can be anticipated that there will be a significant amount of binder buried within the surface irregularities of a crystal in excess of what would be calculated for a purely spherical particle. Cohen's approach reflects this reality. In his most recent model⁸ he assumes that the finest oxidizer fraction burns at the stoichiometric O/F condition. The amount of binder available to the fine fraction will be calculated to be greater than the stoichiometric O/F ratio (i.e. the binder is assumed to be distributed according to the surface area of the particles). Therefore, there is binder left over from the fine fraction which Cohen assumes is available for combustion in the next larger size fraction. That size fraction is also assumed to burn at stoichiometric conditions if there is sufficient fuel, and any excess fuel is then assumed to be available to burn with the coarsest fraction. This approach appears to be very realistic and has been incorporated into the SST model for application with both AP and AN propellants. Furthermore, a preference order of oxidizer must be established. Because AP appears to be the most reactive of the oxidizers considered, it has been assumed that the AP will react whatever binder is available to achieve stoichiometric conditions and that the AN is left to use whatever binder is left over.

AN MONOPROPELLANT MODELING

The model discussed in this section is essentially the BDP monopropellant model^{27,45,46} that has previously been applied to AP, HMX and double base binders burning as monopropellants. The overall model is being developed with the intent of applying it to composite propellant systems. The monopropellant model is a limiting condition of the model, with no binder.

Basic Model Equations

The BDP monopropellant model^{27,45,46} reduces to essentially three equations: one describing the surface kinetics; one resulting from an energy balance at the burning surface; and one related to the gas phase kinetics. The surface regression is described as a one-step, zero-order Arrhenius pyrolysis law (see Equation (1)).

The surface temperature is assumed to be uniform over the burning surface and is determined from an energy balance. The energy balance can be expressed as

$$C_p (T_s - T_o) - Q_L = Q_f e^{-\xi^*} \quad (3)$$

where T_o is the initial temperature, Q_L is the condensed phase heat release and the final term represents the energy transported from the flame back to the surface. For a premixed laminar flame, the nondimensional flame-standoff distance is represented by the expression

$$\xi^* = C_p m^2 / (\lambda k P^\delta) \quad (4)$$

where the δ is the reaction order and the gas-phase rate constant k is expressed by an Arrhenius function of the monopropellant flame.

$$k = A_f e^{(-E_f/RT_f)} \quad (5)$$

The actual flame-standoff distance is then

$$x^* = m / (k P^\delta) \quad (6)$$

In the previous applications of the Beckstead model² for monopropellants, the value of Q_L was taken to be constant with varying pressure, which was considered to be a deficiency in the model. As a result of the concurrent work being done on the Temperature Sensitivity Program⁴³, available data for double base propellants and for HMX monopropellant indicate that the condensed phase heat release varied with

surface temperature and inversely with initial temperature. The expression that has been programmed into the model for Q_L is shown in Equation (2).

This introduces the condensed phase heat release into the calculation as a variable which increases with increasing pressure which is in general agreement with what limited data are available. Pressure does not appear explicitly in Equation (2), but the surface temperature varies with burn rate which is a function of pressure. Although there are no specific data for AN, Q_L will be assumed to follow the form of Equation (2).

The predictions of the most recent application of the Beckstead monopropellant model⁴⁵ were very reasonable. A comparison was made for both AP and HMX, with data at several pressures and three initial temperatures. There was some deviation of the model from experimental data at high pressure, and there was criticism of the activation energy values that were used. However, all of the calculated trends were consistent with observed experimental data.

Pressure Exponent and Temperature Sensitivity

One of the advantages of the BDP approach is its simplicity. The equations are sufficiently tractable that they can be differentiated to obtain a closed-form solution for both pressure and temperature dependence. The pressure exponent can be calculated to be

$$n = \left[\delta + \left(\frac{c_p T_f}{Q_f \xi^*} + \frac{E_f}{RT_f} \frac{d \ln T_f}{d \ln P} \right) \right] / \left[2 + \frac{RT_s}{E_s} \frac{c_p T_s}{Q_f \xi^* e^{-\xi^*}} \right] \quad (7)$$

For most situations the pressure exponent will be ~ half of the reaction order, δ . However, that assumes an equilibrium flame temperature, which is essentially independent of pressure. The monopropellant flame is most likely in equilibrium and therefore, independent of pressure. For double base propellants this is not true.

The temperature sensitivity can be calculated as

$$\sigma_p = \left[\frac{c_p}{Q_f \xi^* e^{-\xi^*}} + \frac{E_f}{RT_f} \frac{d \ln T_f}{dT_o} \right] / \left[2 + \frac{RT_s}{E_s} \frac{c_p T_s}{Q_f \xi^* e^{-\xi^*}} \right] \quad (8)$$

The denominator of the expressions for n and σ_p is identical and therefore, predicted dependencies will be similar. From thermochemical calculations, the rate of change of flame temperature with initial temperature (dT_f/dT_o) is approximately 0.6 for both AP and AN. For a nominal flame temperature of 1500 K and an activation energy of 15 Kcal/mole, the second term in the numerator gives a value of 0.002 1/K which, divided by the value of 2 in the denominator gives a contribution to the σ_p which is the correct order of magnitude for AP monopropellant (σ_p values are typically 0.001 to 0.002 1/K).

Comparison of Monopropellant Model with AP Data

Because of the apparent similarities between AP and AN, and because of the extensive previous work done with AP, it was decided to use AP as a basis of comparison for the monopropellant model. The key parameters that are required to make the calculation are tabulated in Table 4 with a comparison of the values used for both AP and AN. Some of the parameter values are not available from experimental data, and the rationale for selecting the specified value will be discussed in the discussion of the figures that follow.

Table 4 Model Thermochemical and Physical Parameters

	<u>AP</u>	<u>AN</u>
Density (gm/cc)	1.95	1.73
Melting Point (K)	865	443
Heat Capacity, (cal/gm)	0.30	0.30
Gas Thermal Conductivity (cal/cm sec K)	0.0003	0.0003
Condensed Phase Heat Release Coef.	0.20	0.26
Reference Flame Temperature (K)	1405	1247
Reference Surface Temperature (K)	950	530
Reference Burn Rate @ 68 atm (cm/sec)	0.81	0.19
Reaction Order	1.7	2.0
Flame Activation Energy (Kcal/mole)	15	25
Surface Activation Energy (Kcal/mole)	30	14

The burning rate and the burning rate temperature sensitivity, σ_p , have been calculated as a function of pressure and compared to Boggs' data for pressed pellets of AP^{47,48}. The calculated results are compared with the ambient temperature data in Figure 21, and the calculated values of σ_p are shown in Figure 22. Equation (8) of the model indicates that σ_p is very dependent on the gas phase activation energy. Activation energy values of 10, 15 and 20 Kcal/mole were used to calculate the results presented in Figure 22. The precise value of the activation energy does not have a significant effect of the calculated ambient burning rate due to the way that the reference burning rate is incorporated into the model. Within the scatter of the data, any of the three values would be reasonable. The value of 15 was used previously in the model⁴⁵ as this is the value determined experimentally by Pearson, et al⁴⁹, and it is also the value calculated by Guirao and Williams⁵⁰.

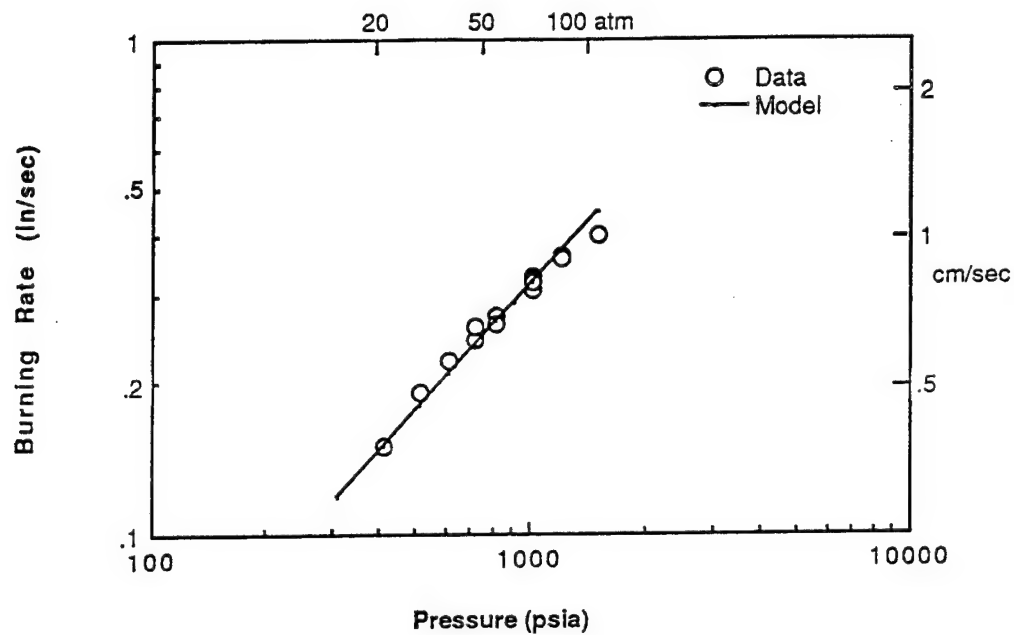


Figure 21. Comparison of AP burning rate data and model calculations for varying pressure.

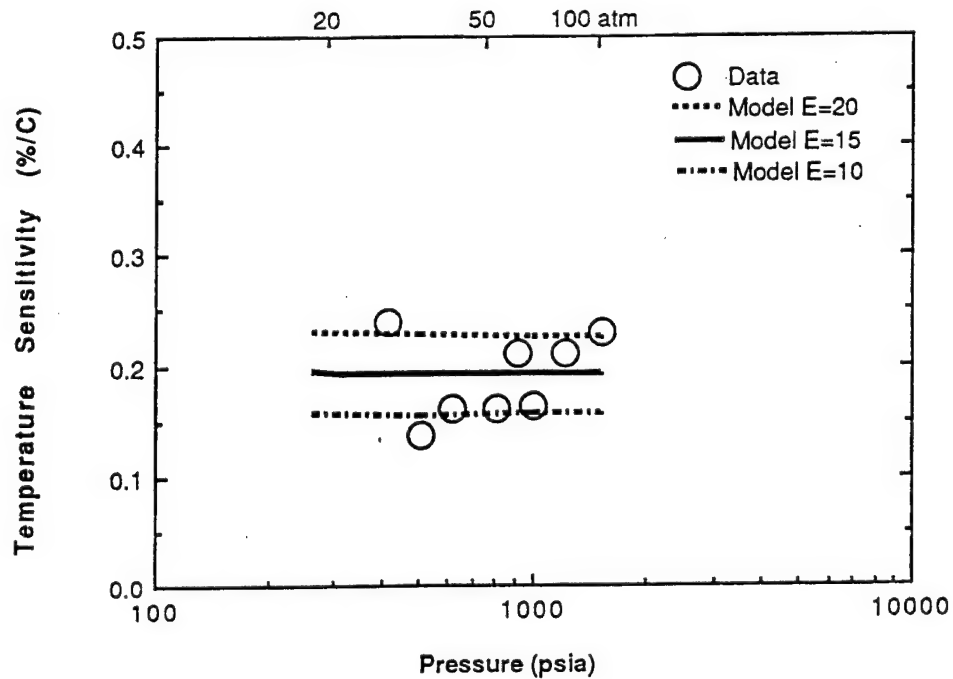


Figure 22. Calculated temperature sensitivity for AP monopropellant for varying flame activation energy.

Three sources of surface temperature data for AP were found in the literature and used for a basis of comparison. Three sources of linear pyrolysis hot plate data^{41,42,51} using burning pressed pellets of AP are compared with the extensive data of Powling⁴⁰ using an IR detector with AP composite propellants. These data are compared with the calculated surface temperatures of Beckstead and Hightower⁵² based on the cubic phase thickness of quenched single crystals of AP. Figure 23 shows the combined data plotted as log rate versus the reciprocal of the surface temperature, compared with the modeling calculations. There appears to be a consistent bias in the linear pyrolysis data relative to the IR detector data. The hot plate data consistently show higher surface temperatures. Variations in the surface activation energy indicate that a value between ~22 and 30 Kcal/mole would fit the data. The calculated surface temperature values from the Price, Boggs, Derr model^{47,48} have also been plotted for reference. Their calculations agree well with the surface temperatures of Beckstead and Hightower. It is also very apparent that most of the data were obtained at burning rates and surface temperatures well below those of normal interest. Again, within the scatter of the data, any of the calculated surface temperature curves would appear to be reasonable. The need for experimental surface temperature for rates above 0.1 cm/sec is also very apparent.

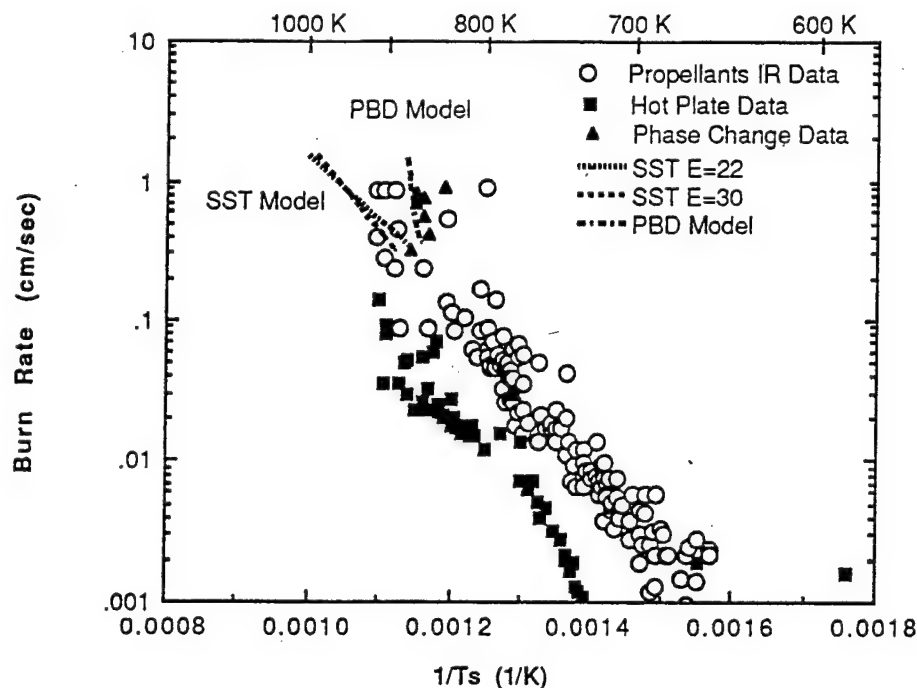


Figure 23. Comparison of AP surface temperature data and model calculations.

For both AP and HMX a significant amount of reaction apparently occurs in the melt layer (up to 75%)^{27,45,50}. The calculated heat release is shown in Figure 24. Although there are no experimental data for the heat release in AP, the calculated values are very comparable to measured values for double base propellants⁴³ and

HMX monopropellant^{53,54}: In the original BDP monopropellant calculations, values of -120 and -150 were used for consistency. The values calculated with the value of Q_c of 0.20 are in this same range and therefore, a value of Q_c equal to 0.20 was used in the model.

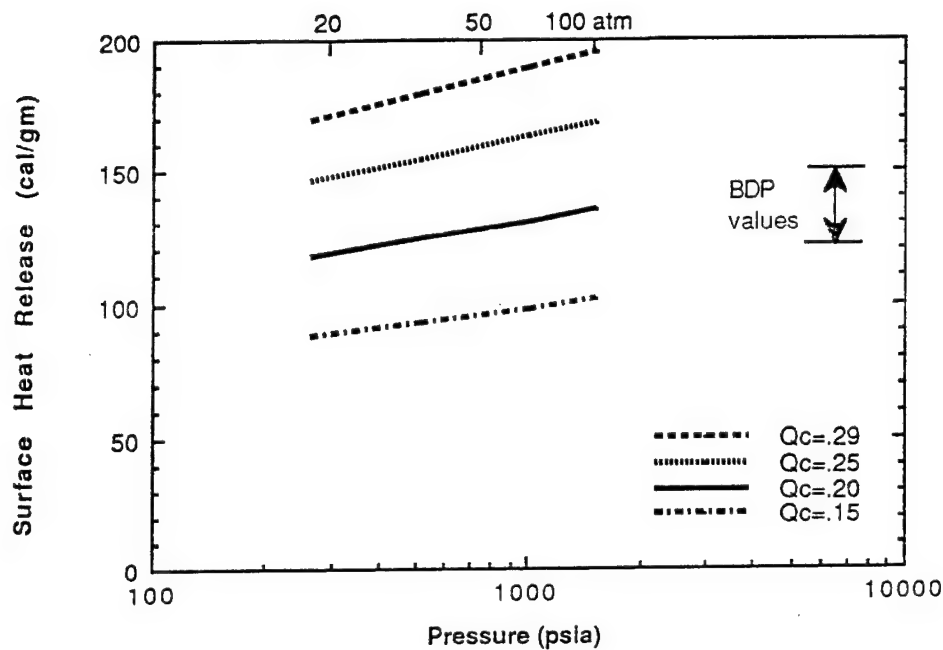


Figure 24. Calculated condensed phase heat release (values are exothermic).

Another variable of interest is the flame standoff distance. Figure 25 is a plot of the flame standoff distance calculated by the model. The flame distances are comparable to those calculated by other models. The calculated values for the original BDP model^{27,45}, from the Price, Boggs, Derr^{47,48} model and the Guirao and Williams model⁵⁰ have all been included for comparison. At low pressure there is a considerable discrepancy between the different calculations but at increasing pressures the BDP, SST and PBD models all come together. The flame standoff distance, Equation (6), is very dependent of the value of the thermal conductivity assumed. Guirao and Williams used a thermal conductivity of 0.0001 while a value of 0.0003 has been used in the BDP modeling. This factor of three accounts for most of the difference. In the Price, Boggs, Derr model a variable thermal conductivity value is used as they integrate through the flame. Their calculations would appear to be the most accurate. For the simplified model used here with a constant thermal conductivity, the standoff distances calculated appear to be reasonable. Again, it is unfortunate that there are no experimental data for comparison purposes.

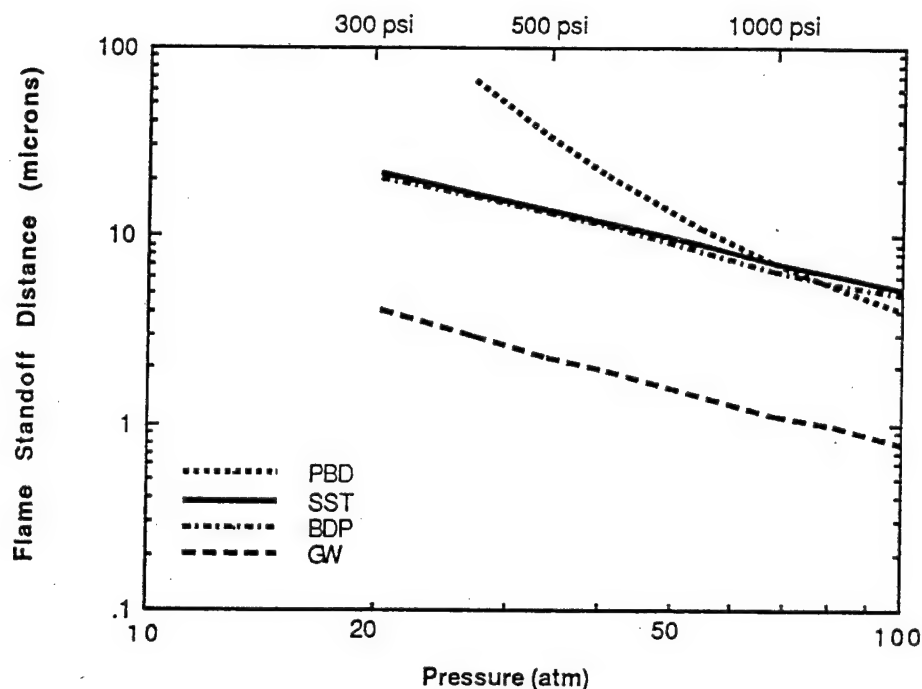


Figure 25. Calculated flame stand-off distance for AP monopropellant.

AN Monopropellant Calculations

Monopropellant parameters have been incorporated into the model to calculate the AN monopropellant burning (see Table 4). The burning rate has been calculated as a function of pressure and compared to Whittaker's data³⁸ for pressed pellets of AN containing up to 2.5% Cr_2O_3 . The calculated burn rates are compared in Figure 26, and the calculated values of σ_p are shown in Figure 27. Using the available physical properties for AN, the following combustion parameters (see Table 4) were selected: a reference burning rate of 0.19 cm/sec at 68 atm, a reference surface temperature of 530 K, reaction order of 2, E_s of 14 Kcal/mole, E_f of 25 Kcal/mole and a Q_c value of 0.26. The reference burning rate is used to calculate the flame kinetic prefactor at a given condition, thus ensuring that the model will calculate the correct burning rate at the reference condition. The burning rate exponent is influenced most by the selected reaction order. An order of 2 gives the observed pressure exponent of slightly less than one.

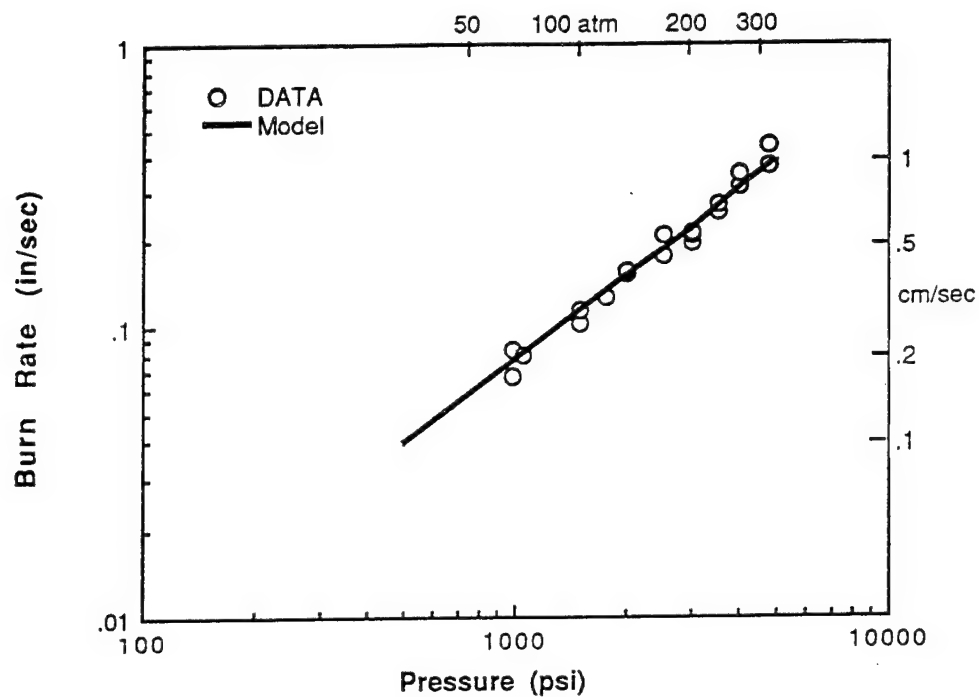


Figure 26. Comparison of AN burning rate data and model calculations for varying pressure.

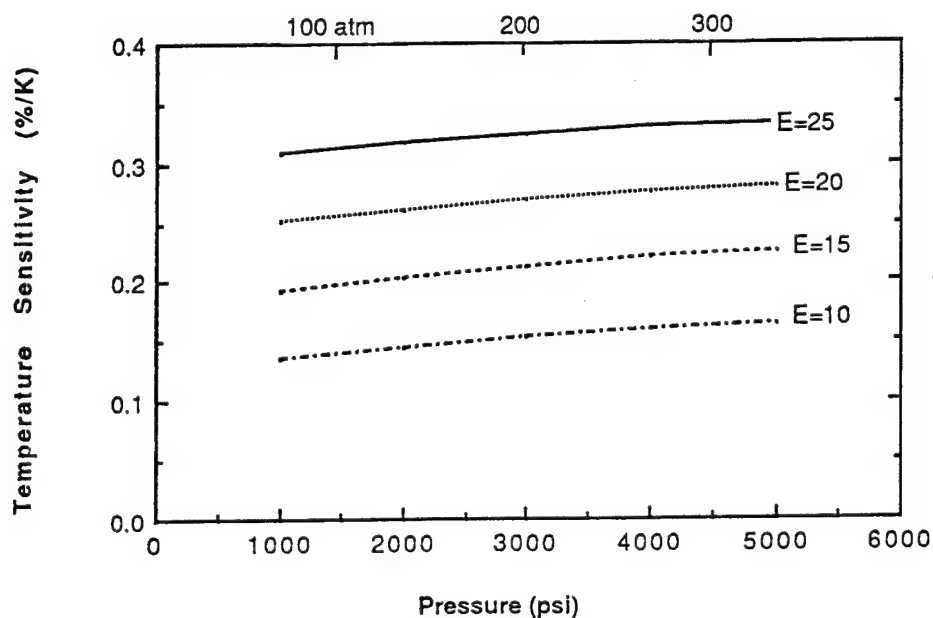


Figure 27. Calculated temperature sensitivity for AN monopropellant varying the flame activation energy.

Unfortunately there are no experimental data available on the burning rate temperature sensitivity, σ_p . The model indicates that the σ_p is very dependent on the gas phase activation energy. Four different values of activation energy were used to calculate the observed results in Figure 27. With the selected flame activation energy of 25 Kcal/mole, a σ_p of ~ 0.3 was calculated. The precise value of the activation energy does not have a significant effect of the calculated ambient burning rate due to the way that the reference burning rate is incorporated into the model. Although AP and HMX have σ_p values on the order of 0.16 and 0.2%/K respectively, it is anticipated that AN would have a relatively high σ_p due to its lower surface temperature and low burning rate (similar to double base propellants which have σ_p values of 0.2 to 0.5 %/K).

Figure 28 shows the combined surface temperature data^{37,38} for AN plotted as log rate versus the reciprocal of the surface temperature, compared with the modeling calculations. It is significant that the burn rate catalyst did not appear to have a significant influence on the surface decomposition characteristics. This seems to verify that the gas phase reaction is the controlling mechanism, and the surface decomposition simply accommodates the heat flux from the gas. Variations in the surface activation energy indicate that a value between ~ 10 and 15 Kcal/mole would fit the data approximately the same (the four curves correspond to activations energies of 11, 13, 14, and 15). The measured and calculated surface temperature varies between 500 and 600 K for the AN monopropellant. This puts AN in the same range of surface temperatures as double base propellants, but significantly below AP.

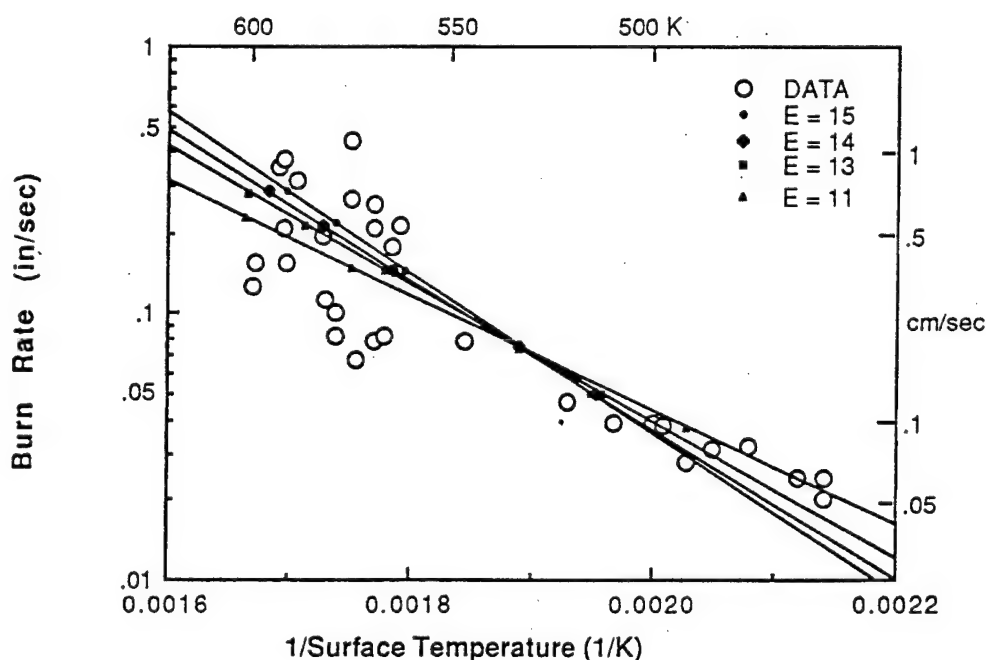


Figure 28. Comparison of AN burning rate data and model calculations for varying surface temperature.

AN is known to melt readily at 443 K. Due to such a low melting point, it is anticipated that there could be a significant amount of condensed phase reaction occur in the melt phase, similar to both AP and HMX. The calculated heat release is shown in Figure 29. Although there are no known experimental data for the heat release in AN, the calculated values are the same order of magnitude as measured values for double base propellants and HMX monopropellant. Also, the calculated values are very close to the heat of reaction calculated for reaction (3) in Table 3 of 83 cal/gm which corresponds to the reduction of nitrogen to NO in the condensed phase. At higher pressure and burning rate the calculated heat release approaches that of reaction (4) in Table (3), 109 cal/gm, corresponding to the reduction of nitrogen to N_2O . Therefore, the coefficient, Q_c , value of 0.29 was used in the modeling work.

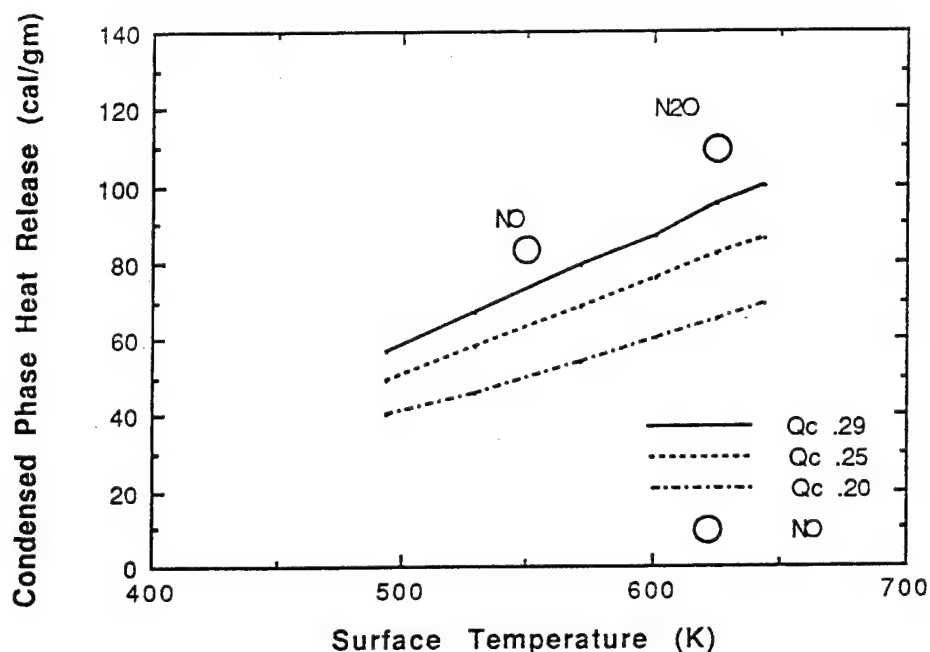


Figure 29. Calculated condensed phase heat release (values are exothermic).

Figure 30 is a plot of distance parameters calculated by the model. The melt layer thickness is calculated assuming an exponential temperature distribution in the condensed phase and an average thermal diffusivity of 1.6×10^{-3} for molten AN. The calculated thicknesses of 15 to 50 microns over the pressure range of interest are in general agreement with the observed window bomb movies of burning propellant³². The calculated flame stand-off distances of 25 to 250 microns are much larger than those values previously calculated for AP and HMX. This is due to the lower burning rate of AN (see Equation 8). The flame distances are comparable to those observed for double base propellants. Again, it is unfortunate that there are no experimental data for comparison purposes.

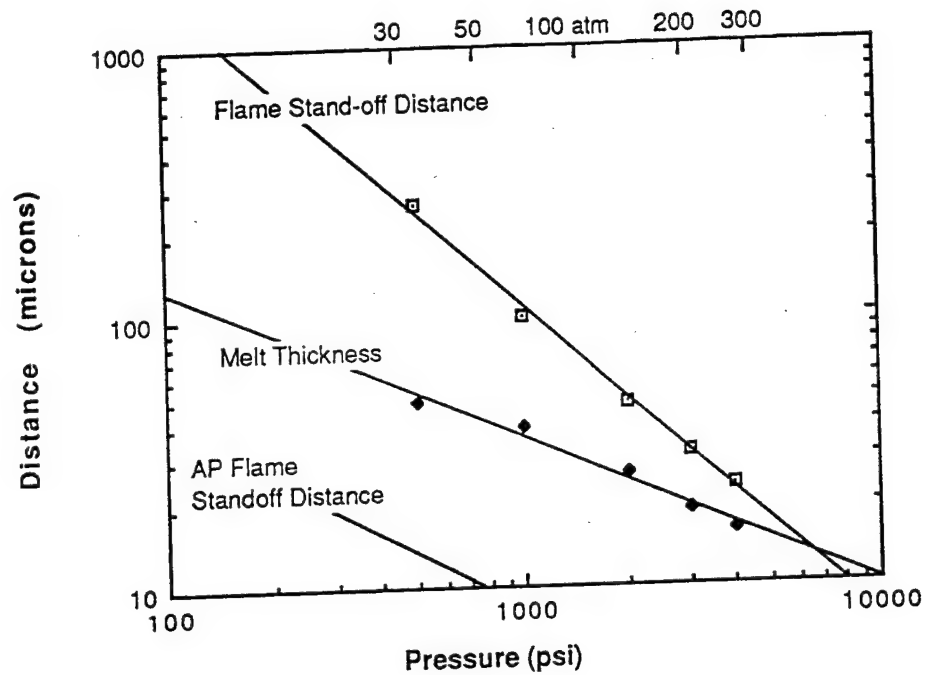


Figure 30. Calculated flame stand-off distance and melt thickness for AN monopropellant.

MODEL EQUATIONS FOR AP AND AN COMPOSITE PROPELLANTS

Surface Temperature Calculation

In the original BDP model, the surface temperature was averaged over the oxidizer as well as the binder. To generalize and improve the model the Beckstead SST model was developed with each separate oxidizer fraction having its own surface temperature and allowing the binder to have its own surface temperature. This approach generalizes the model so as to apply to propellants with very wide distributions of AP, and allows application to double-base propellants, aluminized propellants, and HMX-oxidized propellants.

The basis of the current model is the Beckstead SST (Separate Surface Temperature) model^{5,6,44,55}. The SST model is an adaptation of the original BDP model for composite propellants^{26,27}, but with two major modifications:

- 1) a separate energy balance is written for each ingredient category, resulting in a separate surface temperature calculation for each ingredient, and
- 2) the overall burning rate is calculated on a time averaged basis rather than the original BDP approach of using a space averaged approach.

These concepts have been discussed in detail in previous publications^{5,6,44,55} and only the basic equations will be repeated here.

An energy balance is written for each type and size of oxidizer ingredient. The resultant equation for the oxidizer surface temperature is

$$T_{\text{Soxij}} = T_o - \frac{Q_{\text{Li}}}{C_p} + \beta_{\text{Pij}} \beta_{\text{Fij}} (1 + 1/\Phi_{\text{ST}}) \frac{Q_{\text{PFI}}}{C_p} e^{-\xi^*_{\text{PFij}}} + \beta_{\text{Alj}} \frac{Q_{\text{Al}}}{C_p} e^{-\xi^*_{\text{Alj}}} + (1 - \beta_{\text{Fij}}) \frac{Q_{\text{MONOij}}}{C_p} e^{-\xi^*_{\text{MONOij}}} - \Delta T_{\text{loss}} \quad (9)$$

where the terms denoted PF refer to the primary flame and the terms denoted MONO refer to monopropellant flame. The various terms are all defined in the nomenclature. The j subscript represents different oxidizer fractions sizes, and i represents different oxidizer types (i.e. AP, HMX, AN or SN). It should be noted that the effect of a final flame does not appear explicitly in the equation, but appears indirectly through the ξ^*_{PF} and ξ^*_{MONO} terms which are discussed below.

Because of its relatively large distance from the surface, the final diffusion flame has a small effect on the surface temperature (at low pressures). Its principle influence is likely felt as an effective increase in the monopropellant flame temperature. Therefore, the energy feedback from the final flame was modified in the SST model to represent feedback from the final flame to the oxidizer flame (i.e., its influence is to raise the oxidizer adiabatic flame temperature). The mass of reactants in the final flame is determined from the residual oxidizer species in the monopropellant flame and from the residual fuel species coming from the primary flame. When AP and AN

burn, the combustion products are not fully oxidized and ~34% and 14% oxygen is produced from the monopropellant flame. This is available for further reaction with the fuel in the final diffusion flame. The fraction of the oxidizer flow available for final reaction is denoted as β_{AP} and has the values of 0.34 for AP, 0.14 for AN, and 0.0 for HMX. The oxidizer will react with the stoichiometric amount of fuel from the binder decomposition products. Thus, the expression for the effective oxidizer flame energy becomes:

$$\dot{Q}_{APij} = (\dot{Q}_{AP})_{adj} + \beta_{APij} (1 + 1/\Phi_{ST}) \dot{Q}_{FFij} e^{-\xi_{FFij}^* - \xi_{AP}^*} \quad (10)$$

where $-\xi_{FFij}^* - \xi_{AP}^*$ is the nondimensional distance between the two flames. This term has a minor effect on the overall burn rate of propellants at low pressures, but has an increasing effect above 1000 psi.

The equation for the surface temperature of the binder is developed in a manner analogous to the oxidizer surface temperature^{5,6,55}

$$\begin{aligned} T_{sf} = T_o - \frac{Q_{fuel}}{c_p} + \sum_{ij} (1 - \beta_{Pij}) \beta_{Fij} S_{fij} (1 + \Phi_{ST}) \frac{Q_{PFI}}{c_p} e^{-\xi_{PFI}^*} \\ + \beta_{DB} \frac{Q_{DB}}{c_p} e^{-\xi_{DB}^*} - \frac{m_{AI}}{m_f S_f} \frac{Q_{LM}}{c_p} + \sum_{ij} \frac{m_{AIij}}{m_f S_f} \frac{Q_{AI}}{c_p} e^{-\xi_{AIij}^*} \end{aligned} \quad (11)$$

For a composite propellant the energy feedback from the double base binder flame is zero and the equation reduces to:

$$\begin{aligned} T_{sf} = T_o - \frac{Q_{fuel}}{c_p} + \sum_{ij} (1 - \beta_{Pij}) \beta_{Fij} S_{fij} (1 + \Phi_{ST}) \frac{Q_{PFI}}{c_p} e^{-\xi_{PFI}^*} \\ - \frac{m_{AI}}{m_f S_f} \frac{Q_{LM}}{c_p} + \sum_{ij} \frac{m_{AIij}}{m_f S_f} \frac{Q_{AI}}{c_p} e^{-\xi_{AIij}^*} + \sum \Delta T_{lossij} \end{aligned} \quad (12)$$

Equations (9) and (12) are the backbone of the model and determine the surface temperature of each ingredient. Once the surface temperatures of the various ingredients are determined, the mass burning rate of each ingredient, oxidizers and binder, is calculated from a zero-order Arrhenius expression (see Equation (1)).

$$m_i = A_i e^{(-E_i/RT_{si})} \quad (13)$$

The overall propellant burn rate is calculated from the individual mass burning rates, appropriately weighted. Other aspects of the model and approaches for weighting the individual rates are summarized in the following sections.

The surface temperature equations are based on the assumption of steady state conditions. However, for very small particles, it is very unlikely that a true steady state condition is achieved. Figure 7 of Volume III of reference 44 compares the rates of monomodal propellants to the characteristic thermal wave thickness relative to the binder thickness between particles. In general, for particles greater than 20 to 50 μ , the binder will achieve a steady thermal profile. For smaller particles (depending on the overall rate) the binder will be preheated to 75% of its surface temperature. This represents a significant heat loss from the small particles to the binder. Based on a steady thermal profile in the oxidizer as it burns into binder, the loss is (in degrees of temperature).

$$\Delta T_{\text{loss}} = \frac{C_{pb}}{C_{pox}} (T_{sox} - T_o) \frac{m_b}{m_{ox}} e^{-\frac{\Delta r_{ox}}{\alpha_t}} \quad (14)$$

For particles above 50 μ this heat loss will be very small, but for fine particles, the loss can reach several hundred degrees resulting in a very reduced rate. It is felt that this mechanism is very significant in interpreting self extinguishing phenomena⁵⁶ and the so called "ledge" mechanism discussed in Reference 44 where burning rate can actually decrease with decreasing particle size rather than increase.

The flame standoff distances that are needed in Equations (9) and (11) are calculated as in the BDP and SST models, i.e.

$$\xi_{PF}^* = C_p m_T (x_{PD}^* + x_{PF}^*) / \lambda \quad (15)$$

for the primary flame, and

$$\xi_{MONO}^* = (C_p m_{ox} / \lambda) x_{MONO}^* \quad (16)$$

for the monopropellant flame (see also Equations (4) and (6)).

Rate Averaging Basis

In the BDP approach the local rate is taken as the oxidizer rate, averaged over time, which requires that the overall propellant stoichiometry be maintained. Condon, Glick, and King define the local rate as the rate of a "pseudo propellant" rather than the oxidizer rate as in the original BDP approach. King¹⁴ has recognized what he calls the "end game" problem in determining a time averaged local rate. That is, one must account for left over binder after an oxidizer crystal burns out. In the BDP approach this problem was recognized but avoided by requiring that the overall stoichiometry be maintained. This constraint was assumed to be valid because oxidizer effects dominate the burn rate of AP-composite propellants; the binder having a secondary influence.

The average propellant burning rate is a summation of local rates. However, the binder rate is radically different from the oxidizer rate (see Figure 18). This

difference seriously effects if not invalidates the typical averaging process. If a time integration is performed using the space averaged rate, it is discovered that the oxidizer will invariably burn out before the binder does, leaving residual binder. Accurate modeling requires an accounting of that residual binder and its influence on the overall rate. To date all models other than the SST model have ignored this.

The conventional averaging process depends on two critical assumptions:

1. the local rate is the rate of a pseudo propellant including oxidizer and binder;
2. the oxidizer dominates the overall propellant rate.

If either of these assumptions are not satisfied when the conventional approach breaks down. Based on the results of Beckstead^{13,26} and Condon^{20,25}, it appears that these assumptions are reasonable for a large number of AP/HTPB propellants. However, they obviously do not apply to double base propellants or HMX/composite propellants. Also based on the results summarized in Reference 44, it appears that the assumptions fail for aluminized propellants and for propellants with very wide oxidizer distributions. In other words, it appears that wherever the rate of the binder has a significant influence on the propellant rate, the conventional assumptions will fail.

In the SST model^{5,6} the equation for the average pseudo propellant burn rate is of the form

$$\bar{r}_i = \frac{\sum \text{distances}}{\sum \text{times}} = \frac{\sum \text{distances}}{\sum (\text{distances/rates} + \text{delay times})} \quad (17)$$

The summations for distances and times are performed over the burning path, and therefore, relate to characteristic oxidizer and binder dimensions. This allows the binder to have a significant influence on the rate. Instead of a single local rate, both oxidizer and binder rates are accounted for. Also, for each burning time associated with a given dimension, there is an associated transient time. In the past these delays or transient times have often been neglected. If they are neglected, the time averaging approach can be similar to surface averaging. If the delay times are properly included the results are dramatically different.

The ignition delay time is the time it takes an oxidizer crystal to ignite, assuming that the ignition process starts when a crystal first becomes exposed to the burning surface. As the burning surface sweeps over the crystal, heat is fed to the crystal, which heats up, begins decomposing, and finally ignites. The time required for this process to occur is the ignition delay time. It has been included in previous models based on an empirical data correlation. An improved correlation that is now being used has been developed and reported in previous reports⁵⁵.

The delay time associated with the binder is a binder burn through time. It is related to King's "end game", attempting to account for unburned binder. After a crystal burns out, a pocket of binder remains and must be consumed by pyrolysis, sluffing, or some other mechanism. An approach to describing this phenomenon is discussed later.

In a burning propellant, as the surface approaches a particle of AP or AN, the particle will be heated to a temperature characteristic of the binder pyrolysis rate (i.e. the medium in which it is immersed). Thus, when the particle is exposed to the propellant burning surface, its surface temperature will be that of the binder, not that of a steady burning particle. Because both AP and AN have different surface temperatures than HTPB at a given rate, when they are first exposed to the surface they may not ignite immediately. Each particle will be exposed to the surface conditions, heat up enough to reach ignition, ignite, go through a short transient time, and ultimately reach a steady state burning rate, dependent on the surroundings. The SST model attempts to account for the discrepancies in surface temperature and the associated transient ignition heatup and delay times. The SST equation for the overall propellant burning rate is

$$\bar{r} = \frac{\sum_i N_i D_i' (1 + 2\delta_i)}{\sum_i N_i D_i' \left[\frac{1}{r_{oxi}} + \frac{t_{igni}}{D_i'} + \frac{2\delta_i}{r_b} + \frac{t_{bi}}{D_i'} \right]} \quad (18)$$

where:

- N_i = number of ith oxidizer crystals per unit length
- D_i = statistical intersection diameter of ith oxidizer size
- δ_i = distance from oxidizer to center of adjacent binder
- t_{igni} = ignition delay time of ith oxidizer size
- t_{bi} = binder burnthrough time of ith oxidizer size
- r_{oxi} = rate of ith oxidizer
- r_b = binder rate

The four terms in the denominator represent, respectively, 1) the time to burn through an oxidizer particle, 2) the ignition delay time (or transient heatup time) of the corresponding oxidizer particle, 3) the time associated with burning the binder associated with the oxidizer particle and 4) the transient time associated with burning through any remaining unburned binder.

Multimodal and Mixed Oxidizer Propellants

A significant problem in modeling multimodal and mixed oxidizer propellants is accounting for the effects and influences caused by the fact that different sizes and types of particles can and do have significantly different burn rates (i.e. interaction effects-the particles do not burn independently). What undoubtedly happens is that finer particles along the periphery of a coarse particle burn faster than the coarse particle. The net result is that the overall propellant rate is much closer to the rate of the pseudopropellant corresponding to the fines rather than that of the coarse. The same thing can happen when two components with significantly differing rates burn near each other. This can be visualized in two ways. Either the faster burning components are igniting the slower burning particles all along their periphery, eliminating the normal ignition delay time and coupling with their burn rate, or the

slower burning particles can be visualized as being undercut by the faster burning components which "short circuit" the effect of the slower burning particle. The problem is, how to model this coupling process.

Within the computer program the rates of individual size fractions are monitored relative to the rate of the finest fraction (assumed to have the highest rate). In this manner the fraction of the coarser oxidizer sizes that is effectively contributing to the overall rate is calculated as

$$fr_{oxi} = \frac{\pi \frac{D_{oi}}{2 \bar{r}_{smallest}}}{\frac{D_{oi}}{r_{oxi}} + t_{igni}} \quad (19)$$

The fraction of oxidizer term multiplies the $1/r_{ox}$ term in Equation (18) when HMX is the oxidizer in a double base propellant, and multiplies the $1/r_{ox}$ and t_{ign} terms for the coarse fractions of multimodal propellants as discussed below. Equation (19) accounts for the interaction influence between particles of drastically differing sizes. To allow for the potential interaction of different types of oxidizers, the computer program has been set up to allow the AP to have precedence over the other oxidizers.

Oxidizer Ignition Delay Time

In most models, varying the ignition delay time parameters has little effect on the net burning rate due to the way the term enters into the S_{ox} calculation. A fundamental approach was developed as part of the SST model to calculate the ignition delay time of a crystal in a propellant. A linear regression analysis of Shannon's data⁵⁷ for AP was performed and the ignition delay time has been calculated from the following equation⁵⁵

$$t_{ign} = C_{ign} \frac{D_o^{1.7}}{r} \quad (20)$$

Equation (20) has been programmed into the computer program and is being used for all oxidizer calculations.

The ignition delay time associated with AN is not clear because of the melting characteristics of AN. Under normal conditions AN melts at 443 K. In a combustion environment window bomb photography shows AN melting on the surface of burning propellants. Thus, the AN particles may start to lose their individual size and shape characteristics. Very small particles may melt in their entirety, particularly at low pressures or for low burning rate propellants. Large particles may maintain their integrity and burn with the thin molten layer on their surface. It is not clear that for the times associated with combustion, whether the molten AN is able to move enough in a lateral direction to mix with the surrounding binder significantly. Window bomb photography³² indicates that the lateral flow of molten AN may occur. The general

melting characteristics of AN would prohibit AN crystals from protruding above the surface and would thus reduce the effects of an ignition delay concept. Because of these reasons the coefficient on the ignition delay time was reduced by a factor of four below that used for AP⁵⁴.

Binder Burnthrough Time

In wide distribution propellants the binder is distributed disproportionately so that the fines are very fuel rich and the coarse is oxidizer rich. The fines, being surrounded in their 'sea of binder', are thermally insulated from the rest of the propellant. The binder absorbs heat from the fines, reducing their rate. When they burn, they do so quickly and leave large amounts of binder, which pyrolyzes slowly, thus impeding the overall rate. As the percentage of fines increases or the size decreases, this problem is compounded, leaving more binder unburned and magnifying the impeding effect. If the size of the fines is increased or the percentage reduced, the propellant will burn more efficiently and the rate will be more predictable.

Oxidizers that are not rich in oxygen, such as HMX or AN, will undergo a similar phenomenon. If the oxidizer cannot consume all, or a large majority of the binder surrounding an individual crystal, then the remaining binder must somehow pyrolyze without the aid of an oxidizing species.

This concept shows up in the model in two ways: (1) the loss of energy from the oxidizer to the binder (ΔT_{loss} term in the surface temperature equations), and (2) the binder burnthrough time. The time for binder to cook off (after a crystal has burned past it) should be related to the thickness of the heated binder. If the thermal wave penetrates deeper than the interparticle distance, (as is the case for small particles) the preheated binder will be more prone to pyrolyze. The burnthrough time should also be proportional to the thermal response time of the binder (α_t/r_b^2). Thus, if the response time is short (i.e. if the binder can conduct heat more rapidly than it burns away), then the burnthrough time ought to be short also. The equation for the binder burnthrough time in the SST model was taken as

$$t_b = \frac{\alpha_t}{r_b^2} \left(\frac{298}{T_o} \right) \left(\frac{F}{O} \right) \quad (21)$$

Where O/F is the oxidizer to fuel ratio, α_t is the thermal diffusivity and r_b is the binder rate. The binder rate in the denominator causes the term to be significant for propellants that burn slowly or that have an inherently slow binder rate such as AN propellants.

Calculated Diffusion Flame Heights

The classic work in this area is the Burke-Schumann analysis²⁸ published in 1928. Virtually all subsequent work is either based on the Burke-Schumann analysis or at least references that work extensively. The Burke-Schumann equation was

programmed and used to calculate the diffusion flame standoff distance for many of the Series III propellants⁴⁴. Up to fifty terms had to be used in the summation to obtain flame profile calculations for some of the propellants. Flame profiles for several propellants were reported previously⁴⁴.

The most significant results of that previous study are summarized as follows:

(1) The prevailing concept of the primary flame always closing over the oxidizer crystal is apparently incorrect. Only the finest oxidizer size fraction will do so. The flame shape for coarser fractions within a propellant will close over the binder rather than the oxidizer.

(2) The flame heights are virtually independent of burn rate for the range of conditions covering most propellants. This observation can be a great aid in modeling. It infers that a simpler mathematical solution can be applied (rather than a complete flame analysis), which reduces the complexity of the flame height calculation significantly.

(3) Flame heights (or diffusional distances) of the oxidizer rich flames over the binder can be very small relative to the oxidizer size. If the kinetics also lead to narrow reaction zones, this could be interpreted as a surface reaction relative to the binder with little or no heat feed back to the oxidizer.

As part of the SST model a correlation was developed to predict flame heights, x^* , instead of using a lengthy computer program to compute the heights each time they are needed within the burning rate model. A general correlation for the diffusional flame height as a function of the propellant properties can be expressed as

$$\frac{x^*}{b} = \left(\frac{\gamma_{st}}{a_1} \right)^{a_2} \left(\frac{\alpha_{fi}}{\alpha_{oxi}} \right)^{a_3} \quad (22)$$

where

over the binder

$$a_1 = 0.834$$

$$a_2 = 0.858$$

$$a_3 = 1.871$$

over the oxidizer

$$a_1 = 0.472$$

$$a_2 = 0.929$$

$$a_3 = 1.604$$

This expression gives a single continuous expression for diffusional distances. An arbitrary multiplier, AFH, is included in the computer program to allow for uncertainties between the diffusional calculations and the primary flame calculations. The multiplier is normally set equal to 3.0. This expression has been programmed and is part of the computer model.

Competing Flames

From the general discussion of the model and the primary flame it is apparent that there is a range of pressures where the monopropellant flame and the primary flame are competing for the reactive oxidizer specie. Mathematically this is accounted for by the term β_F in the surface energy balances Equations (9) and (11), where β_F is the fraction of the oxidizing reactants that react in the primary flame. At low pressures

and/or for small particle sizes, β_F is unity. In other words, the combined primary flame mixing and reacting distances are less than the monopropellant flame height, and therefore all of the oxidizing species react directly with the binder products rather than with themselves in the monopropellant flame. As pressure and burning rate increase, the monopropellant flame height is reduced and the primary flame reactive distance is reduced, but the primary diffusive distance is essentially held constant. Thus, near the center of the crystal where the diffusive distance is greatest, the oxidizing species react preferentially in the monopropellant flame, and β_F is between zero and one. At higher pressure, the monopropellant flame standoff becomes very small as does the primary flame reacting distance. Under these conditions only a fraction of the original oxidizing species react with the binder products in the primary flame near the binder-oxidizer interface, and β_F approaches a small number. These effects are illustrated in Figure 31.

The β_F term plays a dominant role in determining burn rates. The primary flame is a high energy flame and can force the propellant burn rate much higher than the low energy monopropellant flame. To determine β_F , the ideal situation would be to calculate (or measure) the actual fraction of the oxidizer species that react in the primary flame versus the total available. This would require the accurate solution of the diffusion equations in conjunction with the monopropellant flame equations. Unfortunately a rigorous approach to do this was considered beyond the scope of the original program. In retrospect it might have been practical to attempt such a solution. The characteristics of the β_F calculation are very dominant within the model in determining the burning rate dependence on pressure and particle size.

For flames closing over the binder, β_F is the fraction of oxidizer reacting in the primary flame relative to the total oxidizer available. The amount of oxidizer reacting in the primary flame is proportional to the stoichiometric ratio, and the total oxidizer available is proportional to the local O/F ratio. The ratio of $\phi_{ST}/O/F$ was used in the definition of β_F to incorporate this proportionality.

The final equation to calculate β_F is

$$\beta_F = \frac{\dot{x}_{AP}}{\dot{x}_{PD} + \dot{x}_{PF}} \frac{\phi_{ST}}{O/F} \quad (23)$$

The determination of \dot{x}_{PD} from Equation 22, assumes that all the oxidizer is available for reaction in the diffusion flame. Once the monopropellant flame becomes active, it robs oxidizing species from the primary flame and a reduced amount of oxidizer is then available. Actually the effective amount available is the total oxidizing species multiplied by β_F . Therefore, within the model an effective O/F ratio is calculated by multiplying β_F times the overall O/F for each oxidizer fraction. Thus, the

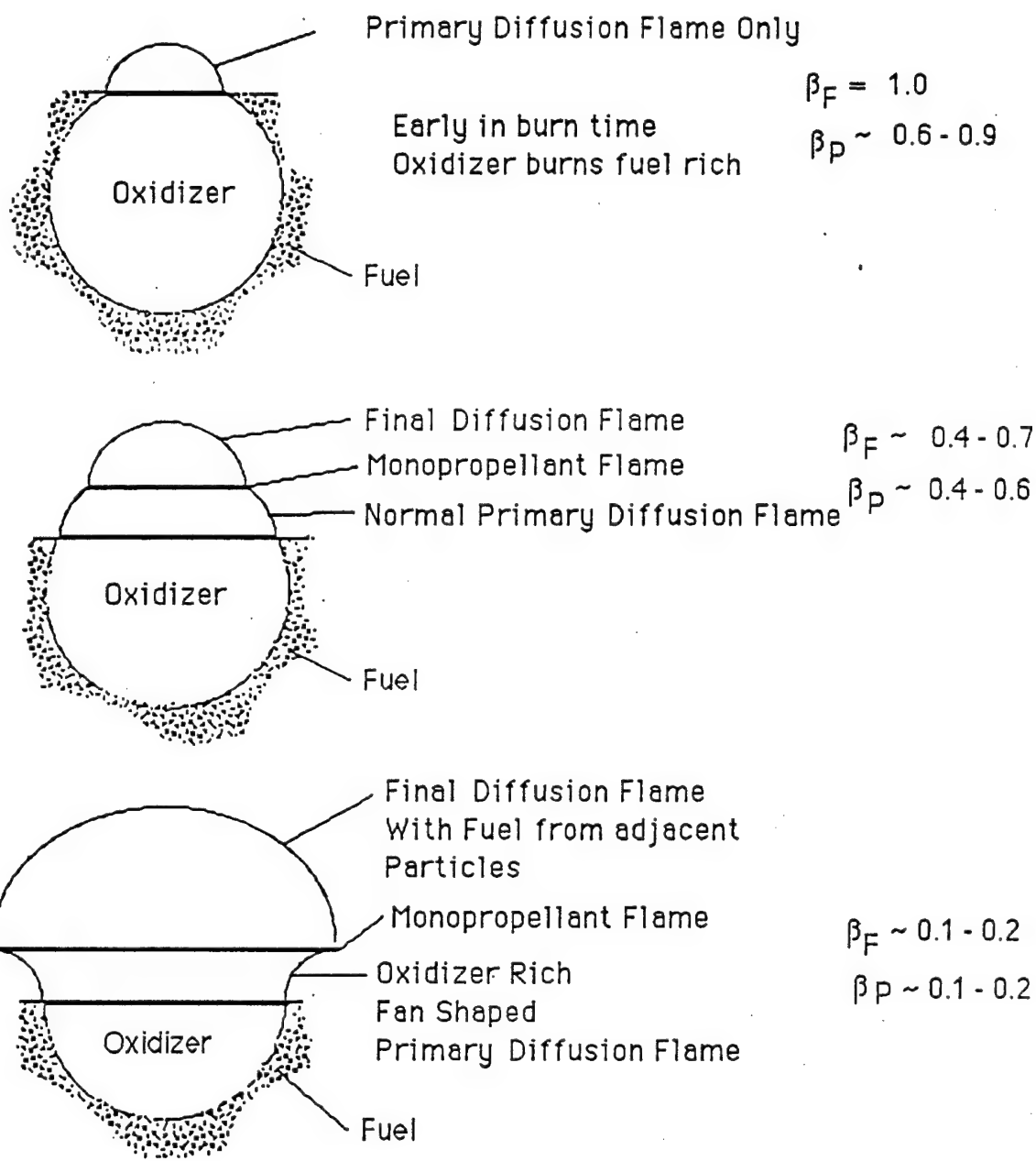


Figure 31. Different flame configurations that can occur during the burning time of an individual particle. Approximate values of β_F and β_P that correspond to the flame structure are noted.

calculation of x_{PD}^* and β_F is an iterative process. The calculation modifies the effective geometry that is used in the calculations, leading to smaller effective diffusion distances as β_F decreases. This is logical and should have been incorporated in the original BDP model. As the monopropellant burns oxidizing species, those gases are not available for reaction in the primary flame. Those gases that are left, are only over the outer part of the oxidizer crystal, and thus have a shorter diffusion path to reach the binder species. Therefore, the actual diffusion distance is dependent on β_F and on the amount of oxidizer reacting in the monopropellant flame. Incorporating this approach into the x_{PD}^* determination leads to an effective diffusion distance which was used in the model.

Heat Transfer from The Primary Flame

Once the amount of oxidizer that participates in the primary flame is determined, then the amount of the heat that is transferred to the oxidizer versus the amount transferred to the binder must be determined. This effect is accounted for by the term β_P in Equations (9) and (11), where β_P is the fraction of heat transferred from the primary flame to the oxidizer. When a particle initially ignites and the flame closes over the oxidizer, as shown in Figure 31, the value of β_P should be greater than 0.5, but less than 1.0. As the particle burns back an increasing amount of the heat will be transferred to the binder, particularly when the flame closes over the binder rather than the oxidizer. During this time the value of β_P should be relatively small (but greater than 0.0). This is obviously a transient effect that is not accounted for within the framework of the assumptions leading to Equations (9) and (11). This general effect has been addressed previously^{58,59}, but a quantitative description of the transient heat transfer is beyond the scope of the current project. Thus an integrated, average value of β_P was estimated in a purely empirical manner. A functional form, based on a hyperbolic tangent, was programmed into the code that would typically be ~ 0.5 and would never exceed one nor fall below zero.

Effect of Catalysts

Modeling the effects of catalysts is another difficult area. Previous efforts in this area by Beckstead and Cohen,⁶⁰ Burnside⁶¹, Beckstead⁶, and Condon and Glick⁶² have been limited. Burnside did little modeling but did get valuable experimental data on catalysis. He concluded that the burn rate augmentation due to Fe_2O_3 is related to the specific surface of the catalyst, pressure and AP specific surface. Mechanistically, he postulates that the catalyzed reaction is promoted by adsorption of reactive species on the heterogeneous catalyst. Flanigan's work⁶³ on catalytic mechanisms, also supports these ideas. In a series of definitive small-scale studies, Flanigan and co-workers⁶³ produced a detailed description of the Fe_2O_3 catalytic process. Similar studies by Musso⁶⁴ support these conclusions. In these studies, it was clearly shown that the Fe_2O_3 catalyzes decomposition of a vapor phase decomposition product of ammonium perchlorate. Since the final flame is too far removed to influence rate and AP flame is geometrically inaccessible to the Fe_2O_3 , the most logical position for the catalyst reaction is in the primary diffusion flame. This basic assumption has been carried over to apply to the catalysis of AN propellants.

The model has been modified to introduce catalytic rate augmentation by the heterogeneous mechanism in the primary flame reaction. The net rate is assumed to be the sum of the normal rate plus a catalytic effect. The equation for the catalyzed rate is assumed to have the form of a general heterogeneous reaction.

$$r_{cat} = \frac{C_{cat}}{A_1 + C_{cat}} A_{cat} e^{-E_{cat}/RT_{PF}} P_{cat}^{\delta_{cat}} \quad (24)$$

C_{cat} = catalyst concentration x specific surface area
 A_1 = specific surface dependent constant
 A_{cat} = prefactor for catalytic reaction
 E_{cat} = activation energy for catalytic reaction
 δ_{cat} = reaction order of catalytic reaction
 T_{PF} = temperature of primary flame

To evaluate the effectiveness of this format, a reaction order of 1 was assumed to simulate adsorption ($\delta_{cat} = -1$ would correspond to desorption, $\delta_{cat} = 0$ would correspond to surface reaction); E_{cat} was taken to be the same as the basic primary flame reaction; and A_{cat} was taken as some number much greater than A_{PF} , the primary flame frequency factor. The prefactor ratio (A_{cat}/A_{PF}) was adjusted to give rates in the right order of magnitude. C_{cat} was taken as the weight fraction of catalyst times the specific surface area of the catalyst (meter²/gm). The constant A_1 was selected to give an asymptotic rate at ~5 percent catalyst. The net reaction rate for the catalyzed primary flame becomes

$$rate_{PF} \sim A_{PFE} e^{-E_{PF}/RT_{PF}} P_{PF}^{\delta_{PF}} \left[1 + \frac{C_{cat}}{A_1 + C_{cat}} \frac{A_{cat}}{A_{PF}} \frac{1}{P_{PF}^{\delta_{PF}-1}} \right] \quad (25)$$

Using this equation, rates were calculated with the SST model⁶ for the 1 percent Fe₂O₃ propellants from Miller's Series VI propellants⁴⁴. The calculated rates compared reasonably well to the experimental data. Based on this general approach the same equations have been applied to the AN propellants that are being modeled as part of this program.

AP COMPOSITE PROPELLANT RESULTS

The primary objective of the modeling effort was to model AN based composite propellants with mixed oxidizers. The separate surface temperature and the time averaging approaches were used to accommodate the description of several oxidizers within the same model. As has been outlined above, the model is designed to accommodate AP, HMX, AN, and SN in any combination. Because of the very extensive data base of AP propellants, the approach used was to evaluate the model by comparing the calculated results for AP propellants varying composition, pressure, particle size, etc, with known data. For a given propellant, or family of propellants, the various parts of the model can then be examined individually to determine their influence on the overall rate within the given formulation or test variables. Optimization of the unknown model parameters is then performed to try to match the experimental behavior. The various combustion properties such as surface temperatures, flame standoff distances, fraction of binder reacting, etc. are all monitored. If unrealistic values are calculated, then the source of the discrepancy is traced within the model. That particular part of the model is then explored to determine what must be done to produce more realistic calculations.

The data of Miller, et al⁴⁴ for non-metallized AP/HTPB propellants was used as the comparative data base, because of the large number of propellants with the same consistent binder and a wide range of compositions, pressure, particle size, and initial temperatures. The data used were from the Series III and Series XI non-metallized propellants⁴⁴. The available data consist of 19 propellants from the Series III and 17 propellants from the Series XI. These propellant families covered a range of compositions from monomodal, to tetramodal, from 77% to 87.37% AP, and from 0.7 to 400 micron AP. Test data were used for 500, 1000, and 2000 psi (3.4, 6.8, 13.6 MPa). Eleven of the Series III propellants also had temperature sensitivity data. A total of 151 datum points were used in the overall parameter optimization. Based on this comparison procedure, model parameters such as the primary flame prefactor, the coefficient in the primary flame standoff distance, the coefficient in the expression for β_p or β_F , etc., were optimized to provide the best fit of the model to the data base. After optimization 47% of the calculated points were within 10% of the experimental data and 74% were within 20%, with a correlation coefficient of 0.92.

With the optimized parameters the model was compared directly with the Series III data at 1000 psi (6.8 MPa) and the results are shown in Figure 32. The agreement is very reasonable with only a few of the widest distribution propellants falling outside of the 10% predictive goal. Datum points lying outside of 10% bounds have been labeled with their identification number.

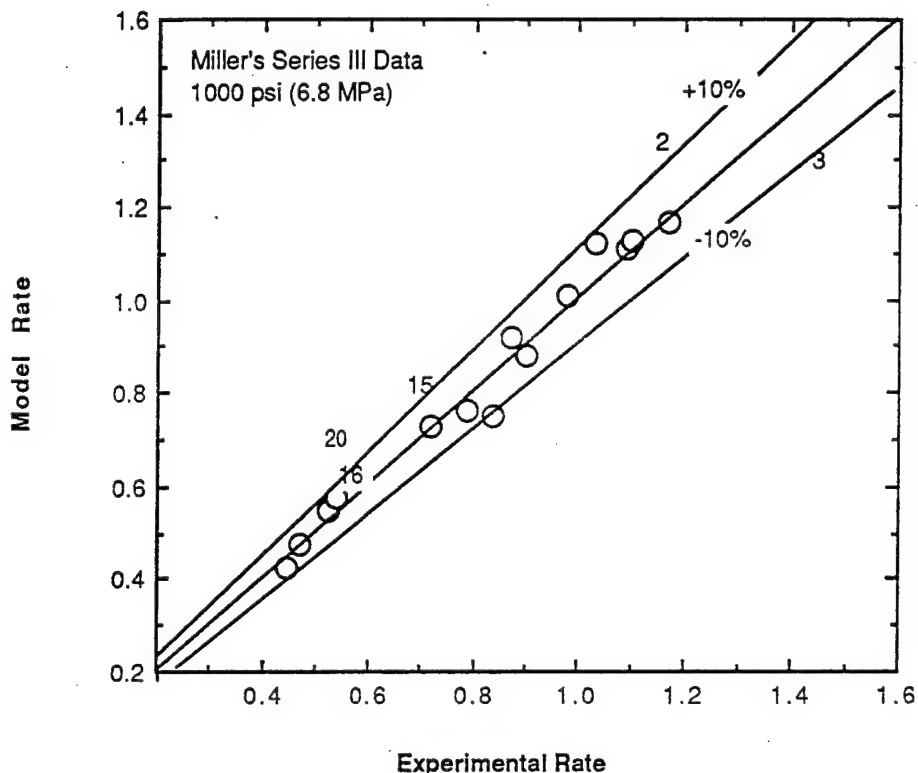


Figure 32. A comparison of calculated and experimental burning rates for Miller's Series III propellants at 1000 psi (6.8 MPa). Datum points lying outside of +10% have been labeled with their identification number.

The correct prediction of the pressure exponent is a significant challenge in modeling. The pressure dependence is caused by two main factors: (1) the reaction order of the primary flame, and (2) the relationship between the primary flame and the monopropellant flame. A second order primary flame reaction was assumed, as a second order gas phase reaction seems most consistent with high temperature, gas phase kinetics. The second factor contributing to pressure dependence is much more difficult to evaluate. The relationship between the primary diffusion flame and the premixed monopropellant flame is very complex. Within the model this interaction enters into the equations through two terms, β_F and β_P . β_F represents the fraction of the oxidizer decomposition products that react in the primary diffusion flame. The β_P term represents the fraction of energy fed back from the primary flame to the oxidizer. The exact nature of these terms and how they vary with propellant composition and test variables is an area that is not well understood, but still needs extensive study in the future.

The pressure exponent calculations are compared with the Series III data at 1000 psi (6.8 MPa) in Figure 33. In the calculations that were made the pressure

exponent was consistently low for all of the propellants. For most of the propellants simulated, the pressure exponent was within 20% of the measured values, but several datum points, particularly for the propellants containing 400 μ AP were more than 20% in error. The very wide distribution propellants containing 400 μ AP have been particularly difficult to model in the past also^{7,8,13,17}, due to the extreme variation in the particle sizes.

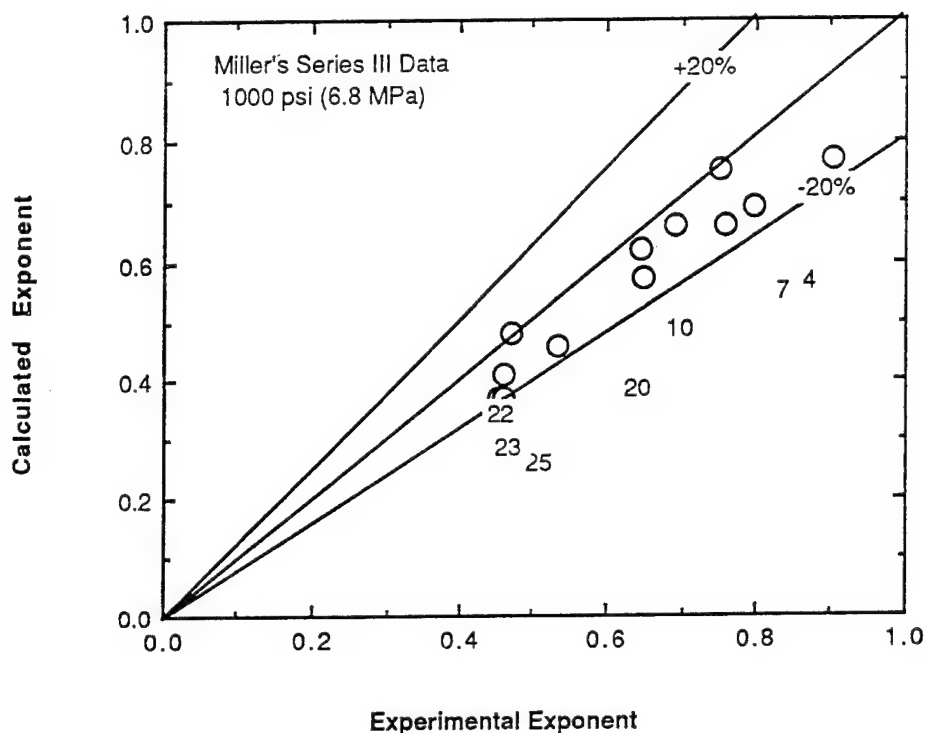


Figure 33. A comparison of calculated and experimental pressure exponents for Miller's Series III propellants at 1000 psi (6.8 MPa). Datum points lying outside of $\pm 20\%$ have been labeled with their identification number.

The model was also used to calculate the temperature sensitivity of the Series III propellants where there were data available. The calculations comparing the calculated values to the experimental values are shown in Figure 34. The agreement is very reasonable with only three calculations lying outside of the 20% range and two of those calculations were for propellants containing 400 μ AP. The calculations are also compared with data in Figure 35 where the temperature sensitivity has been plotted versus the size of the fine AP fraction for propellants containing 400 μ and 200 μ coarse AP. Other than the calculation for 400 μ coarse and 20 μ fine AP the calculated trends are in the right direction, but the model underpredicts the observed trend in the data.

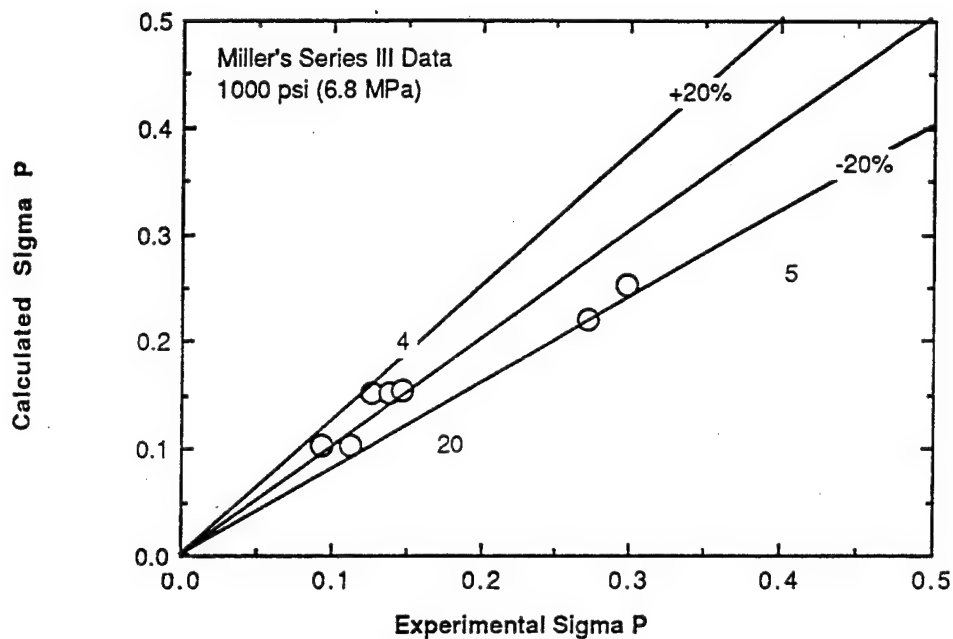


Figure 34. A comparison of calculated and experimental temperature sensitivity for Miller's Series III propellants at 1000 psi (6.8 MPa). Datum points lying outside of +20% have been labeled with their identification number.

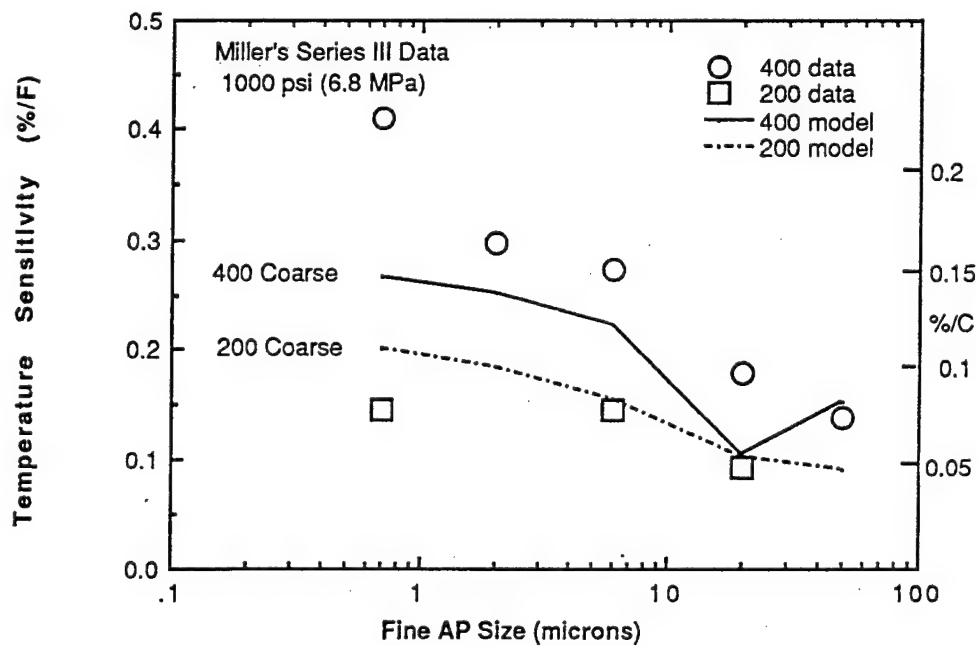


Figure 35. Calculated temperature sensitivity for Miller's Series III propellants at 1000 psi (6.8 MPa), compared with experimental data as a function of fine AP fraction size.

AN COMPOSITE PROPELLANT RESULTS

The primary objective of the program was to model AN based composite propellants with mixed oxidizers. As has been outlined above, the model is designed to accommodate AP, HMX, AN, and SN as the mixed oxidizers. The unknown model parameters were evaluated by comparing the calculated results for AP propellants with known data varying composition, pressure, particle size, etc. Those parameters that are anticipated to be independent of the chemical nature of the oxidizer have been frozen in the model with the values determined from the AP propellant optimization. These include the functional form of the equations describing the terms, β_F , β_P , x^* , etc, and the coefficients and limits on those parameters. On the other hand, parameters such as the primary flame activation energy and prefactor will obviously vary with oxidizer type. Because there is not a consistent set of data for AN propellants, such as that available for AP propellants, the unknown parameters were determined by comparing calculated trends with what appeared to be reasonable.

AN/HTPB Propellant

AN/HTPB propellants can be expected to have a much lower burning rate than AP/HTPB propellants. This is because of the lower flame temperature of the AN propellants. The flame temperature calculations presented in Figure 12 show that at an 86% loading an AP propellant has a primary flame temperature of 2700 K, while an AN propellant has a flame temperature of 1700 K. For an activation energy of 15 Kcal/mole, such as used in the model for the primary flame activation energy, a 1000 K change in flame temperature should cause a change in rate of a factor of five. Thus, if a typical AP propellant has a rate of 0.5, then a corresponding AN propellant will have a rate of ~0.1. This is approximately the ratio of burning rates that are observed for the two types of propellants.

Most AN based propellants have catalysts or additives of some type to augment the rate of the propellant. For standardization of the model however, it is very desirable to have a propellant with no additives to provide a basis of comparison. One such propellant developed by Talley Corporation⁶⁵ was identified at the AFAL sponsored workshop on AN Combustion held in November 1987. That propellant contained 77.5% AN with an HTPB binder. Its burning rate at 1000 psi (6.8 MPa) was 0.47 in/sec (0.119 cm/sec), and it was reported to have an exponent of 0.59. Using these characteristics as a standard a series of calculations were made calculating the burn rate as a function of pressure for varying AN content. The AN particle size was not known, and was assumed to be ~50 μ . Parametric calculations indicated that the particle size has little effect on the burn rate. The results are presented in Figure 36. The rates at 1000 psi (6.8 MPa) vary from ~0.05 to 0.1 (0.1 to 0.2 cm/sec), which seems very reasonable. The data at the reference pressure have also been plotted in Figure 37 as both burn rate and pressure exponent versus AN content. The burn rate increases almost linearly with AN content which also seems very reasonable. The pressure exponent is higher than the datum point of 0.59 at 78% and the exponent reaches a maximum at 80% AN, which is probably not consistent with data. The reason that the model predicts the maximum is not totally clear.

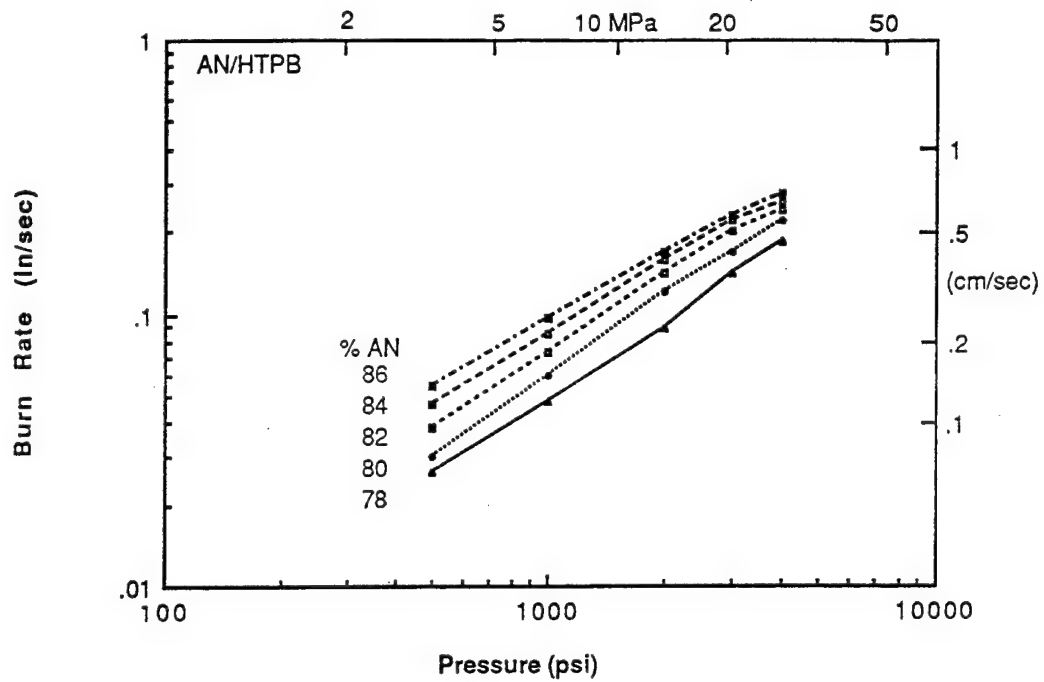


Figure 36. Calculated burn rates of AN/HTPB propellants with varying amounts of AN.

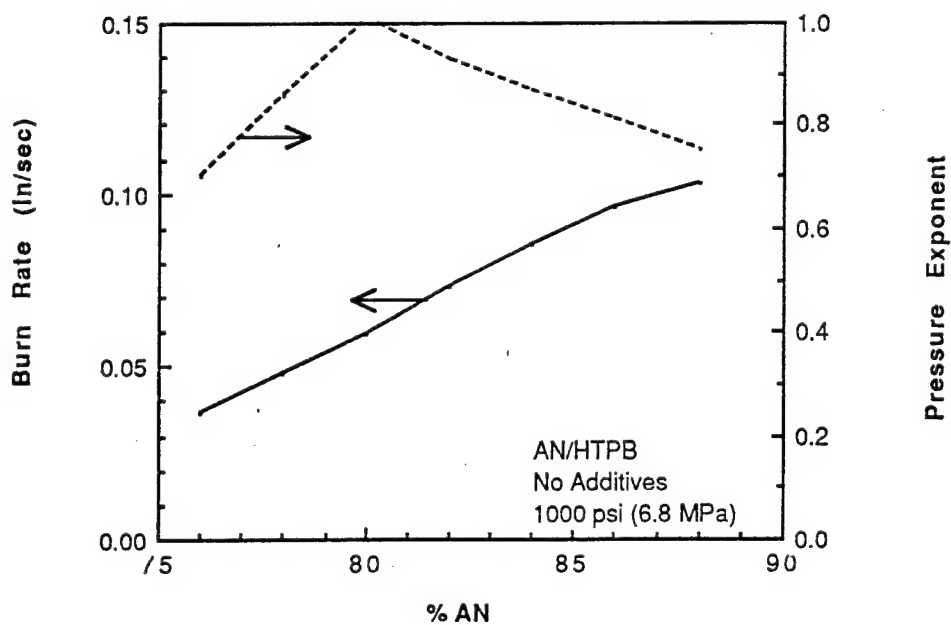


Figure 37. Burn rate and pressure exponent of AN/HTPB propellants for varying AN content.

An unknown parameter of great significance within the model is the primary flame activation energy. For AP and HMX/HTPB propellants a value of 15 Kcal/mole is normally used as the primary flame activation energy, based on flame kinetics work with ammonia-perchloric acid flames⁴⁹ and previous propellant modeling work. Parametric calculations were made to evaluate the effect of the primary flame activation energy for AN propellants. Figure 38 shows the calculated results varying the activation energy from values of 10 to 15 Kcal/mole. In each case the primary flame prefactor was adjusted to give the burning rate of the Talley propellant at 78% AN. The effect of the primary flame activation energy is to cause the burn rate to increase with increasing activation energy as the AN content (and the corresponding primary diffusion flame temperature) increases. An activation energy of 15 seemed to give rates higher than would be expected, while a value of 10 seemed to give more reasonable results and was used in all of the AN calculations.

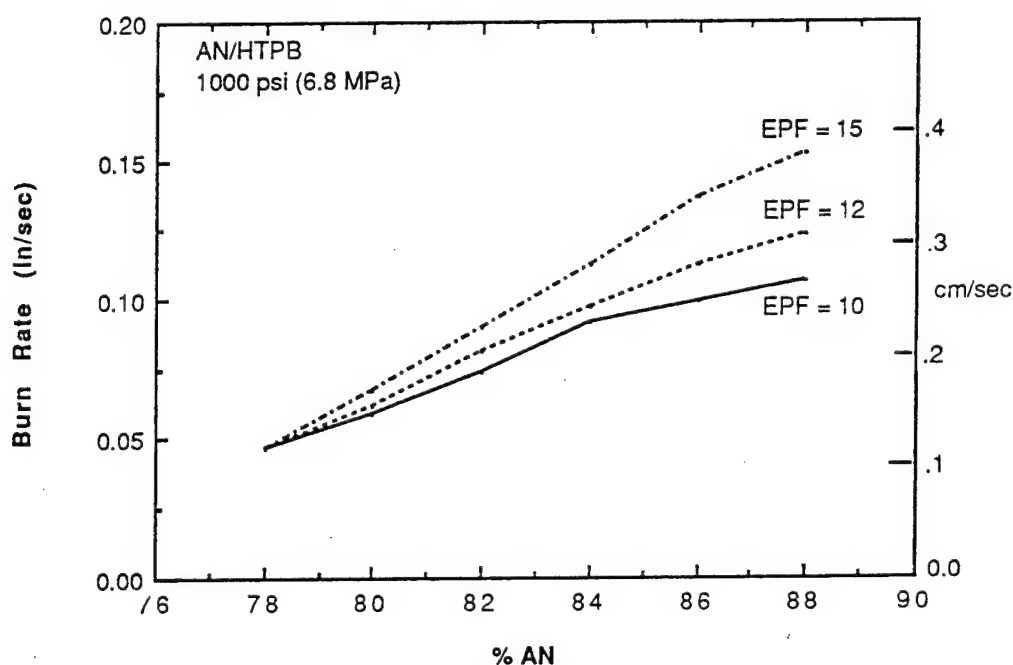


Figure 38. The effect of the primary flame activation energy on burn rate for varying AN content.

The calculations were extended to calculate the temperature sensitivity of the same family of propellants. The temperature sensitivity results are shown in Figure 39. The calculated temperature sensitivity decreases significantly with increasing AN content and with decreasing activation energy. With no precise data to compare with the values predicted with an activation energy of 10 again appeared to give reasonable values of temperature sensitivity, particularly at the lower concentration levels. The values of temperature sensitivity are quite high compared to conventional AP propellants, but based on limited data⁶⁵ for AN propellants where typical values of π_K values of 0.2 to 0.3%/F were quoted, which are about double those normally expected for AP propellants.

The effect of particle size was also explored. For particle sizes ranging from 50 to 200 microns there was no significant difference in the calculated burning rates, at the low solids loadings. At the higher solids loading there is a slight effect which will be discussed later.

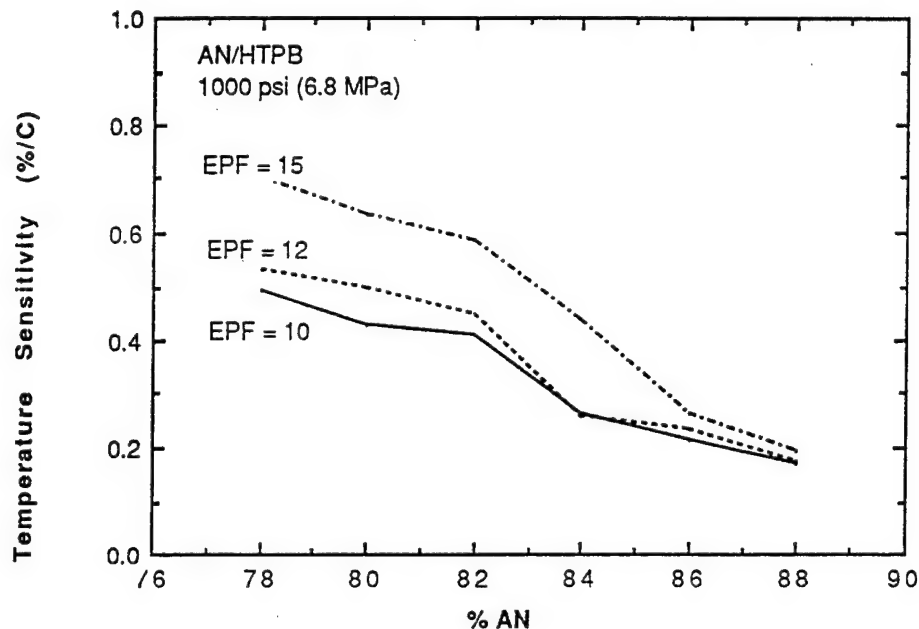


Figure 39. The effect of the primary flame activation energy on temperature sensitivity for varying AN content.

Effect of Catalysts

Because of the very low inherent burning rate of AN propellants, catalysts are usually used to increase the burning rate. To accommodate this effect within the model, the catalytic activity is described in Equations (24) and (25), the inherent assumptions being that the primary flame is catalyzed through the adsorption of reactants on the catalyst. The general characteristics of the functional form of the equation for the catalyzed primary flame were previously evaluated by comparison to AP propellants⁶. As a part of an experimental task of this program, a propellant (BRM-1) was made and burned, which contained 80% 150 μ AN with 2% ammonium dichromate (AD) and 18% HTPB binder. This datum point plus the Talley propellant discussed in the previous section, gave two reference points for comparison with the calculations.

Burn rate calculations were made for a family of AN/AD/HTPB propellants varying the catalyst concentration and the percentage solids. The results are presented in Figure 40 and compared to the two datum points. The calculations show the rate increasing with increasing catalyst concentration and with increasing percentage solids. The trends appear to be consistent and reasonable. The calculations are in agreement with the experimental data.

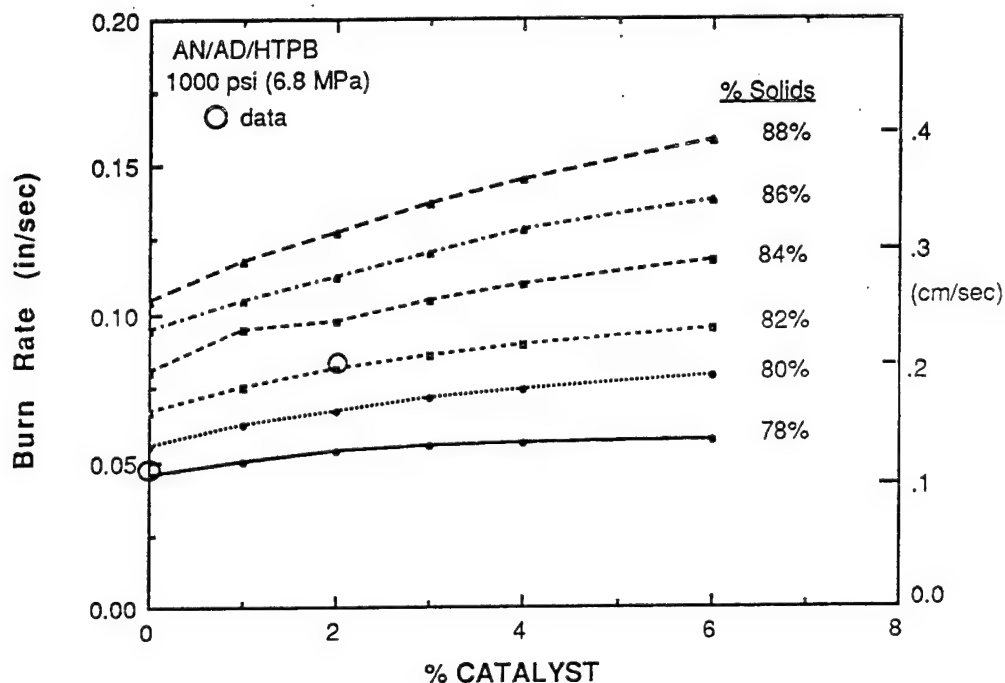


Figure 40 . Burn rate calculations for AN/AD/HTPB propellants, varying the catalyst concentration and the percentage solids. Two experimental datum points are included for reference.

The calculated effect of the catalyst is not great. This is due to the inherently low energy of AN. The primary flame temperature for the AN/HTPB system is relatively low (see Figure 12), and no amount of catalysis is going to increase the burning rate to values comparable to an AP propellant because of the low flame temperature (i.e. the low energy) compared to the flame temperature of AP propellants.

The corresponding pressure exponent calculations for these propellants at 1000 psi (6.8 MPa) are plotted in Figure 41 versus the catalyst concentration. In the calculations that were made the pressure exponent consistently decreases with increasing catalyst concentration and is generally lower for the higher concentration of solids. The decrease in exponent is a direct result of the manner in which the catalytic effect is modeled (see Equation (25)). The catalysis is assumed to occur through adsorption of the primary flame gases onto the catalyst surface. The adsorption process is normally assumed to be proportional to the pressure. In comparison, the global kinetics of the primary flame are assumed to have an order of 1.5. Thus, the catalysis has a lower pressure dependence than the uncatalyzed process. The net effect of the catalysis is to reduce the pressure dependence of the overall reaction.

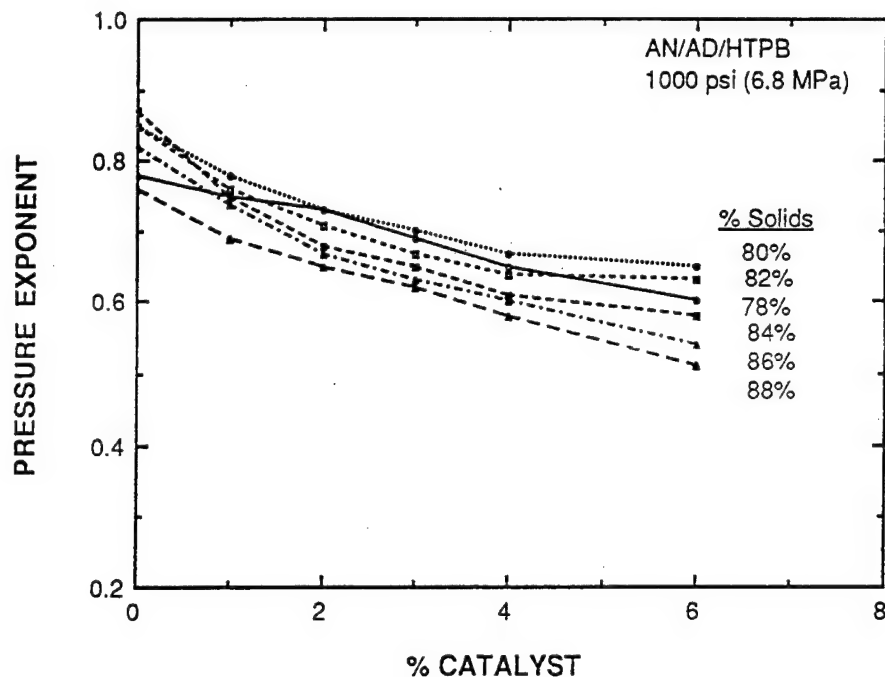


Figure 41. Calculated pressure exponent for AN/AD/HTPB propellants, varying the catalyst concentration and the percentage solids.

The corresponding temperature sensitivity calculations for these propellants at 1000 psi (6.8 MPa) are plotted in Figure 42 versus the catalyst concentration. In the calculations, the temperature sensitivity is virtually independent of catalyst concentration except for the lowest concentration of solids where it increases slightly. The magnitude of the temperature sensitivity appears to be somewhat high especially when compared to AP propellants, but it probably not unreasonable for AN propellants. Anticipating that a typical propellant would probably have about 2% catalyst in its formulation, the zero and 2% data have been replotted in Figure 43. The decrease in temperature sensitivity with increasing solids loading is dramatic. This trend is probably consistent also.

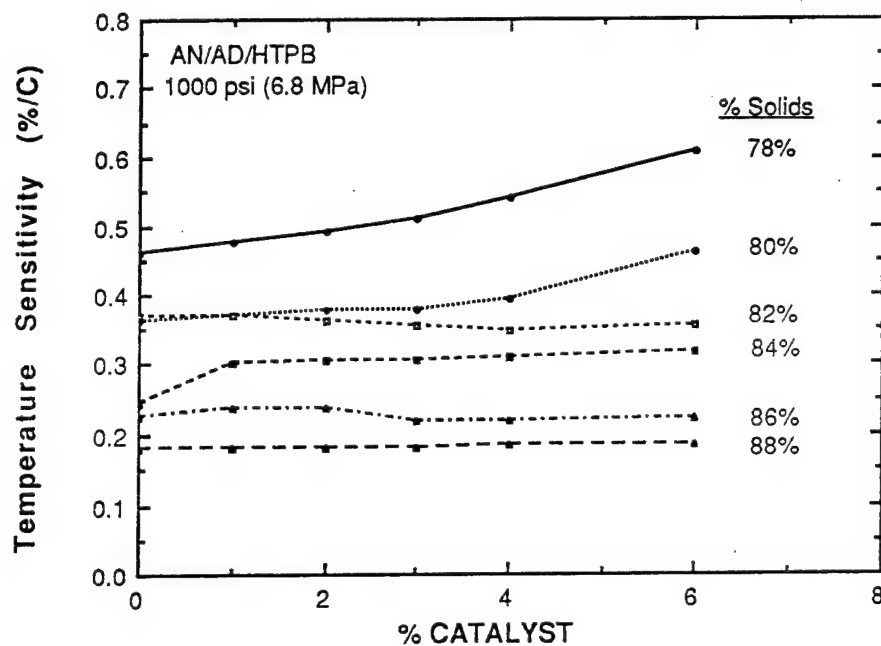


Figure 42. Calculated temperature sensitivity for AN/AD/HTPB propellants, varying the catalyst concentration and the percentage solids.

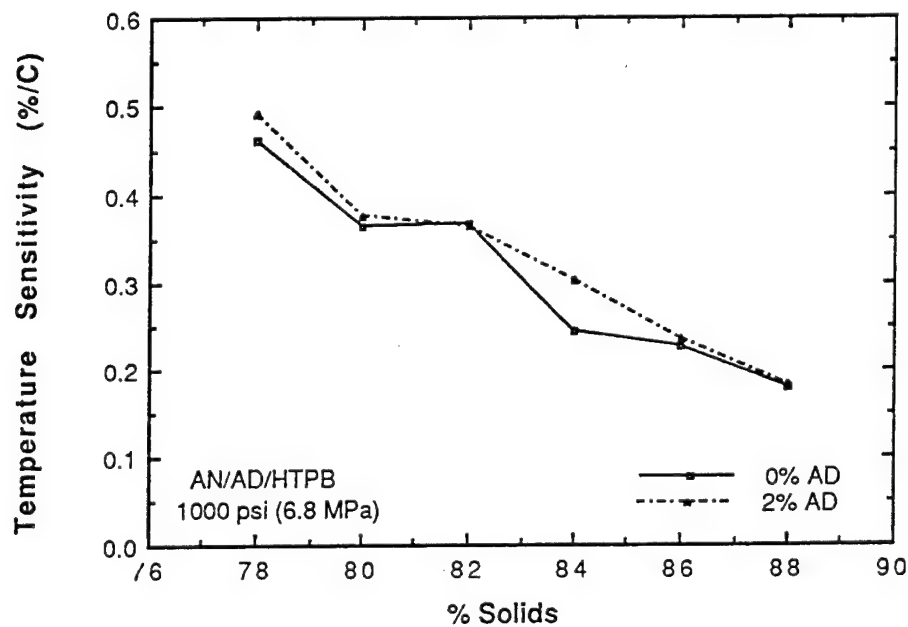


Figure 43. Calculated temperature sensitivity for AN/HTPB propellants, comparing the catalyzed and uncatalyzed temperature sensitivities for varying solids percentage.

Calculations were also made to evaluate a potential effect of particle size. Although virtually no particle size effect was calculated for the 78% AN propellant discussed previously, there was an effect calculated for an 86% solids loading propellant with 2% catalyst. The calculated results are shown in Figure 44. The fine size was varied from 10 to 100 microns and the coarse to fine ratio was varied from 70/30 to 30/70. Increasing the concentration of fine particles did in fact increase the burn rate, but changing the particle size had little effect. For the lowest concentration of fines the rate actually decreased slightly with decreasing size, which is the opposite effect from what is generally observed with AP propellants. However, the AN environment is much more fuel rich than AP propellants (i.e. relative to CO the stoichiometric condition for AP is 85% AP while for AN it is 90%). Within the model the decrease in rate with decreasing particle size corresponds to an excessive energy loss to the binder (see Equation (21)). The corresponding effect has been seen with very wide distribution AP propellants and in self extinguishing AP propellants⁵⁶.

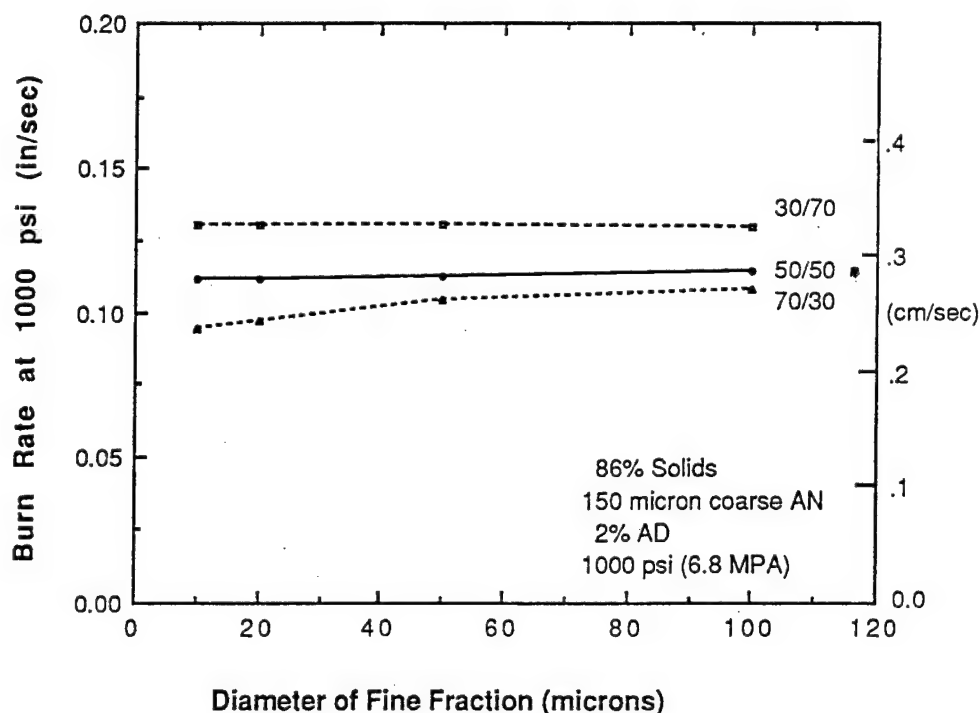


Figure 44. Burn rate calculations for AN/AD/HTPB propellants, varying the concentration and size of the AN fine fraction at 86% solids.

Temperature sensitivity calculations were performed for the same family of propellants, and the calculated results are shown in Figure 45. There is a slight effect calculated for the 86% solids loading propellant. Decreasing the concentration of fine particles did increase the temperature sensitivity slightly for decreasing fine particle size, but had the opposite effect for larger particles.

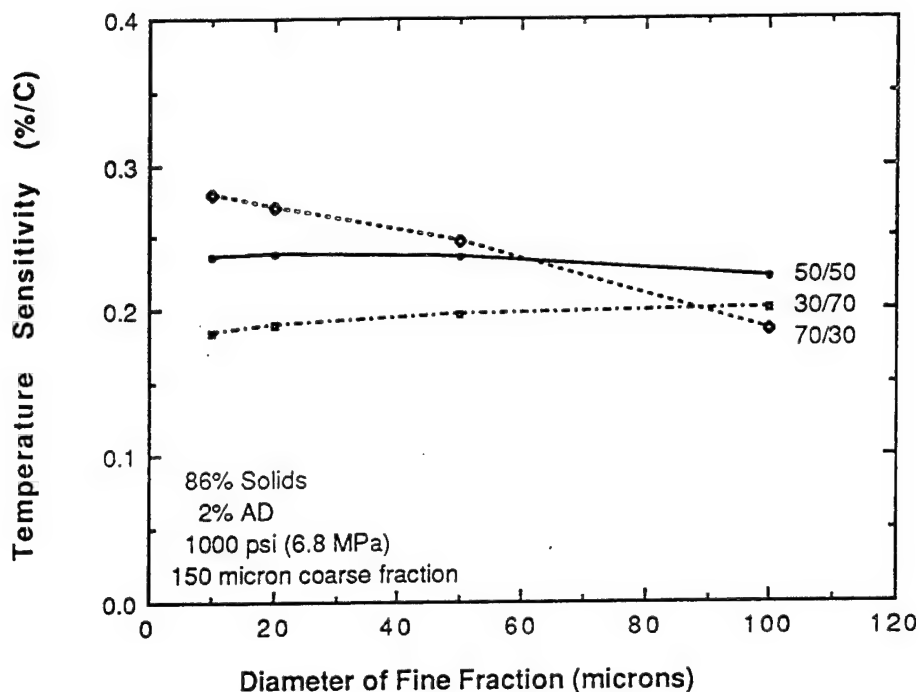


Figure 45. Temperature sensitivity calculations for AN/AD/HTPB propellants, varying the concentration and size of the AN fine fraction at 86% solids.

Effect of AP on AN Propellants

A critical aspect in the development of the model is the ability to handle mixed oxidizers, specifically AP and AN. A series of calculations were made for an 86% solids loading propellant with 2% catalyst, varying the concentrations and particle size of the AP. The AN was assumed to be 150 micron coarse with 50 micron fine in equal amounts. The calculated results are shown in Figure 46. The AP size was varied from 5 to 200 microns, and from 0 to 20% concentration. Increasing the concentration of AP particles increased the burn rate, and decreasing the AP particle size also increased the burn rate. Both of these effects are in agreement with experimental observation. The propellant with 200 micron AP actual showed a slight decrease in the burning rate with increasing concentration. This trend may not be consistent with experimental data, but the effect of 200 micron AP would not be expected to increase the rate very much.

The pressure exponent calculations for the same family of propellants are shown in Figure 47. Increasing the concentration of fine AP particles increases the exponent, but the exponent for the larger particles passes through a maximum with increasing AP concentration. This trend could very well be consistent with experimental data.

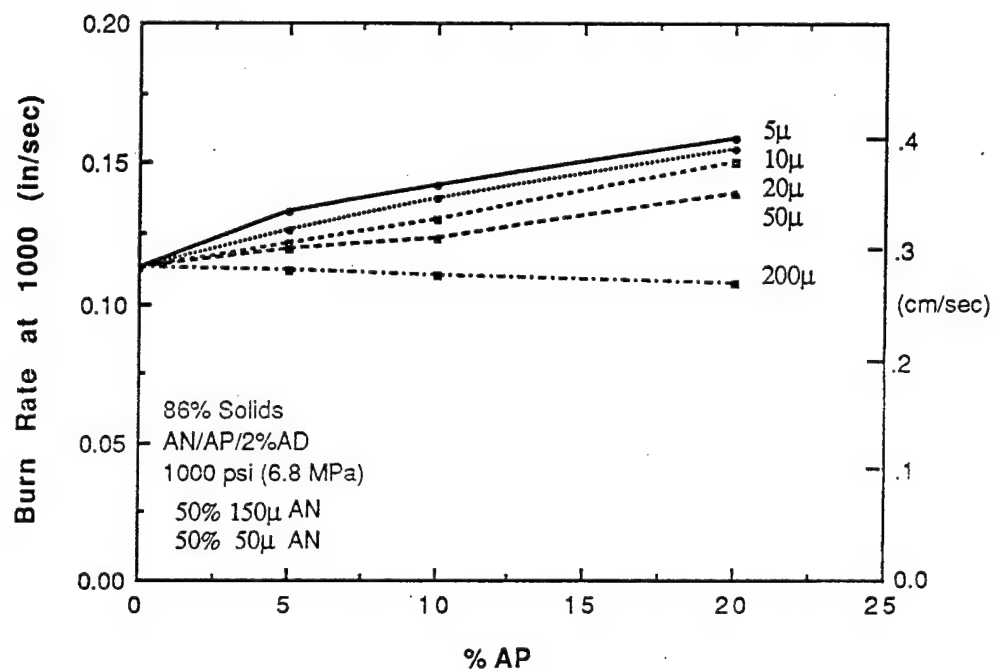


Figure 46. Burn rate calculations for 86% solids AN/AP/HTPB propellants, varying the concentration and size of the AP.

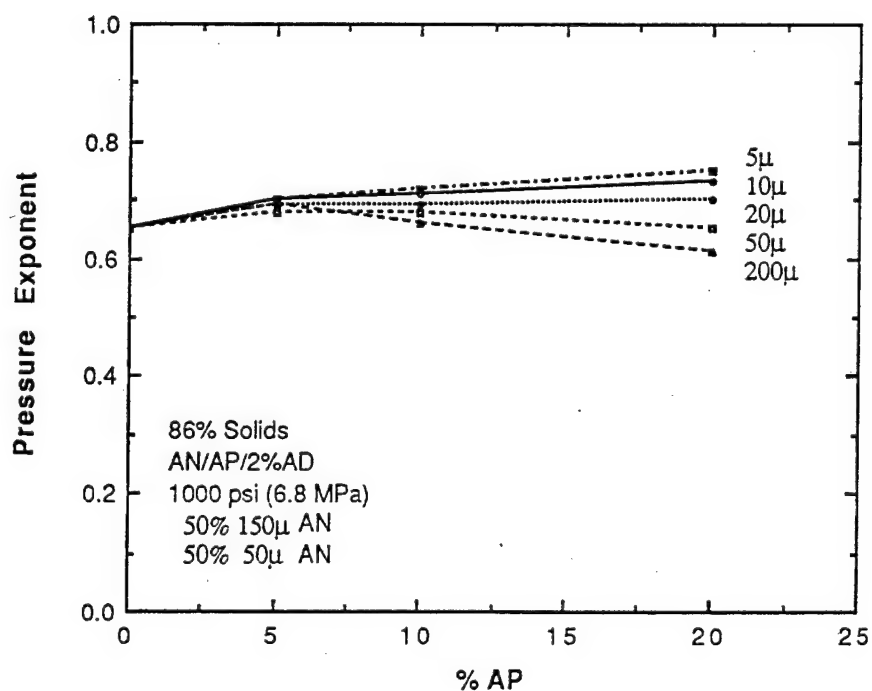


Figure 47. Calculated pressure exponents for 86% solids AN/AP/HTPB propellants, varying the concentration and size of the AP.

During the experimental part of the program three propellants corresponding to some of the conditions of Figures 46 and 47 were actually formulated and data obtained. The data are compared with the calculated results in Figure 48. The propellants were designated BRM-275, 277, and 278 and contained 150 micron coarse and 50 micron fine AN in equal amounts. The BRM-275 propellant had 5% 5 micron AP; the BRM-277 propellant had 10% 5 micron AP; and the BRM-278 propellant had 10% 200 micron AP. The 5 micron propellant calculations are in very reasonable agreement with the data, but the 200 micron calculations are lower than the corresponding data.

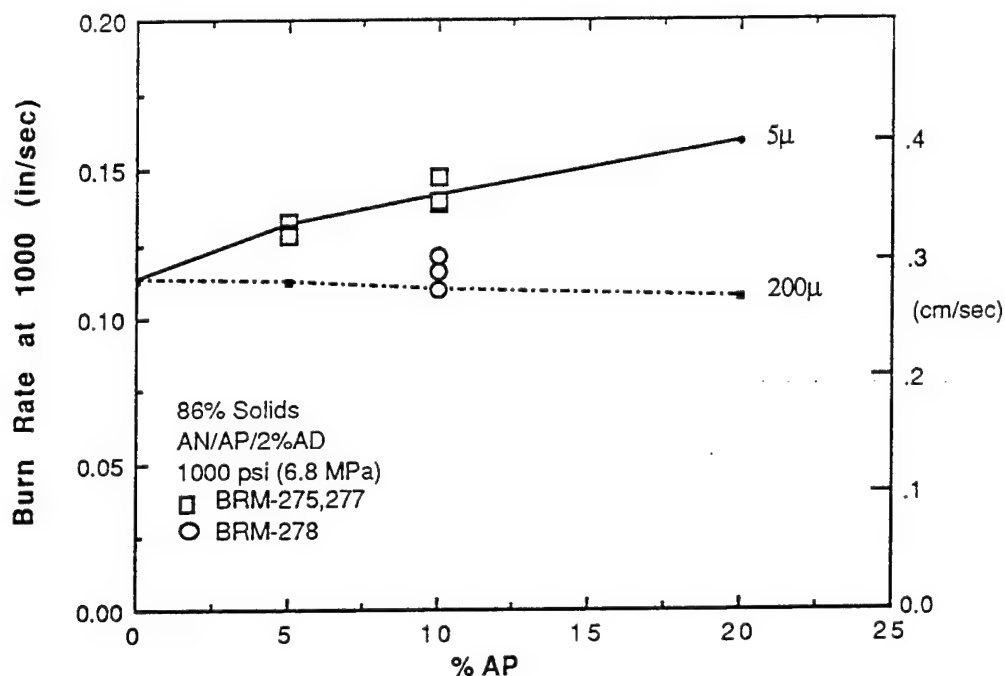


Figure 48. Comparison of calculated and experimental burn rates for 86% solids AN/AP/HTPB propellants, varying the concentration and size of the AP.

Temperature sensitivity calculations were performed for the same family of propellants, and the calculated results are shown in Figures 49 and 50. In Figure 49 the calculations are plotted versus the AP concentration with particle size as a parameter. The temperature sensitivity is virtually constant with only the 200 micron AP propellant deviating significantly from the values between 0.22 and 0.24 %/C. Although there are no experimental data with which to make a comparison, the magnitude of the calculated the temperature sensitivity appears to be reasonable. The effect of particle size is illustrated in Figure 50 and is seen to be small.

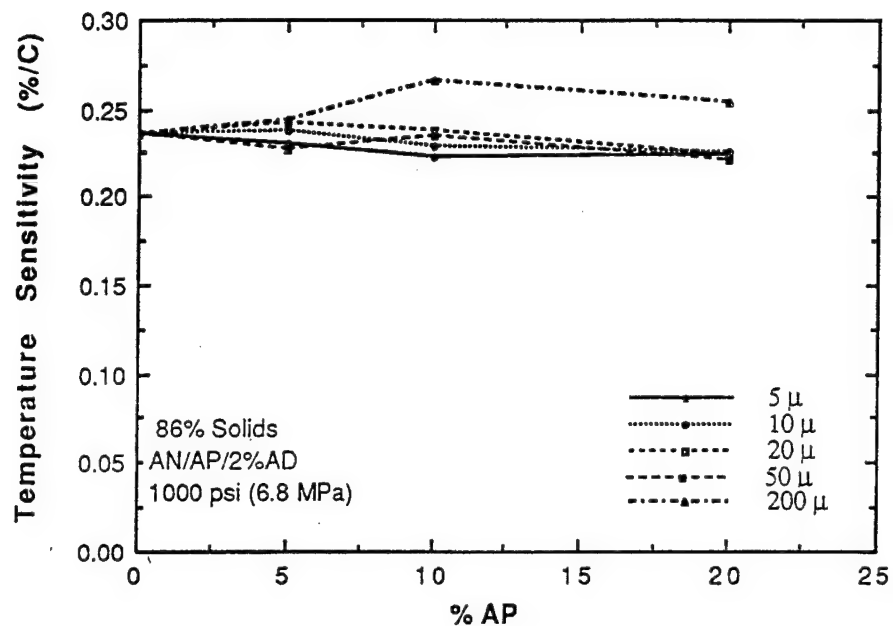


Figure 49. Temperature sensitivity calculations for 86% solids AN/AP/HTPB propellants, varying the concentration and size of the AP.

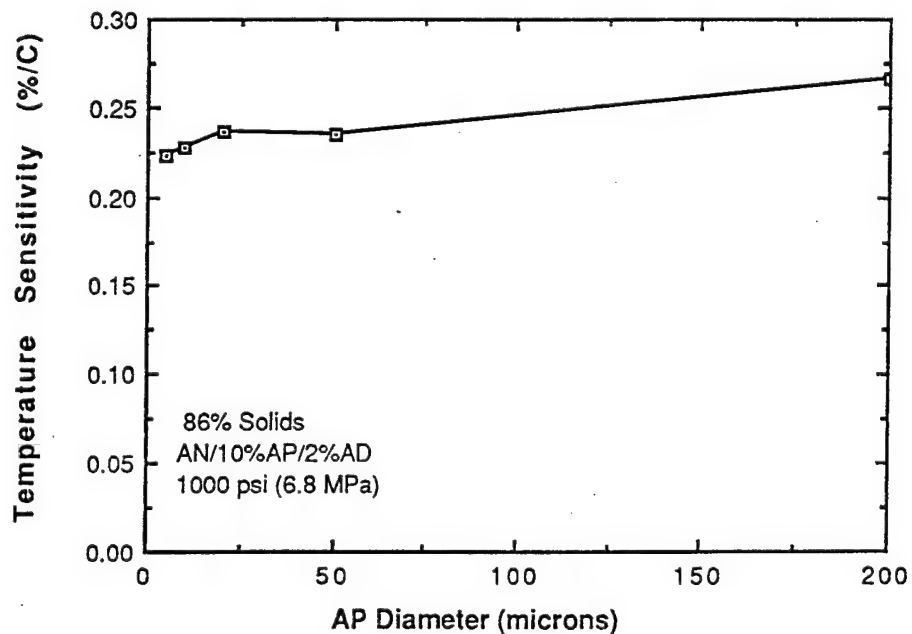


Figure 50. AP particle size effect on the temperature sensitivity calculations for 86% solids AN/AP/HTPB propellants.

Effect of SN on AN Propellants

A significant aspect of the model is the ability to handle AN and SN as mixed oxidizers. A series of calculations were made for an 86% solids loading propellant with 2% catalyst, varying the concentrations and particle size of the SN similar to those for AP. As with the AP calculations the AN was assumed to be 150 micron coarse with 50 micron fine in equal amounts. The calculated results are shown in Figure 51. The SN size was varied from 10 to 200 microns, and from 0 to 20% concentration. Increasing the concentration of the SN particles increased the burn rate, and decreasing the SN particle size increased the burn rate. Both of these effects are the same trend as observed with the AP containing propellant, except that the SN is predicted to have a larger effect than the AP. This is apparently due to the primary flame temperature of SN which is significantly higher than that of AN for similar concentrations. Although there are no experimental data available with which to compare, the trends would seem to be overpredicted. Intuitively, one would expect AP to have a greater effect than SN.

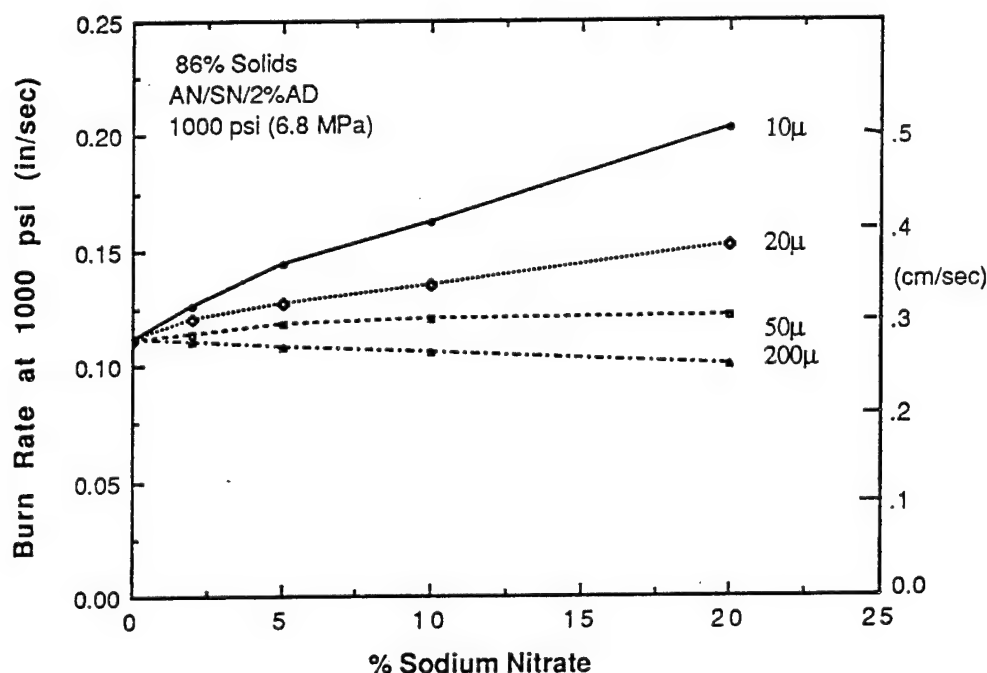


Figure 51. Burn rate calculations for 86% solids AN/SN/HTPB propellants, varying the concentration and size of the SN.

Propellants Containing AN/AP/SN

A primary objective of the program was to model AN based composite propellants including additional oxidizers of AP and SN. A series of AN propellants were formulated and tested as part of the experimental part of the program³¹. These propellants contained AP and SN as well as 2% AD as a catalyst. One of those

propellants, BRM-270 has been compared to two other propellants that are comparable with respect to the AN fractions. The other two propellants are the Talley propellant, representing a propellant without additives, and the BRM-1 propellant which is an 82% solids propellant containing AD but no additional oxidizer. The data and the model calculations are compared in Figure 52. As would be expected, the Talley propellant without catalyst and with a relatively low amount of AN has the lowest burn rate. Increasing the AN content and adding a catalyst increases the rate from 0.047 to 0.080 in/sec (0.12 to 0.20 cm/sec). Increasing the solids content to 86% with 10% AP and 10% SN increases the rate to 0.135 in/sec (0.34 cm/sec). The calculated rates are in very good agreement with the data for the three propellants. However, there is some deviation at the higher pressures. The BRM-1 propellant without any mixed oxidizers has a lower exponent than predicted while the mixed oxidizer propellant has a higher exponent than predicted. In the model a primary flame reaction order of 1.5 was assumed which will give pressure exponents on the order of 0.7. Had an order of 2.0 been assumed there would have been better agreement with the mixed oxidizer propellant, but not with the other propellant. Apparently the single global reaction used in the model is not adequate to model the wide variation of oxidizer/fuel ratios and environments of the different propellants. A more comprehensive kinetics model is needed.

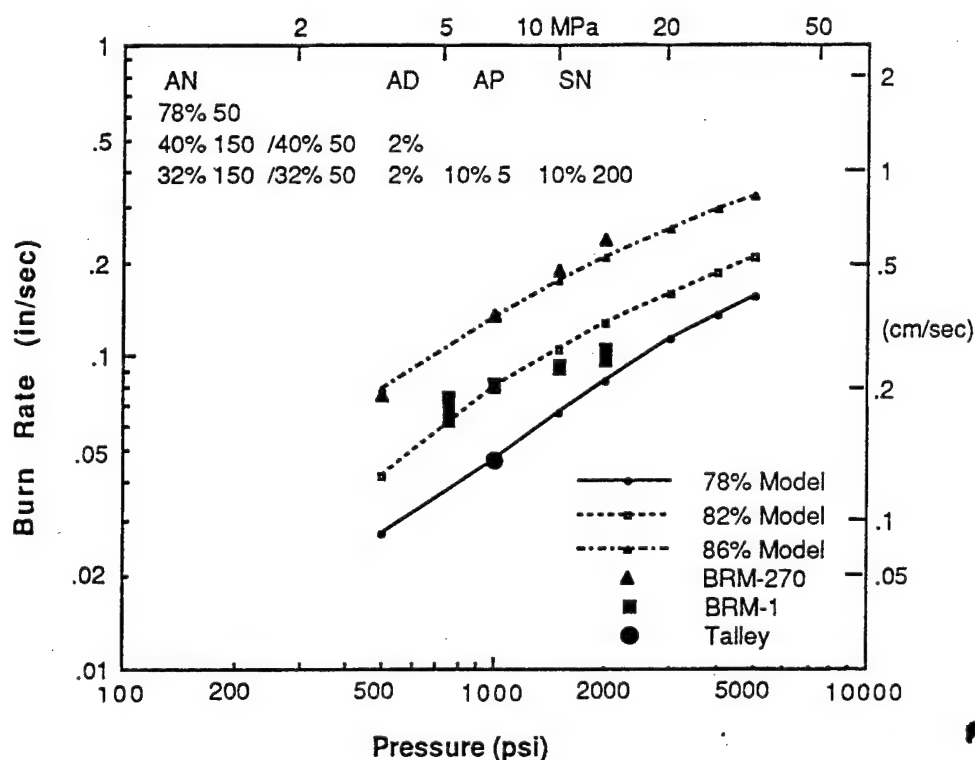


Figure 52. Calculated burning rates of AN/HTPB propellants with varying amounts of AN, AP, and SN compared to experimental data.

Temperature sensitivity calculations were also made for the same propellants, although there is not any temperature sensitivity data for comparison purposes. The

temperature sensitivity calculations are shown in Figure 53. As in the calculations above, the temperature sensitivity decreases with increasing solids loading (with the exception of the 78% 500 psi point). The 78% solids loading propellant has the highest temperature sensitivity, and it increases slightly with increasing pressure. Both of the other propellants show a decreasing temperature sensitivity with increasing pressure, and the 86% solids propellant has the lowest temperature sensitivity. The calculated temperature sensitivity values are all higher than would be calculated for similar AP propellants. The 87.4% AP propellants shown in Figure 35 had temperature sensitivity values between 0.08 to 0.22 %/C. In Figure 53 the 86% AN propellant has temperature sensitivity values from 0.29 to 0.20%/C. It appears that the temperature sensitivity of AN containing propellants will, in general, be higher than AP propellants due to the inherently lower burn rate of the AN propellants. This can be seen from Equation 8. The flame stand-off distance, ξ , appears in the denominator and is proportional to the burning rate squared (Equation 4), which leads to a higher σ_p for lower burning rate propellants.

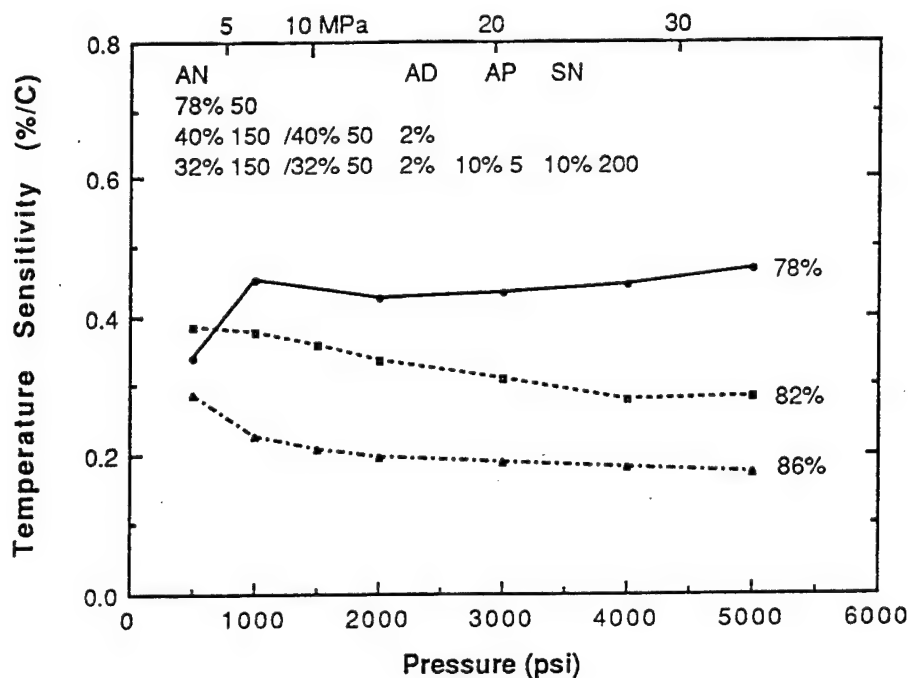


Figure 53. Calculated temperature sensitivity for AN/AP/SN propellants, varying the oxidizer concentrations and the percentage solids.

The six mixed oxidizer propellants from the experimental part of the program were BRM-270, 271, 272, 275, 277 and 278. These propellant had a solids content of 86% with 2% AD, 5 to 10% AP and 0 or 10% SN. Calculations were performed to simulate each of these propellants, and a comparison of calculated and experimental burning rates is presented in Figure 54. The data were taken at four pressures. The agreement between the model and the data is reasonable, although the model predicts slightly lower rates at the higher pressures.

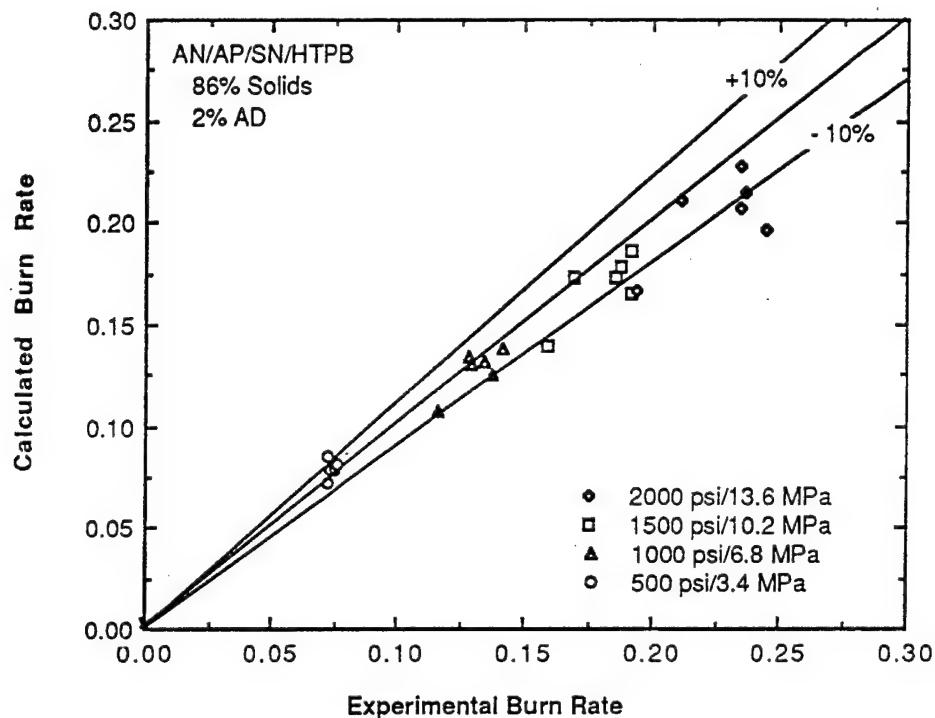


Figure 54. A comparison of calculated and experimental burning rates for the six propellants BRM-270, 271, 272, 275, 277 and 278 at varying pressure.

Formulations corresponding to three of the mixed oxidizer propellants (BRM-270, 271 and 272) were used to study the effect of AN particle size and distribution. The propellants had a solids content of 86% with 2% AD, 10% AP and 10% SN. The results are shown in Figures 55 and 56 and should be compared to the results shown in Figures 44 and 45 for a propellant without the mixed oxidizers. The fine size was varied from 10 to 100 microns and a coarse to fine ratio of 70/30, 50/50 and 30/70 was used. Increasing the concentration of fine particles caused a very small increase in the burn rate, and changing the particle size had a similar small effect. This is essentially the same as noted in the discussion of Figure 44 for AN propellants without added oxidizers. It seems very apparent that in AN propellants the primary flame temperature (energy release) is so low that the kinetic aspects of the primary flame dominate over the diffusion aspects, virtually eliminating the possibility of using the AN particle size to tailor the propellant burn rate. This is a major conclusion from the modeling effort.

For the smallest particle size of fines the rate actually decreased slightly with decreasing size, more so than without the mixed oxidizers. As noted in the discussion of Figure 44, this effect is felt to be a real effect, due to the fuel richness of the environment surrounding the fine particles. This effect is introduced into the model through Equation (14).

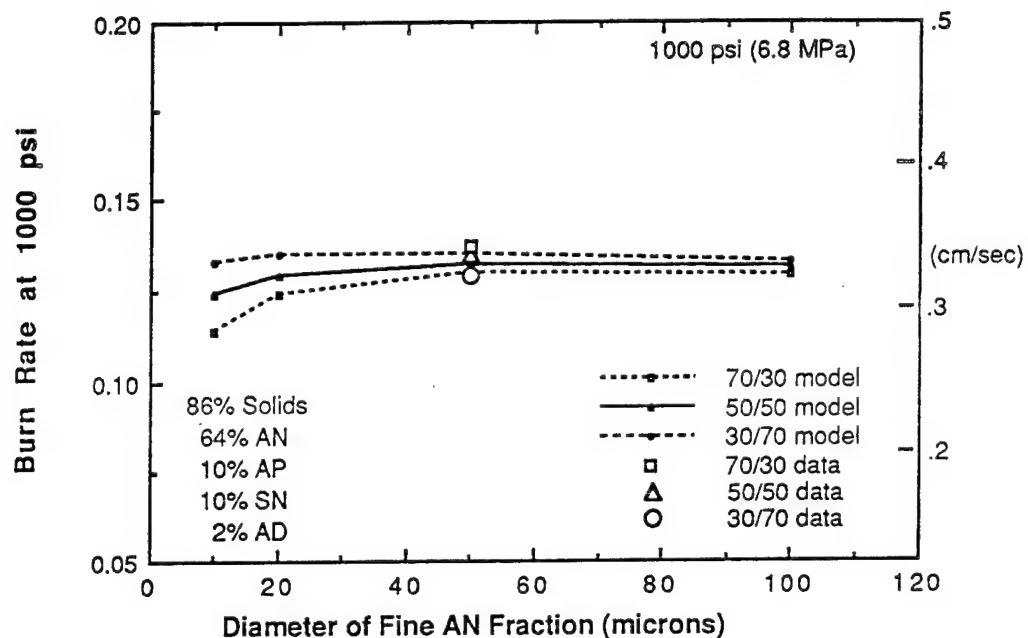


Figure 55. Burn rate calculations for AN/AP/SN/HTPB propellants, varying the concentration and size of the AN fine fraction at 86% solids. Data from propellants BRM-270, 271, 272 are included for reference.

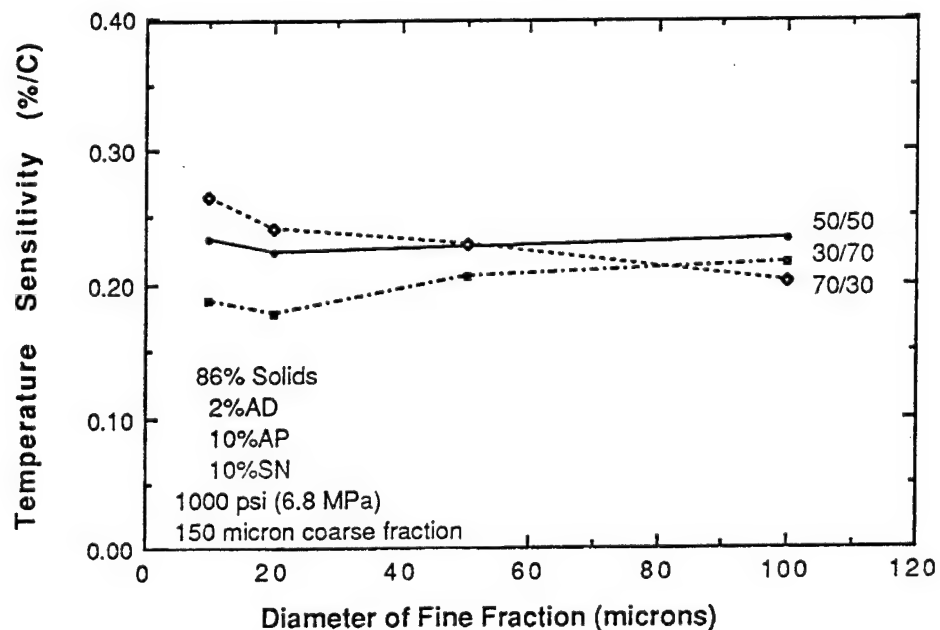


Figure 56. Temperature sensitivity calculations for AN/AP/SN/HTPB propellants, varying the concentration and size of the AN fine fraction at 86% solids.

Temperature sensitivity calculations performed for the same family of propellants, show a slight effect on the calculated temperature sensitivity, but almost identical to the temperature sensitivity for the propellant without the mixed oxidizers. Decreasing the concentration of fine particles did increase the temperature sensitivity slightly for decreasing fine particle size, but had the opposite effect for larger particles. The value of temperature sensitivity remains significantly higher than corresponding AP propellants.

SUMMARY AND CONCLUSIONS

Performance Calculations

A thermochemical investigation was conducted evaluating the performance of AN based propellants. AP/HTPB propellants have a maximum I_{sp} at 22% aluminum, while AN/HTPB propellants have an equivalent maximum at 28%. Unfortunately, it is difficult to get good combustion efficiency above about 20% aluminum, which reduces the potential practical usage of AN propellants.

Performance calculations were made evaluating lithium nitrate (LN), sodium nitrate (SN), and potassium nitrate (KN) as additives to scavenge HCl in the exhaust. LN appears to be the best HCl scavenger, and has a higher I_{sp} than SN or KN. However, it is more hygroscopic and less compatible than SN or KN, and SN improves propellant agglomeration characteristics. SN also has a higher density than either AN or AP which makes it attractive on an I_{sp} -density basis. Therefore, SN ultimately became the additive of choice for the study.

Calculations for AN propellants, with sufficient SN to scavenge HCl to less than 2% of the exhaust gases, shows that increasing AP content improves the I_{sp} dramatically due to its inherently higher performance. The low energy of AN plus its low density result in very poor performance numbers for AN containing propellants.

Combustion Mechanisms

Due to the nitrate in AN, it was initially speculated that the AN flame structure might be similar to double base propellants, where a dual stage flame exists. Therefore, thermochemical calculations were made simulating different potential flames. The flame temperature calculated assuming NO as a product (analogous to the double base propellant dark zone) is less than 600 K, which is the nominally measured surface temperature of burning AN. Therefore, it is highly unlikely that there is an inner flame with NO as a product of AN combustion. It was finally concluded that there is probably a single AN flame which is in equilibrium with the final products of N_2 , H_2O , and O_2 and at a monopropellant flame temperature of 1247 K.

A critically important part of the model is the primary diffusion flame. Initially four separate flame structures were postulated with nitrogen and carbon at various stages of oxidation. Previous work on AP has led to the conclusion that the formation of CO_2 is relatively slow and that CO is the product of importance in the primary flame. It was finally concluded that the AN primary flame occurs with N_2 , CO and H_2O as the final products. Based on this assumption, AP/HTPB propellants have a peak temperature of 2750 K at a loading of 85%; SN/HTPB propellants have a peak temperature slightly greater than 2300 K at a loading of 84%; while the peak temperature for AN/HTPB propellants is barely 2000 K and occurs at a loading of 90%.

A composite propellant flame structure for AP, AN, and SN has been postulated. AP and AN each burn with a monopropellant flame whose products are approximately 30 and 14% O_2 , respectively. This leads to a final diffusion flame where the oxygen-rich products from the monopropellant flame react with the binder pyrolysis products.

SN on the other hand, does not burn with a monopropellant flame but only burns with a single diffusion flame.

Because of lower flame temperatures, AN propellants have a much lower burn rate than AP propellants. For example, at an 86% loading an AP propellant has a primary flame temperature of 2700 K, while at the same loading an AN propellant has a flame temperature of 1700 K. A 1000 K decrease in flame temperature leads to an AN propellant burn rate five times lower than an AP propellant rate. This is approximately the ratio of experimental burn rates that is observed.

Flame temperatures calculated for a silicone binder were significantly higher than for a corresponding HTPB binder propellant for both AP and AN. Thus, one would expect the silicone propellant to burn better, both faster and more efficiently, than the corresponding HTPB propellant which is in agreement with experimental observation.

Experimental data for AN indicate surface temperatures from 500 to 600 K, with an apparent surface activation energy of ~10 Kcal/mole. Data for SN indicate surface temperatures of ~1000 K, and an activation energy of ~4.5 Kcal/mole. Apparently there is a wide diversity of surface temperatures and individual rates occurring simultaneously on a propellant surface. Because of its higher surface temperature for an overall propellant rate, an ingredient such as SN will be slow to ignite while the thermal profile adjusts to a configuration compatible with the SN surface kinetics. Once ignited, it should burn very rapidly, possibly leaving an empty pocket of binder or disrupting adjacent surface regions with an explosive type of flow due to its high relative rate. AN on the other extreme could possible puddle and flow along a surface due to its low melting point, surface temperature and combustion rate, and long residence time.

AN Monopropellant Modeling

The literature was reviewed for pertinent articles on AN combustion and modeling, but few articles were found. Because of the extensive previous work done with AP, it was decided to use AP as a basis of comparison for the monopropellant model. The key parameters that are required to make the calculation are tabulated in Table 4 (page 31) with a comparison of the values used for both AP and AN. The AP burn rate, temperature sensitivity, surface temperature, surface heat release, and flame standoff distance were calculated and compared to experimental data, where available, or other modeling results.

Using the known physical properties for AN, the following combustion parameters were selected: a reference burning rate of 0.19 cm/sec at 68 atm, a reference surface temperature of 530 K, reaction order of 2, E_s of 14 Kcal/mole, E_f of 25 Kcal/mole and a Q_c value of 0.26. The calculated burn rates agree very well with experimental data, and a σ_p of ~0.3 %/K was calculated (which is a very dependent on the selected value of the flame activation energy). Although AP and HMX have σ_p values on the order of 0.16 and 0.2%/K respectively, it seems logical that AN would have a relatively high σ_p due to its lower surface temperature and low burning rate

(similar to double base propellants which have σ_p values of 0.2 to 0.5 %/K). The measured and calculated surface temperature varies between 500 and 600 K for the AN monopropellant. This puts AN in the same range of surface temperatures as double base propellants, but significantly below AP. Variations in E_s indicate that a value between ~10 and 15 Kcal/mole would fit the surface temperature data equally well. The molten AN layer was calculated to be 15 to 50 microns over the pressure range of interest, which compares qualitatively with window bomb movies of burning AN propellants. The calculated flame stand-off distances of 25 to 250 microns are much larger than those values calculated for AP or HMX, but are comparable to those observed for double base propellants.

AN Composite Propellant Model

The basis of the AN model is the Beckstead SST model. The SST model is based on a separate energy balance for each ingredient type and size, and the overall burning rate is calculated on a time averaged basis rather than the original BDP approach of using a space averaged approach. Other aspects of the SST model that influence AN propellants are summarized briefly.

To model composite propellant combustion one must assume a distribution of fuel among the different oxidizer fractions. In the SST model it has been assumed that the binder is distributed according to the oxidizer specific surface area. However, binder thicknesses for intermediate and coarse oxidizer fractions are ~1% of the particle diameter which is smaller than the roughness and non-sphericity of actual crystals. Thus, a significant amount of binder can be buried within the surface irregularities of a crystal in excess of what would be calculated for a purely spherical particle. To compensate for this, Cohen assumes that the finest oxidizer fraction burns at the stoichiometric O/F condition, and the fuel left over from one particle size is available to be burned in the diffusion flame of the next larger size fraction. This approach appears to be quite realistic on a mechanistic basis, and has been adopted.

Multimodal and mixed oxidizer propellants experience interaction effects and influences caused by different sizes and types of particles having significantly different burn rates. Either faster burning components are igniting slower burning particles all along their periphery, or slower burning particles can be undercut by faster burning components. The model attempts to account for this effect also.

A critical aspect of a composite propellant model is the description of the monopropellant flame and primary diffusion flame interaction. Within the BDP type of approaches, the β_F term accounts for this interaction, and is very dominant within the model in determining the effect of pressure and particle size on burn rate. This effect is still accounted for in a relatively crude manner, and a more rigorous calculational procedure needs to be developed.

Once the amount of oxidizer that participates in the primary flame is determined, then the amount of the heat that is transferred to the oxidizer versus the amount transferred to the binder must be determined. This effect is accounted for by the term β_p in the model. Evaluation of this effect is complicated by the fact that the primary

flame flips back and forth from being over the oxidizer to being over the binder, during the lifetime of a particle. This general effect has been addressed previously, but a quantitative description of the transient heat transfer was beyond the scope of the current project, and an integrated, average value of β_p is estimated empirically.

AP Propellant Results

Miller's non-metallized AP/HTPB propellants were used as a comparative data base, because of the large number of propellants with the same binder and a wide range of compositions, pressure, particle size, and initial temperatures. Calculations were compared to the experimental data, and model parameters were optimized to provide the best fit of the model to the data. Model calculations for Miller's Series III data at 1000 psi (6.8 MPa) are very reasonable with only a few of the widest distribution propellants falling outside of a 10% predictive goal. The calculated pressure exponents for most of data were within 20% of the measured values, but the calculations were consistently low with several datum points for propellants containing 400 μ AP more than 20% in error. Calculated σ_p values were very reasonable with only three calculations lying outside of the 20% range of the data and two of those calculations were for propellants containing 400 μ AP.

AN Propellant Results

Burn rate calculations were made for AN/HTPB propellants (with no additives) varying AN content from 76% to 88%. The calculated rates vary almost linearly from 0.05 to 0.1 in/sec (0.1 to 0.2 cm/sec) which seems very reasonable. Pressure exponents of 0.7 to 1.0 were calculated, which appear to be a little high.

Increasing the primary flame activation energy causes burn rate to increase as AN content (and the corresponding primary flame temperature) increases. An activation energy of 15 seemed to give rates higher than would be expected, while a value of 10 seemed to give more reasonable results. For AP and HMX/HTPB propellants a value of 15 Kcal/mole is normally used as the primary flame activation energy.

Burn rate calculations for propellants containing ammonium dichromate as a catalyst show the rate increases with increasing catalyst concentration and with increasing percentage solids, which is in general agreement with experimental data. The calculated effect of the catalyst is small due to the inherently low energy of AN. The low flame temperature (i.e. the low energy) of AN propellants prohibits a catalysis comparable to AP propellants. The catalysis process has a lower pressure dependence than the uncatalyzed process, and the net effect is to increase the burn rate slightly, but reduce the pressure exponent.

Virtually no particle size effect was calculated for a 78% AN propellant, but there was a slight effect calculated for an 86% solids loading. For the lowest concentration of fines the rate actually decreased slightly with decreasing size. The AN environment is very fuel rich and the decrease in rate with decreasing particle size corresponds to

an excessive energy loss to the binder. The corresponding effect has been seen with very wide distribution AP propellants and in self extinguishing AP propellants.

A critical aspect in the development of the model is the ability to handle mixed oxidizers, specifically AP, SN, and AN. Increasing AP concentration increased burn rate, and decreasing AP particle size increased burn rate. Both of these effects are in agreement with experimental observation. Increasing fine AP concentration increased the exponent slightly, but in general, the exponent did not change significantly with increasing AP concentration. The calculations were compared with propellants containing 5% 5 micron AP, 10% 5 micron AP; and 10% 200 micron AP. The 5 micron propellant calculations are in very reasonable agreement with the data, but the 200 micron calculations are lower than the corresponding data.

Increasing the concentration of SN increased the burn rate, and decreasing the SN particle size increased the burn rate. Both of these effects are the same trend as observed with AP, except that the SN is predicted to have a larger effect than the AP. Although there are no experimental data available with which to compare, the trends would seem to be overpredicted. Intuitively, one would expect AP to have a greater effect than SN.

Calculations were performed to simulate six propellants containing 86% solids with 2% AD, 5 to 10% AP and 0 or 10% SN. The agreement between the model and the data is reasonable, although the model predicts slightly lower rates at the higher pressures. Increasing the concentration of fine AN particles caused a very small increase in the burn rate, and changing the AN particle size had a similar small effect. In AN propellants the primary flame temperature is so low that the kinetic aspects of the primary flame dominate over the diffusion aspects, virtually eliminating the possibility of using AN particle size to tailor propellant burn rate. This is a major conclusion from the modeling effort.

Calculated temperature sensitivity decreases significantly with increasing AN content (i.e. solids loading) and with decreasing activation energy. With no precise data to compare with the values predicted with an activation energy of 10 Kcal/mole appeared to give reasonable σ_p values, 0.2 to 0.3 %/K, particularly at the lower concentration levels. The σ_p values are quite high compared to conventional AP propellants, but limited data for AN propellants indicate π_K values of 0.2 to 0.3%/F, which are about double those normally expected for AP propellants and in very reasonable agreement with the calculated σ_p values. The addition of AP and SN to the propellants had little effect on the calculated σ_p values. For the mixed oxidizer propellants, decreasing the concentration of fine AN particles did increase the temperature sensitivity slightly for decreasing fine AN particle size, but had the opposite effect for larger AN particles. The calculated σ_p value remains significantly higher than corresponding AP propellants.

Modeling Needs

The following is an abbreviated list of areas where additional work is needed to further advance the understanding of composite propellant combustion.

- Phenomenological needs in composite propellant modeling:
 - a better understanding of binder pyrolysis
 - a better description of how the fuel is distributed relative to oxidizer particles in the combustion process
 - an accurate description of the interaction of the diffusion flame and the monopropellant flame (i.e. β_F)
 - a better understanding of the dynamic diffusion flame shape during the life time of a burning particle
 - a description of the diffusion flame heat transfer both to the oxidizer as well as the binder (i.e. β_P) during the life time of a burning particle
 - a description of the interaction between flames from adjacent oxidizer particles
 - the effect of aluminum agglomeration and combustion on all of the above
 - determination of the number of kinetic steps necessary to describe the essential combustion features of typical flames including the condensed phase reactions
- Experimental needs to support modeling of composite propellants:
 - accurate surface temperature measurements of any ingredient intended for use in composite propellants (i.e. AP, AN, SN, HMX, HTPB, etc)
 - surface decomposition products of composite propellant ingredients (i.e. AP, AN, SN, HMX, HTPB, etc) closer to actual burn rate conditions
 - surface heat release and heat flux values
 - σ_p data of oxidizers intended for use in composite propellants (i.e. AP, AN, SN, HMX, etc)
 - systematic combustion data (i.e. r , n , and σ_p) varying the oxidizer content and particle size to allow identification of global kinetic parameters
 - systematic combustion data (i.e. r , n , and σ_p) varying the oxidizer content and particle size to allow identification of global kinetic parameters
 - species composition data through flames to identify which gas phase species are important in the flames
 - identification of key species needed to describe the principal kinetic steps in both the condensed and gas phases

NOMENCLATURE

A	Arrhenius frequency factor
a	numerical coefficients in flame standoff expression
AP	Ammonium perchlorate
AN	Ammonium nitrate
b	Characteristic surface dimension
BDP	Beckstead-Derr-Price model
C_{ign}	Coefficient in ignition delay time calculation
CMDB	Composite-modified double-base
C_p	Average mean heat capacity for the solid and gases
D_i	Statistical intersection diameter
D_o	Particle diameter
E	Activation energy
f_{rb}	Fraction of binder reacted
f_{rox}	Fraction of oxidizer reacted
H_{ex}	Heat of explosion
HMX	Cyclotetramethylene tetranitramine
HTPB	Hydroxyterminated polybutadiene
k	Kinetic rate constant
KN	Potassium nitrate
LN	Lithium nitrate
m	Mass flux associated with propellant components
m_T	Total mass flux of propellant
MW	Molecular weight
n	Pressure exponent of burn rate
P	Pressure
Q	Heat release associated with combustion steps
Q_c	Proportionality constant in the equation for Q_L
Q_{fuel}	Heat of pyrolysis of the fuel binder
Q_f	Heat release in monopropellant flame
Q_L	Heat of gasification of the oxidizer
Q_{LM}	Heat of fusion of the metal
r or r_b	Linear burning rate
R	Gas constant
RDX	Cyclotrimethylene trinitramine
S_o	Total surface area
SN	Sodium nitrate
SST	Separate surface temperature
t	Characteristic time
t_b	Binder burnthrough time
t_{ign}	Ignition delay time
T	Temperature
T_f	Adiabatic flame temperature of the propellant
T_o	Initial temperature of the propellant
v	Gas velocity
x^*	Flame standoff distance
XLDB	Crosslinked double-base
α	Weight fraction oxidizer

α_t	Thermal diffusivity
β_{AP}	Fraction of oxidizer reactants available for final flame
β_f	Fraction of oxidizer reactants involved in the primary diffusion flame
β_p	Fraction of heat transferred from primary flame to oxidizer
γ_{st}	Stoichiometric oxidizer to fuel ratio in primary diffusion flame
ΔT_{loss}	Temperature loss differential from oxidizer to binder
δ_i	Distance from oxidizer to center of adjacent binder
δ	Reaction order
ϕ_{ST}	Stoichiometric oxidizer to fuel ratio
ξ^*	Nondimensional flame standoff distance
σ_p	Temperature sensitivity of burn rate
ρ	Density
λ	Thermal conductivity of gases

Subscripts

Al	Aluminum
b	Fuel binder
Comb	Combustion
DB	Double base
f	Monopropellant flame conditions
fuel	Fuel binder
FF	Final flame conditions
g	Gas
i	Particle size counter
ign	Ignition
j	Oxidizer type counter
MONO	Oxidizer monopropellant flame conditions
o	Initial conditions
ox	Oxidizer
P	Solid propellant
PD	Diffusion part of primary flame
PF	Primary flame
s	Propellant surface conditions

REFERENCES

1. McDonald, A. "Design Evolution of the Space Shuttle Solid Rocket Motors," AIAA-85-1265, 21st AIAA/SAE/ASME/ASEE Joint Propulsion Conference, (1985).
2. Chaiken, R. F., "A Thermal Layer Mechanism of Combustion of Solid Composite Propellants: Application to Ammonium Nitrate Propellants", Combustion and Flame, Vol. 3, (1959), pp. 285-300.
3. Andersen, W. H. , Bills, K. W., Mishuck, E., Moe, G., and Schultz, R. D., "A Model Describing Combustion of Solid Composite Propellants Containing Ammonium Nitrate", Combustion and Flame, Vol. 3, (1959), pp. 301-318.
4. Chaiken, R. F. and Andersen, W.H., "The Role of Binder in Composite Propellant Combustion", ARS Progress in Astronautics and Rocketry Vol I: Solid Propellant Rocket Research, (1960), pp. 141-182.
5. Beckstead, M.W., "A Model for Solid Propellant Combustion", 18th Symposium (International) on Combustion, The Combustion Institute, (1981), pp. 175-183.
6. Beckstead, M. W., "A Model for Solid Propellant Combustion", 14th JANNAF Combustion Meeting, (1977), pp. 281-306.
7. Cohen, N. S., "Review of Composite Propellant Burn Rate Modeling", AIAA J., Vol. 18, No. 3, (1980), pp. 277-293.
8. Cohen, N. S. , and Strand, L.D., "An Improved Model for the Combustion of AP Composite Propellants", AIAA J., Vol. 20, No. 12, (1982), pp. 1739-1746.
9. Gusachenko, L. K. , and Zarko, V.E., "Analysis of Contemporary Models of Steady State Combustion of Composite Solid Fuels", Combustion, Explosions & Shock Waves, Vol. 22, No. 6, (1986), pp. 643-653.
10. Cohen, N.S., Derr, R.L., and Price, C.F., "Extended Model of Solid Propellant Combustion Based on Multiple Flames," 9th JANNAF Combustion Meeting, CPIA Publication 321, (1972), pp. 25-42.
11. Cohen, N. S. and Price, C.F., "Combustion of Nitramine Propellants", J. of Spacecraft and Rockets, Vol 12, (1975), pp. 608-612.
12. Cohen, N. S. , Price, C.F. and Strand, L.D., "Analytical Model of the Combustion of Multicomponent Solid Propellants", AIAA-77-927, (1977),
13. Beckstead, M.W., "Combustion Calculations for Composite Solid Propellants," 13th JANNAF Combustion Meeting, Vol. II, CPIA Publication 281, (1976), p. 299; See also, Beckstead, M.W., Hercules Computer Program No. 64026, Steady State Combustion Program, January 21, 1972.

14. King, M. K., "Model for Steady State Combustion of Unimodal Composite Solid Propellants", AIAA 16th Aerospace Sciences Meeting, AIAA-78-216, (1978).
15. King, M. K., "A Model of the Effects of Pressure and Crossflow Velocity on Composite Propellant Burning Rate", AIAA/SAE/ASME 15th Joint Propulsion Conference, AIAA-79-1171, (1979).
16. King, M. K., "Composite Propellant Combustion Modeling", AIAA/SAE/ASME 16th Joint Propulsion Conference, AIAA-80-1124, (1980).
17. Glick, R. L., "On Statistical Analysis of Composite Solid Propellant Combustion", AIAA J., Vol 12, (1974), pp. 384-385; See also, Glick, R. L., "Statistical Analysis of Non-Metallized Composite Solid Propellant Combustion", 10th JANNAF Combustion Meeting, Vol I, CPIA No 243, (1973), pp. 157-184.
18. Glick, R. L., "Distribution Functions for Statistical Analysis of Monodisperse Solid Propellant Combustion", AIAA J., Vol. 14, (1976), pp. 1631-1633.
19. Condon, J. A. , Glick , R. L. and Osborn, J. R., "Statistical Analysis of Polydisperse, Heterogeneous Propellant Combustion: Nonsteady-State", 13th JANNAF Combustion Meeting, Vol. II, CPIA #281, (1976).
20. Condon, J. A. , Osborn, J. R. and Renie, J. P., "Temperature Sensitivity of Combustion Propellants", 13th JANNAF Combustion Meeting, CPIA #281, (1976), pp. 367-383.
21. Glick, R.L., and Condon, J.A., "Statistical Combustion Modeling: The Effect of Additives," 14th JANNAF Combustion Meeting, CPIA Publication 292, Vol. I, (1977), pp. 341-378.
22. Osborn, J. R. and Renie, J. P., "An Implicit Flame Interaction Combustion Model", 15th JANNAF Combustion Meeting, CPIA #297, Vol. II, (1979).
23. Osborn, J. R. and Renie, J. P., "Combustion Modeling of Aluminized Propellants", AIAA/SAE/ASME 15th Joint Propulsion Conference, AIAA-79-1131, (1979).
24. Glick, R. L., "Statistical Analysis of Steady-State Combustion of Composite Solid Propellants", AIAA/SAE/ASME 15th Joint Propulsion Conference, AIAA-79-1130, (1979).
25. Condon, J. A. , Osborn, J. R. and Renie, J. P., "Oxidizer Size Distribution Effects on Propellant Combustion", AIAA J., Vol. 17, No. 8, (1979), pp. 877-883.
26. Beckstead, M.W., Derr, R.L., and Price, C.F., "A Model of Composite Solid Propellant Combustion Based on Multiple Flames," AIAA J., Vol. 8, No. 4, December 1970, pp. 2200-2207.

27. Beckstead, M.W., Derr, R.L., and Price, C.F., "The Combustion of Solid Monopropellants & Composite Propellants", 13th Symposium (International) on Combustion, The Combustion Institute, 1971, p. 1047.
28. Burke, S.P., and Schumann, T.E.W., "Diffusion Flames," Industrial And Engineering Chemistry, Vol. 20, p. 998, 1928; also First and Second Symposium on Combustion, The Combustion Institute, Pittsburgh, PA, pp. 2-11; 1965.
29. Gladun, V. D. and Frolov, Yu. V., "A Model for Detachment of a Condensed Particle from a Combustion Surface", Combustion, Explosion and Shock Waves, 12, 2, (1976), pp. 191-197.
30. Gladun, V. D. and Frolov, Yu.V., "Coalescence of Powdered Aluminum Particles on Combustion Surface of Metallized Compositions", Combustion, Explosion and Shock Waves, 13, 5, (1977), pp. 705-710.
31. Simonenko, V. N. , Zarko, V.E., Kiskin, A.B., Gladun, V.D., Kashporov, L.Ya. and Silin, N.A., "Stability of the Combustion of Composite Metallized Samples", Combustion, Explosion and Shock Waves, 19, 5, (1983), pp. 62-64.
32. Muhlfeith, C. M. and Thacher, J. H., "Burn Rate Mechanism Studies," Vol. I, AFAL-TR-89-XXX, Hercules, Inc., Magna, Utah, (1989); see also AFAL-TR-88-015, Interim Report, 1988.
33. Beckstead, M.W., "Combustion Mechanisms of Composite Solid Propellants," 19th JANNAF Combustion Meeting, Vol. II, CPIA No. 366, (1982), pp. 93-100.
34. Moore, J.G. and Moore, J., "The Distributions of Temperature and Major Species in Laminar Diffusion Flames," 16th Symposium (Int) on Combustion, The Combustion Institute, Pittsburgh, Penn. (1977), p. 1123-1132.
35. Leining, R. B., Muhlfeith, C. M. and Thacher, J.H., "Aluminum Water Rocket," AFAL-TR-88-051, Hercules, Inc., Magna, Utah, (1988).
36. Boggs, T.L., Zurn, D.E., Cordes, H.F., and Covino, J., "Combustion of Ammonium Perchlorate and Various Inorganic Additives," J. Propulsion, Vol. 4, No. 1, (1988) pp. 27-40.
37. Andersen, W. H. , Bills, K.W., Dekker, A.O., Mishuck, E., Moe, G. and Schultz, R.D., "The Gasification of Solid Ammonium Nitrate", Jet Propulsion, (1958), pp. 831-832.
38. Whittaker, A. G. and Barham, D.C., "Surface Temperature Measurements on Burning Solids," J. Phys. Chem., Vol. 68, No. 1, (1964), pp. 196-199.

39. Girdhar, H. L. and Arora, A.J., "Role of Some Additives on Burning Rate of Phenol-Formaldehyde Composite Propellants", Combustion Science and Technology, 17, (1978), pp. 237-240.
40. Powling, J., "Experiments Relating to the Combustion of Ammonium Perchlorate-Based Propellants", 11th Symposium (International) on Combustion, The Combustion Institute, (1967) pp 447-456.
41. Coates, R.L., "Linear Pyrolysis Rate Measurements of Propellant Constituents", AIAA J., Vol 3, No 7, (1965) pp 1257-1261.
42. Anderson, W. H., and Chaiken, R. F., "On the Detonability of Composite Propellants," American Rocket Society Conference on Solid Propellants, (1961).
43. Beckstead, M. W., "Temperature Sensitivity Verification Study: Vol II, A Model for Double Base Propellant Temperature Sensitivity," AFAL-TR-88-109, (1989).
44. Miller, R.R., Jones, M.L., Foster, R.L., and Condon, J.A. "Ballistic Control of Solid Propellants," Final Report, Vol. I, AFRPL-TR-81-058, April 1982; see also Miller, R.R., Foster, R.L., Beckstead, M.W., and Jones, M.L., "Ballistic Control of Solid Propellants," Interim Report, AFRPL-TR-80-10, November 1980.
45. Beckstead, M.W. and McCarty, K.P., "Calculated Combustion Characteristics of Nitramine Monopropellants", 13th JANNAF Combustion Meeting, Vol. I, (1976), pp. 57-68.
46. Beckstead, M.W., "Model for Double-Base Propellant Combustion", AIAA J., 18,8, (1980), pp. 980-985.
47. Price, C. F. , Boggs, T.L. and Derr, R.L., "Modeling of Solid Monopropellant Deflagration", AIAA-78-219, (1978).
48. Price, C.F., Boggs, T.L., and Derr, R.L., "The Steady-State Combustion Behavior of Ammonium Perchlorate and HMX", AIAA-79-0164, (1979);
49. Combourieu, J., et al., "Ammonium Perchlorate Combustion Analogue: Ammonia-Chlorine Dioxide Flames," AIAA J., Vol. 8, No. 3, (1970), pp. 594-597.
50. Guirao, C., and Williams, F. A., "A Model for Ammonium Perchlorate Deflagration Between 20 and 100 Atm," AIAA J., Vol. 9, (1971), pp. 1345-1356.
51. Barrere, M. and Williams, F. A., "Analytical and Experimental Studies of the Steady-State Combustion Mechanism of Solid Propellants," 25th Meeting of the AGARD Combustion and Propulsion Panel, La Jolla, California (1965).

52. Beckstead, M. W. and Hightower, J. D., "Surface Temperature of Deflagrating Ammonium Perchlorate Crystals," AIAA J., Vol. 5, No.10, (1967), pp. 1785-1790.
53. Mitani, T., and Williams, F.A., "A Model for the Deflagration of Nitramines", SAND86-8230, Sandia National Labs, Livermore, Calif., 1986.
54. Lengelle, G., and Duterque, J., "Combustion Des Propergols a Base D'Octogene", AGARD-CP-391 on Smokeless Propellants (1985) p. 8-1.
55. McCarty, K.P. and Beckstead, M.W., "HMX Propellant Combustion Studies", Final Report, AFRPL-TR-79-61, November 1979; see also, McCarty, K.P., and Beckstead, M.W., "HMX Propellant Combustion Studies", Second Interim Report, AFRPL-TR-78-73, November 1978.
56. Miller, R. R., et. al., "Self-Extinguishing Propellant Development," AFRPL-TR-84-026, Hercules, Inc., Cumberland, MD, April 1984.
57. Shannon, L.J., and Peterson, E.E., "Deflagration Characteristics of Ammonium Perchlorate Strands," AIAA J., Vol. 2, No. 1, Jan. 1964, pp. 168-169.
58. Renie, J. and Cor, J., "A Continuous Surface Regression Model for the Combustion of Composite Solid Propellants," WSS/CA Paper No. 87-11, presented at the Western States Section Meeting, Provo, Utah, 1987.
59. Eldredge, H. B. , Beckstead, M.W. and White, S.C., "Solid Propellant Diffusion Flame Structure", 19th JANNAF Combustion Meeting, CPIA No. 366, Vol I, (1982), pp. 99-108.
60. M. W. Beckstead and N. S. Cohen, "Temperature and Pressure Sensitivity of Composite Propellants," Seventh JANNAF Combustion Conference, CPIA Publication 204, Vol. II, (1971), pp. 85-98.
61. C. H. Burnside, "Effect of Solid Particle Size Distributions on Propellant Temperature Sensitivity," presented at JANNAF Propulsion Meeting, (1976).
62. Condon, J. A. and Glick, R. L., "Statistical Combustion Modeling - The Effect of Additives," 14th JANNAF Combustion Meeting, CPIA #292, Vol. I, (1977) pp. 341-378.
63. D. A. Flanigan, "Investigation of the Mechanism of Solid Propellant Burn Rate," Final Technical Report AFRPL-TR-67-18, Thiokol Chemical Corporation, Huntsville Division, Huntsville, Alabama, (1967).
64. Hercules Incorporated, Combustion of Mechanism of Low Burning Rate Propellant (U), AFRPL-TR-69-130, (1969).
65. Donohue, M., Talley Inc., presentation at AFAL Workshop on Ammonium Nitrate Combustion, November 1987.

APPENDIX A

Computer Test Cases

<u>Test Case</u>	<u>Description</u>
#1	AN Monopropellant test case calculating temperature sensitivity. (Note: A binder must be included for program to run. Use small weight % ~ 0.01)
#2	AN monopropellant data compared statistically with statistics input.
#3	AN/AP/SN/HTPB mixed oxidizer calculation with standard output.
#4	AN/HTPB test case with simplified output.

```

0, 0, 0, 1
'AN MONOPROPELLANT -- TEST CASE'
'AN', 'HTPB'
0.0,0.0,0.0, 0.0,0.0,0.0, 1.0,0.0,0.0, 0.0,0.0,0.0
1.0,1.0,1.0, 1.0,1.0,1.0, 999.,1.0,1.0, 1.0,1.0,1.0
300.0, 0.0, , , , 0.0, 0.0, 0.0
$NAM1 PSTOP=280., $END
$NAM1 NJOB = 3 $END

```

```

0000000001111111112222222223333333333444444444555555555666666666777
12345678901234567890123456789012345678901234567890123456789012

```

13-MAR-89

AN MONOPROPELLANT -- TEST CASE

OXIDIZER DEPENDENT VARIABLES:

TYPE	WT %	DIA(MICRONS)	BDSQ	ARATIO	ERATIO	D0XNUM	DELTA	SFE	DEL
AN 1	99.9	999.00	1.0002	9999.00	9999.00	1.22	0.00	1.000	0.0000

OXIDIZER CONSTANTS:

TYPE	QCOEF	RHOX	AOX	EOX	HINAP	EAP	TMONO	AAP	KAP1
AN	0.290	1.72	4.51E+05	12000.	2.0	25000.	1191.	127.	0.328E-02
	CIGN	TMELT	POWD	TLOSS	FRD	GEOM	HIEAP	TMONOH	HIAAP
	0.00	443.0	2.00	0.00	0.0	0.000	25000.	1191.	182.

MISC PARAMETERS:

CSUBP	XLAMB	AFH	TZERO	BPI	RHOP	BETMIN	BPMIN	BFDIV
0.30	0.0003	3.00	219.	1.50	1.72	0.00	0.10	999999.00

PRESSURE DEPENDENT RESULTS:

OX	P(ATM)/PSI	ROX	TSOX	X*PD	BETAP	BETAF	X*PF	X*AP
		QL	ZAP	ZPF	DNOM1	DNOM2	DNOM3	DNOM4
AN	34.0/ 500.							
1		0.029	492.	0.000	0.001	0.002	0.29	335.7
		-79.2	4.28	0.15	13.485	0.000	0.000	0.000
AN	68.0/ 1000.							
1		0.058	524.	0.000	0.001	0.002	0.17	166.4
		-88.3	4.23	0.15	6.799	0.000	0.000	0.000
AN	136.1/ 2000.							
1		0.114	559.	0.000	0.001	0.002	0.10	81.6
		-98.6	4.07	0.15	3.466	0.000	0.000	0.000

BINDER	RB	TSB	FRB	DELTB	ZP	EXZP	QFUEL
HTPB	0.0296	850.0	0.99	0.0	0.02	10.	433.0 7
HTPB	0.0288	850.0	0.99	0.0	0.01	10.	433.0 6
HTPB	0.0290	850.0	0.99	0.0	0.00	10.	433.0 6

BURN RATE SUMMARY

PTA	RBAR	N	IT	RB	ROX
500.	0.0292	0.00	5	0.0296	0.0292
1000.	0.0579	0.98	6	0.0288	0.0579
2000.	0.1136	0.97	6	0.0290	0.1136

0.370 CPU SECONDS USED

13-MAR-89

AN MONOPROPELLANT -- TEST CASE

OXIDIZER DEPENDENT VARIABLES:

TYPE	WT %	DIA(MICRONS)
AN 1	99.9	999.00

BDSQ	ARATIO	ERATIO	D0XNUM	DELTA	SFE	DEL
1.0002	9999.00	9999.00	1.22	0.00	1.000	0.0000

OXIDIZER CONSTANTS:

TYPE	QCOEF	RHOX	AOX	EOX	HINAP	EAP	TMONO	AAP	KAP1
AN	0.290	1.72	4.51E+05	12000.	2.0	25000.	1247.	127.	0.528E-02
	CIGN	TMELT	POWD	TLOSS	FRD	GEOM	HIEAP	TMONOH	HIAAP
	0.00	443.0	2.00	0.00	0.0	0.000	25000.	1247.	182.

MISC PARAMETERS:

CSUBP	XLAMB	AFH	TZERO	BPI	RHOP	BETMIN	BPMIN	BFDIV
0.30	0.0003	3.00	298.	1.50	1.72	0.00	0.10	999999.00

PRESSURE DEPENDENT RESULTS:

OX	P(ATM)/PSI	ROX	TSOX	X*PD	BETAP	BETAF	X*PF	X*AP	CNVRG
AN	34.0/ 500.	QL	ZAP	ZPF	DNOM1	DNOM2	DNOM3	DNOM4	
1		0.037	496.	0.000	0.001	0.002	0.27	267.8	
		-57.4	4.35	0.15	10.503	0.000	0.000	0.000	2
AN	68.0/ 1000.								
1		0.074	529.	0.000	0.001	0.002	0.16	133.0	
		-66.9	4.31	0.15	5.290	0.000	0.000	0.000	2
AN	136.1/ 2000.								
1		0.148	567.	0.000	0.001	0.001	0.09	66.0	
		-77.9	4.26	0.15	2.665	0.000	0.000	0.000	2

BINDER	RB	TSB	FRB
HTPB	0.0307	850.0	0.99
HTPB	0.0309	850.0	0.99
HTPB	0.0312	850.0	0.99

DELTB	ZP	EXZP	QFUEL
0.0	0.02	10.	433.0 6
0.0	0.00	10.	433.0 6
0.0	0.00	10.	433.0 7

BURN RATE SUMMARY

PTA	RBAR	N	IT	RB	ROX
500.	0.0375	0.00	6	0.0307	0.0375
1000.	0.0744	0.99	6	0.0309	0.0744
2000.	0.1477	0.99	6	0.0312	0.1477

0.180 CPU SECONDS USED

13-MAR-89

AN MONOPROPELLANT -- TEST CASE

OXIDIZER DEPENDENT VARIABLES:

TYPE	WT %	DIA(MICRONS)
AN 1	99.9	999.00

BDSQ	ARATIO	ERATIO	D0XNUM	DELTA	SFE	DEL
1.0002	9999.00	9999.00	1.22	0.00	1.000	0.0000

OXIDIZER CONSTANTS:

TYPE	QCOEF	RHOX	AOX	EOX	HINAP	EAP	TMONO	AAP	KAP1
AN	0.290	1.72	4.51E+05	12000.	2.0	25000.	1282.	127.	0.695E-02
	CIGN	TMELT	POWD	TLOSS	FRD	GEOM	HIEAP	TMONOH	HIAAP
	0.00	443.0	2.00	0.00	0.0	0.000	25000.	1282.	182.

MISC PARAMETERS:

CSUBP	XLAMB	AFH	TZERO	BPI	RHOP	BETMIN	BPMIN	BFDIV
0.30	0.0003	3.00	347.	1.50	1.72	0.00	0.10	999999.00

PRESSURE DEPENDENT RESULTS:

OX	P(ATM)/PSI	ROX	TSOX	X*PD	BETAP	BETAF	X*PF	X*AP
		QL	ZAP	ZPF	DNOM1	DNOM2	DNOM3	DNOM4
AN	34.0/ 500.							
1		0.043	496.	0.000	0.001	0.002	0.26	235.4
		-43.3	4.39	0.15	9.093	0.000	0.000	0.000
AN	68.0/ 1000.							
1		0.086	530.	0.000	0.001	0.002	0.15	116.8
		-53.2	4.35	0.15	4.581	0.000	0.000	0.000
AN	136.1/ 2000.							
1		0.171	569.	0.000	0.001	0.001	0.09	57.9
		-64.5	4.30	0.15	2.309	0.000	0.000	0.000

BINDER	RB	TSB	FRB	DELTB	ZP	EXZP	QFUEL
HTPB	0.0317	850.0	0.99	0.0	0.01	10.	433.0
HTPB	0.0324	850.0	0.99	0.0	0.00	10.	433.0
HTPB	0.0327	850.0	0.99	0.0	0.00	10.	433.0

BURN RATE SUMMARY

PTA	RBAR	N	IT	RB	ROX
500.	0.0433	0.00	7	0.0317	0.0433
1000.	0.0859	0.99	6	0.0324	0.0859
2000.	0.1705	0.99	6	0.0327	0.1705

0.180 CPU SECONDS USED

TEMPERATURE SENSITIVITY DATA BETWEEN -65. AND 165. DEG F

PSI	RATE (IN/SEC)	EXPONENT	SIG P (1/C)	PI K (1/F)	AVE TS(K)
500.	0.038	0.00	0.00307	1.00000	496.6
1000.	0.074	0.99	0.00309	0.14850	530.7
2000.	0.148	0.99	0.00317	0.15789	569.6

COMBUSTION INSTABILITY CHARACTERISTICS USING THE DENISON AND BAUM MODEL
TDIFF = 0.000300 IN.

P=1000. A= 3.9 B=1.40				P=2000. A= 4.1 B=1.17				P= 0. A= 0.0 B=0.00			
FREQ	OMEGA	REAL PC	IMAG	OMEGA	REAL PC	IMAG		OMEGA	REAL PC	IMAG	
100.	34.04	0.67	-0.44	8.64	1.26	-0.49		0.00	0.00	0.00	
200.	68.08	0.48	-0.36	17.29	0.91	-0.55		0.00	0.00	0.00	
300.	102.12	0.39	-0.31	25.93	0.73	-0.51		0.00	0.00	0.00	
400.	136.16	0.33	-0.28	34.57	0.62	-0.47		0.00	0.00	0.00	
500.	170.20	0.30	-0.26	43.21	0.55	-0.44		0.00	0.00	0.00	
600.	204.24	0.27	-0.24	51.86	0.50	-0.41		0.00	0.00	0.00	
700.	238.28	0.25	-0.22	60.50	0.46	-0.39		0.00	0.00	0.00	
800.	272.32	0.24	-0.21	69.14	0.43	-0.37		0.00	0.00	0.00	
900.	306.37	0.22	-0.20	77.79	0.40	-0.35		0.00	0.00	0.00	
1000.	340.41	0.21	-0.19	86.43	0.38	-0.33		0.00	0.00	0.00	
2000.	680.81	0.15	-0.14	172.86	0.26	-0.25		0.00	0.00	0.00	
3000.	1021.22	0.12	-0.11	259.29	0.21	-0.20		0.00	0.00	0.00	
4000.	1361.62	0.10	-0.10	345.72	0.18	-0.18		0.00	0.00	0.00	
5000.	1702.03	0.09	-0.09	432.14	0.16	-0.16		0.00	0.00	0.00	
6000.	2042.44	0.09	-0.08	518.57	0.15	-0.15		0.00	0.00	0.00	
7000.	2382.84	0.08	-0.08	605.00	0.14	-0.14		0.00	0.00	0.00	
8000.	2723.25	0.07	-0.07	691.43	0.13	-0.13		0.00	0.00	0.00	
9000.	3063.66	0.07	-0.07	777.86	0.12	-0.12		0.00	0.00	0.00	

13-MAR-89

AN MONOPROPELLANT -- TEST CASE

OXIDIZER DEPENDENT VARIABLES:

TYPE	WT %	DIA (MICRONS)
AN 1	99.9	999.00

BDSQ	ARATIO	ERATIO	D0XNUM	DELTA	SFE	DEL
1.0002	9999.00	9999.00	1.22	0.00	1.000	0.0000

OXIDIZER CONSTANTS:

TYPE	QCOEF	RHOX	AOX	EOX	HINAP	EAP	TMONO	AAP	KAP1
AN	0.290	1.72	4.51E+05	12000.	2.0	25000.	1191.	127.	0.328E-02
	CIGN	TMELT	POWD	TLOSS	FRD	GEOM	HIEAP	TMONOH	HIAAP
	0.00	443.0	2.00	0.00	0.0	0.000	25000.	1191.	182.

MISC PARAMETERS:

CSUBP	XLAMB	AFH	TZERO	BPI	RHOP	BETMIN	BPMIN	BFDIV
0.30	0.0003	3.00	219.	1.50	1.72	0.00	0.10	999999.00

PRESSURE DEPENDENT RESULTS:

OX	P(ATM)/PSI	ROX	TSOX	X*PD	BETAP	BETAF	X*PF	X*AP	CNVRG
		QL	ZAP	ZPF	DNOM1	DNOM2	DNOM3	DNOM4	
AN	34.0/ 500.	0.029	492.	0.000	0.001	0.002	0.29	335.7	
1		-79.2	4.28	0.15	13.485	0.000	0.000	0.000	2
AN	68.0/ 1000.	0.058	524.	0.000	0.001	0.002	0.17	166.4	
1		-88.3	4.23	0.15	6.799	0.000	0.000	0.000	2
AN	136.1/ 2000.	0.114	559.	0.000	0.001	0.002	0.10	81.6	
1		-98.6	4.07	0.15	3.466	0.000	0.000	0.000	2
AN	204.1/ 3000.	0.174	584.	0.000	0.001	0.002	0.07	51.9	
1		-105.8	3.96	0.16	2.262	0.000	0.000	0.000	2
AN	272.1/ 4000.	0.239	604.	0.000	0.001	0.001	0.06	37.0	
1		-111.6	3.87	0.15	1.648	0.000	0.000	0.000	2
AN	340.1/ 5000.	0.303	620.	0.000	0.001	0.001	0.05	28.7	
1		-116.3	3.81	0.15	1.300	0.000	0.000	0.000	2

BINDER	RB	TSB	FRB
HTPB	0.0286	850.0	0.99
HTPB	0.0288	850.0	0.99
HTPB	0.0290	850.0	0.99
HTPB	0.0310	850.0	0.99
HTPB	0.0312	850.0	0.99
HTPB	0.0366	850.0	0.99

DELTB	ZP	EXZP	QFUEL
0.0	0.02	10.	433.0
0.0	0.01	10.	433.0
0.0	0.00	10.	433.0
0.0	0.00	10.	433.0
0.0	0.00	10.	433.0
0.0	0.00	10.	433.0

BURN RATE SUMMARY

PTA	RBAR	N	IT	RB	ROX
500.	0.0292	0.00	6	0.0286	0.0292
1000.	0.0579	0.98	6	0.0288	0.0579
2000.	0.1136	1.00	6	0.0290	0.1136
3000.	0.1738	1.07	5	0.0310	0.1741
4000.	0.2387	1.08	5	0.0312	0.2389
5000.	0.3012	1.04	4	0.0366	0.3029

0.320 CPU SECONDS USED

13-MAR-89

AN MONOPROPELLANT -- TEST CASE

OXIDIZER DEPENDENT VARIABLES:

TYPE WT % DIA(MICRONS)

AN 1 99.9 999.00

BDSQ	ARATIO	ERATIO	D0XNUM	DELTA	SFE	DEL
1.0002	9999.00	9999.00	1.22	0.00	1.000	0.0000

OXIDIZER CONSTANTS:

TYPE	QCOEF	RHOX	AOX	EOX	HINAP	EAP	TMONO	AAP	KAP1
AN	0.290	1.72	4.51E+05	12000.	2.0	25000.	1247.	127.	0.528E-02

	CIGN	TMELT	POWD	TLOSS	FRD	GEOM	HIEAP	TMONOH	HIAAP
	0.00	443.0	2.00	0.00	0.0	0.000	25000.	1247.	182.

MISC PARAMETERS:

CSUBP	XLAMB	AFH	TZERO	BPI	RHOP	BETMIN	BPMIN	BFDIV
0.30	0.0003	3.00	298.	1.50	1.72	0.00	0.10	999999.00

PRESSURE DEPENDENT RESULTS:

OX	P(ATM)/PSI	ROX	TSOX	X*PD	BETAP	BETAF	X*PF	X*AP	
		QL	ZAP	ZPF	DNOM1	DNOM2	DNOM3	DNOM4	CNVRG
AN	34.0/ 500.								
1		0.037	496.	0.000	0.001	0.002	0.27	267.8	
		-57.4	4.35	0.15	10.503	0.000	0.000	0.000	2
AN	68.0/ 1000.								
1		0.074	529.	0.000	0.001	0.002	0.16	133.0	
		-66.9	4.31	0.15	5.290	0.000	0.000	0.000	2
AN	136.1/ 2000.								
1		0.148	567.	0.000	0.001	0.001	0.09	66.0	
		-77.9	4.26	0.15	2.665	0.000	0.000	0.000	2
AN	204.1/ 3000.								
1		0.228	593.	0.000	0.001	0.001	0.07	42.3	
		-85.6	4.22	0.15	1.726	0.000	0.000	0.000	2
AN	272.1/ 4000.								
1		0.313	615.	0.000	0.001	0.001	0.06	30.2	
		-91.8	4.14	0.15	1.257	0.000	0.000	0.000	2
AN	340.1/ 5000.								
1		0.397	631.	0.000	0.001	0.001	0.05	23.4	
		-96.7	4.06	0.15	0.992	0.000	0.000	0.000	2

BINDER	RB	TSB	FRB	DELTB	ZP	EXZP	QFUEL	
HTPB	0.0302	850.0	0.99	0.0	0.02	10.	433.0	5
HTPB	0.0309	850.0	0.99	0.0	0.00	10.	433.0	6
HTPB	0.0312	850.0	0.99	0.0	0.00	10.	433.0	7
HTPB	0.0334	850.0	0.99	0.0	0.00	10.	433.0	8
HTPB	0.0337	850.0	0.99	0.0	0.00	10.	433.0	8
HTPB	0.0398	850.0	0.99	0.0	0.00	10.	433.0	10

BURN RATE SUMMARY

PTA	RBAR	N	IT	RB	ROX
500.	0.0375	0.00	7	0.0302	0.0375
1000.	0.0744	0.99	6	0.0309	0.0744
2000.	0.1477	1.02	6	0.0312	0.1477
3000.	0.2277	1.08	5	0.0334	0.2281
4000.	0.3129	1.08	5	0.0337	0.3133
5000.	0.3947	1.04	4	0.0398	0.3968

0.340 CPU SECONDS USED

13-MAR-89

AN MONOPROPELLANT -- TEST CASE

OXIDIZER DEPENDENT VARIABLES:

TYPE	WT %	DIA(MICRONS)
AN 1	99.9	999.00

BDSQ	ARATIO	ERATIO	D0XNUM	DELTA	SFE	DEL
1.0002	9999.00	9999.00	1.22	0.00	1.000	0.0000

OXIDIZER CONSTANTS:

TYPE	QCOEF	RHOX	AOX	EOX	HINAP	EAP	TMONO	AAP	KAP1
AN	0.290	1.72	4.51E+05	12000.	2.0	25000.	1282.	127.	0.695E-02
	CIGN	TMELT	POWD	TLOSS	FRD	GEOM	HIEAP	TMONOH	HIAAP
	0.00	443.0	2.00	0.00	0.0	0.000	25000.	1282.	182.

MISC PARAMETERS:

CSUBP	XLAMB	AFH	TZERO	BPI	RHOP	BETMIN	BPMIN	BFDIV
0.30	0.0003	3.00	347.	1.50	1.72	0.00	0.10	999999.00

PRESSURE DEPENDENT RESULTS:

UX	P(ATM)/PSI	ROX	TSOX	X*PD	BETAP	BETAF	X*PF	X*AP
		QL	ZAP	ZPF	DNOM1	DNOM2	DNOM3	DNOM4
AN	34.0/ 500.							
1		0.043	496.	0.000	0.001	0.002	0.26	235.4
		-43.3	4.39	0.15	9.093	0.000	0.000	0.000
AN	68.0/ 1000.							
1		0.086	530.	0.000	0.001	0.002	0.15	116.8
		-53.2	4.35	0.15	4.581	0.000	0.000	0.000
AN	136.1/ 2000.							
1		0.171	569.	0.000	0.001	0.001	0.09	57.9
		-64.5	4.30	0.15	2.309	0.000	0.000	0.000
AN	204.1/ 3000.							
1		0.263	597.	0.000	0.001	0.001	0.07	37.1
		-72.5	4.26	0.15	1.495	0.000	0.000	0.000
AN	272.1/ 4000.							
1		0.364	619.	0.000	0.001	0.001	0.05	26.6
		-79.0	4.23	0.15	1.082	0.000	0.000	0.000
AN	340.1/ 5000.							
1		0.463	637.	0.000	0.001	0.001	0.05	20.8
		-84.2	4.21	0.15	0.850	0.000	0.000	0.000

BINDER	RB	TSB	FRB	DELTB	ZP	EXZP	QFUEL
HTPB	0.0315	850.0	0.99	0.0	0.01	10.	433.0 4
HTPB	0.0324	850.0	0.99	0.0	0.00	10.	433.0 6
HTPB	0.0327	850.0	0.99	0.0	0.00	10.	433.0 7
HTPB	0.0351	850.0	0.99	0.0	0.00	10.	433.0 8
HTPB	0.0353	850.0	0.99	0.0	0.00	10.	433.0 8
HTPB	0.0420	850.0	0.99	0.0	0.00	10.	433.0 10

BURN RATE SUMMARY

PTA	RBAR	N	IT	RB	ROX
500.	0.0433	0.00	8	0.0315	0.0433
1000.	0.0859	0.99	6	0.0324	0.0859
2000.	0.1705	1.02	6	0.0327	0.1705
3000.	0.2629	1.09	5	0.0351	0.2633
4000.	0.3632	1.10	5	0.0353	0.3637
5000.	0.4607	1.07	4	0.0420	0.4633

0.300 CPU SECONDS USED

TEMPERATURE SENSITIVITY DATA BETWEEN -65. AND 165. DEG F

PSI	RATE (IN/SEC)	EXPONENT	SIG P (1/C)	PI K (1/F)	AVE TS(K)
500.	0.038	0.00	0.00307	1.00000	496.6
1000.	0.074	0.99	0.00309	0.14818	530.7
2000.	0.148	1.02	0.00317	-0.09697	569.6
3000.	0.228	1.08	0.00323	-0.02156	597.3
4000.	0.313	1.08	0.00328	-0.02388	619.6
5000.	0.395	1.04	0.00332	-0.04587	637.4

COMBUSTION INSTABILITY CHARACTERISTICS USING THE DENISON AND BAUM MODEL TDIFF = 0.000300 IN#:

P=1000. A= 3.9 B=1.40				P=2000. A= 4.1 B=1.17				P=3000. A= 4.2 B=1.05			
FREQ	OMEGA	REAL PC	IMAG	OMEGA	REAL PC	IMAG	OMEGA	REAL PC	IMAG		
100.	34.04	0.67	-0.44	8.64	1.30	-0.50	3.63	1.82	-0.18		
200.	68.08	0.48	-0.36	17.29	0.94	-0.56	7.27	1.54	-0.58		
300.	102.12	0.39	-0.31	25.93	0.75	-0.53	10.90	1.26	-0.68		
400.	136.16	0.33	-0.28	34.57	0.64	-0.49	14.54	1.07	-0.68		
500.	170.20	0.30	-0.26	43.21	0.57	-0.45	18.17	0.94	-0.66		
600.	204.24	0.27	-0.24	51.86	0.51	-0.42	21.81	0.84	-0.63		
700.	238.28	0.25	-0.22	60.50	0.47	-0.40	25.44	0.77	-0.60		
800.	272.32	0.24	-0.21	69.14	0.44	-0.38	29.07	0.71	-0.58		
900.	306.37	0.22	-0.20	77.79	0.41	-0.36	32.71	0.66	-0.55		
1000.	340.41	0.21	-0.19	86.43	0.39	-0.34	36.34	0.62	-0.53		
2000.	680.81	0.15	-0.14	172.86	0.27	-0.25	72.68	0.42	-0.39		
3000.	1021.22	0.12	-0.11	259.29	0.22	-0.21	109.03	0.34	-0.33		
4000.	1361.62	0.10	-0.10	345.72	0.19	-0.18	145.37	0.29	-0.28		
5000.	1702.03	0.09	-0.09	432.14	0.17	-0.16	181.71	0.26	-0.25		
6000.	2042.44	0.09	-0.08	518.57	0.15	-0.15	218.05	0.23	-0.23		
7000.	2382.84	0.08	-0.08	605.00	0.14	-0.14	254.39	0.22	-0.22		
8000.	2723.25	0.07	-0.07	691.43	0.13	-0.13	290.74	0.20	-0.20		
9000.	3063.66	0.07	-0.07	777.86	0.13	-0.12	327.08	0.19	-0.19		

```

0, 0, 1, 0
'AN MONOPROPELLANT STATISTICAL DATA -- TEST CASE'
, 'AN', , 'HTPB'
1.0,0.0,0.0, , ,0.0
1.0,1.0,1.0, 1.0,1.0,1.0, 999.,1.0,1.0, 1.0,1.0,1.0
298.0, , , ,0.0, 0.0, 0.0
, 298., ,985., ,.067
, , , ,1.0 ,0.0,0.0, , ,0.0
1.0,1.,1., 1.,1.,1., 999.,1.0,1.0, 1.0,1.,1.
298., 1050., ,.079
0.0,0.0,0.0,0.0,0.0,0.0, 1.0 ,0.0,0.0,0.0,0.0,0.0
1.0,1.0,1.0,1.0,1.0,1.0, 999.0 ,1.0,1.0,1.0,1.0,1.0
298., ,988., ,.083
0.0,0.0,0.0,0.0,0.0,0.0, 1.0 ,0.0,0.0,0.0,0.0,0.0
1.0,1.0,1.0,1.0,1.0,1.0, 999.0 ,1.0,1.0,1.0,1.0,1.0
298., ,1500., ,.102
0.0,0.0,0.0,0.0,0.0,0.0, 1.0 ,0.0,0.0,0.0,0.0,0.0
1.0,1.0,1.0,1.0,1.0,1.0, 999.0 ,1.0,1.0,1.0,1.0,1.0
298., ,1500., ,.114
0.0,0.0,0.0,0.0,0.0,0.0, 1.0 ,0.0,0.0,0.0,0.0,0.0
1.0,1.0,1.0,1.0,1.0,1.0, 999.0 ,1.0,1.0,1.0,1.0,1.0
298., ,1750., ,.126
0.0,0.0,0.0,0.0,0.0,0.0, 1.0 ,0.0,0.0,0.0,0.0,0.0
1.0,1.0,1.0,1.0,1.0,1.0, 999.0 ,1.0,1.0,1.0,1.0,1.0
298., ,2000., ,.154
0.0,0.0,0.0,0.0,0.0,0.0, 1.0 ,0.0,0.0,0.0,0.0,0.0
1.0,1.0,1.0,1.0,1.0,1.0, 999.0 ,1.0,1.0,1.0,1.0,1.0
298., ,2000., ,.157
0.0,0.0,0.0,0.0,0.0,0.0, 1.0 ,0.0,0.0,0.0,0.0,0.0
1.0,1.0,1.0,1.0,1.0,1.0, 999.0 ,1.0,1.0,1.0,1.0,1.0
298., ,2500., ,.177
0.0,0.0,0.0,0.0,0.0,0.0, 1.0 ,0.0,0.0,0.0,0.0,0.0
1.0,1.0,1.0,1.0,1.0,1.0, 999.0 ,1.0,1.0,1.0,1.0,1.0
298., ,2500., ,.209
0.0,0.0,0.0,0.0,0.0,0.0, 1.0 ,0.0,0.0,0.0,0.0,0.0
1.0,1.0,1.0,1.0,1.0,1.0, 999.0 ,1.0,1.0,1.0,1.0,1.0
298., ,3000., ,.197
0.0,0.0,0.0,0.0,0.0,0.0, 1.0 ,0.0,0.0,0.0,0.0,0.0
1.0,1.0,1.0,1.0,1.0,1.0, 999.0 ,1.0,1.0,1.0,1.0,1.0
298., ,3000., ,.209
0.0,0.0,0.0,0.0,0.0,0.0, 1.0 ,0.0,0.0,0.0,0.0,0.0
1.0,1.0,1.0,1.0,1.0,1.0, 999.0 ,1.0,1.0,1.0,1.0,1.0
298., ,3000., ,.213
0.0,0.0,0.0,0.0,0.0,0.0, 1.0 ,0.0,0.0,0.0,0.0,0.0
1.0,1.0,1.0,1.0,1.0,1.0, 999.0 ,1.0,1.0,1.0,1.0,1.0
298., ,3500., ,.256
0.0,0.0,0.0,0.0,0.0,0.0, 1.0 ,0.0,0.0,0.0,0.0,0.0
1.0,1.0,1.0,1.0,1.0,1.0, 999.0 ,1.0,1.0,1.0,1.0,1.0
298., ,3500., ,.268
0.0,0.0,0.0,0.0,0.0,0.0, 1.0 ,0.0,0.0,0.0,0.0,0.0
1.0,1.0,1.0,1.0,1.0,1.0, 999.0 ,1.0,1.0,1.0,1.0,1.0
298., ,4000., ,.315
0.0,0.0,0.0,0.0,0.0,0.0, 1.0 ,0.0,0.0,0.0,0.0,0.0
1.0,1.0,1.0,1.0,1.0,1.0, 999.0 ,1.0,1.0,1.0,1.0,1.0
298., ,4000., ,.350
0.0,0.0,0.0,0.0,0.0,0.0, 1.0 ,0.0,0.0,0.0,0.0,0.0
1.0,1.0,1.0,1.0,1.0,1.0, 999.0 ,1.0,1.0,1.0,1.0,1.0
298., ,4800., ,.374
0.0,0.0,0.0,0.0,0.0,0.0, 1.0 ,0.0,0.0,0.0,0.0,0.0
1.0,1.0,1.0,1.0,1.0,1.0, 999.0 ,1.0,1.0,1.0,1.0,1.0
298., ,4800., ,.437
0.0,0.0,0.0,0.0,0.0,0.0, 1.0 ,0.0,0.0,0.0,0.0,0.0
1.0,1.0,1.0,1.0,1.0,1.0, 999.0 ,1.0,1.0,1.0,1.0,1.0
'END',0.0,0.0,0.0

```

```

$NAM1 ISTAT=2, QCOEF(3)=0.28,
$NAM1
$NAM1

```

```
$END
```

```

NJOB = 3 $END
NJOB = 3 $END

```

13-MAR-89

AN MONOPROPELLANT STATISTICAL DATA -- TEST CASE

OXIDIZER DEPENDENT VARIABLES:

TYPE	WT %	DIA(MICRONS)
AN 1	99.9	999.00

OXIDIZER CONSTANTS:

TYPE	QCOEF	RHOX	AOX	EOX	HINAP	EAP	TMONO	AAP	KAP1
AN	0.290	1.72	4.51E+05	12000.	2.0	25000.	1247.	127.	0.528E-02
	CIGN	TMELT	POWD	TLOSS	FRD	GEOM	HIEAP	TMONOH	HIAAP
	0.00	443.0	2.00	0.00	0.0	0.000	25000.	1247.	182.

MISC PARAMETERS:

CSUBP	XLAMB	AFH	TZERO	BPI	RHOP	BETMIN	BPMIN	BFDIV
PSI	TZERO	RBAR	CNVRG	DATA	%ERROR	CNVRG	AN	DIA WT%
985.	298.	0.073	6	0.067	9.4	2	999.100.00	
1050.	298.	0.078	4	0.079	-1.3	2	999.100.00	
988.	298.	0.074	6	0.083	-11.4	2	999.100.00	
1500.	298.	0.111	5	0.102	8.8	2	999.100.00	
1500.	298.	0.111	6	0.114	-2.5	2	999.100.00	
1750.	298.	0.129	4	0.126	2.3	2	999.100.00	
2000.	298.	0.147	4	0.154	-4.4	2	999.100.00	
2000.	298.	0.148	5	0.157	-5.8	2	999.100.00	
2500.	298.	0.183	4	0.177	3.5	2	999.100.00	
2500.	298.	0.184	4	0.209	-11.8	2	999.100.00	
3000.	298.	0.227	4	0.197	15.2	2	999.100.00	
3000.	298.	0.227	4	0.209	8.7	2	999.100.00	
3000.	298.	0.227	4	0.213	6.7	2	999.100.00	
3500.	298.	0.270	4	0.256	5.4	2	999.100.00	
3500.	298.	0.271	5	0.268	1.0	2	999.100.00	
4000.	298.	0.312	4	0.315	-0.9	2	999.100.00	
4000.	298.	0.313	5	0.350	-10.7	2	999.100.00	
4800.	298.	0.378	4	0.374	1.2	2	999.100.00	
4800.	298.	0.379	5	0.437	-13.2	2	999.100.00	

SQUARE OF THE CORRELATION COEFFICIENT FOR THE DATA IS 0.95949

STANDARD ERROR OF ESTIMATE IS 0.0045

NUMBER OF DATA POINTS IS 19

73% OR 14 POINTS ARE WITHIN 10% 100% OR 19 POINTS ARE WITHIN 20%
MAXIMUM DEVIATIONS ARE + 15.2%, AND -13.2%

1.050 CPU SECONDS USED

13-MAR-89

AN MONOPROPELLANT STATISTICAL DATA -- TEST CASE

OXIDIZER DEPENDENT VARIABLES:

TYPE WT % DIA(MICRONS)

AN 1 99.9 999.00

BDSQ	ARATIO	ERATIO	D0XNUM	DELTA	SFE	DEL
1.0002	9999.00	9999.00	1.22	0.00	1.000	0.0000

OXIDIZER CONSTANTS:

TYPE	QCOEF	RHOX	AOX	EOX	HINAP	EAP	TMONO	AAP	KAP1
AN	0.280	1.72	4.51E+05	12000.	2.0	25000.	1247.	150.	0.622E-02
	CIGN	TMELT	POWD	TLOSS	FRD	GEOM	HIEAP	TMONOH	HIAAP
	0.00	443.0	2.00	0.00	0.0	0.000	25000.	1247.	218.

MISC PARAMETERS:

CSUBP	XLAMB	AFH	TZERO	BPI	RHOP	BETMIN	BPMIN	BFDIV
0.30	0.0003	3.00	298.	1.50	1.72	0.00	0.10	999999.00
PSI	TZERO	RBAR	CNVRG	DATA	%ERROR	CNVRG	AN	DIA WT%
985.	298.	0.075	6	0.067	12.4	2		999.100.00
1050.	298.	0.080	4	0.079	1.2	2		999.100.00
988.	298.	0.076	6	0.083	-9.0	2		999.100.00
1500.	298.	0.113	5	0.102	10.5	2		999.100.00
1500.	298.	0.113	6	0.114	-1.0	2		999.100.00
1750.	298.	0.130	4	0.126	3.5	2		999.100.00
2000.	298.	0.148	4	0.154	-3.6	2		999.100.00
2000.	298.	0.149	5	0.157	-5.1	2		999.100.00
2500.	298.	0.184	4	0.177	3.7	2		999.100.00
2500.	298.	0.185	4	0.209	-11.6	2		999.100.00
3000.	298.	0.227	4	0.197	15.0	2		999.100.00
3000.	298.	0.227	4	0.209	8.6	2		999.100.00
3000.	298.	0.227	4	0.213	6.5	2		999.100.00
3500.	298.	0.269	4	0.256	5.1	2		999.100.00
3500.	298.	0.270	5	0.268	0.7	2		999.100.00
4000.	298.	0.311	4	0.315	-1.2	2		999.100.00
4000.	298.	0.312	5	0.350	-10.9	2		999.100.00
4800.	298.	0.377	4	0.374	0.9	2		999.100.00
4800.	298.	0.378	5	0.437	-13.5	2		999.100.00

SQUARE OF THE CORRELATION COEFFICIENT FOR THE DATA IS 0.95804

STANDARD ERROR OF ESTIMATE IS 0.0046

NUMBER OF DATA POINTS IS 19

68% OR 13 POINTS ARE WITHIN 10% 100% OR 19 POINTS ARE WITHIN 20%
 MAXIMUM DEVIATIONS ARE + 15.0%, AND -13.5%


```

0, 0, 0, 1
'AN/AP/SN MIXED OXIDIZER TEST CASE'
'AP', , 'AN', 'SN', 'HTPB'
0.0001, 0.0, 0.0, 0.0, .0, .0, 0.39, 0.39, 0.0, 0.0001, 0.0, 0.0
5., 1.0, 1.0, 20., 1.0, 1.0, 50., 50., 1.0, 200., 1.0, 1.0
298.0, 0.0, , 0.0, 0.0, 0.0, , 0.12, , 0.0, 0.0, 0.0
$NAM1 ALF(3,1)=0.4, ALF(3,2)=0.4, DZERO(3,1)=150., CATCON(3)=0.02, $END
$NAM1 ALF(3,1)=0.32, ALF(3,2)=0.32, ALF(1,1)=0.1, ALF(4,1)=0.1, $END
$NAM1 NJOB = 3 $END
$NAM1 NJOB = 3 $END

00000000011111111122222222223333333333444444444455555555556666666666777
123456789012345678901234567890123456789012345678901234567890123456789012

```

PAGES 100, 101
ARE
MISSING
IN
ORIGINAL
DOCUMENT

13-MAR-89

AN/AP/SN MIXED OXIDIZER TEST CASE

OXIDIZER DEPENDENT VARIABLES:

TYPE	WT %	DIA (MICRONS)	BDSQ	ARATIO	ERATIO	DØXNUM	DELTA	SFE	DEL
AP 1	0.0	5.00	8.2904	0.30	5.70	0.939E-04	0.90	0.002	0.2205
AN 1	40.0	150.00	1.2143	8.92	2.83	0.426	6.94	0.785	0.056
2	40.0	50.00	1.6430	2.97	10.40	0.426	4.01	0.214	0.0
SN 1	0.0	200.00	1.2113	11.89	5.20	0.810E-04	9.19	0.000	0.0

OXIDIZER CONSTANTS:

TYPE	QCOEF	RHOX	AOX	EOX	HINAP	EAP	TMONO	AAP	KAP1
AP	0.200	1.95	3.22E+08	30000.	1.7	15000.	1413.	365.	1.75
	CIGN	TMELT	POWD	TLOSS	FRD	GEOM	HIEAP	TMONOH	HI AAP
	4.32	865.0	1.70	1.00	900.0	0.200	15000.	1413.	12 1.
AN	0.290	1.72	4.51E+05	12000.	2.0	25000.	1247.	127.	0.528 E-02
	CIGN	TMELT	POWD	TLOSS	FRD	GEOM	HIEAP	TMONOH	HI AAP
	0.50	443.0	1.70	1.00	100.0	0.300	25000.	1247.	1.02.
SN	0.260	2.26	1.15E+02	4500.	2.0	25000.	999.	800.	0.27 1E-02
	CIGN	TMELT	POWD	TLOSS	FRD	GEOM	HIEAP	TMONOH	HI AAP
	0.10	580.0	1.70	1.00	100.0	0.300	25000.	999.	97.3

HTPB BINDER CONSTANTS:

QFUEL	RHOF	AF	EF	CSUBPB	ALFF
433.0	0.90	6.74E+02	10200.	0.43	0.180

CATALYST PROPERTIES:

OX	CONC	ECAT	ACAT	CATK	AAA	CATSSA	XNC1
AN	0.020	10000.	183.6		0.1000	0.1200	1.00
			1)	0.22			
			2)	1.00			

MISC PARAMETERS:

CSUBP	XLAMB	AFH	TZERO	BPI	RHOP	BETMIN	BPMIN	BFDIV
0.30	0.0003	3.00	298.	1.50	1.49	0.30	0.10	0.10

PRIMARY FLAME CONSTANTS:

QPF	KPF	TPF (K)	XNPF	APF	EPF	X*PD	STOIC	FROXM
261.	0.784	1169.	2.00	500.	15000.	1.45	5.70	1.00
273.	0.507E-01	1266.	1.50	2.70	10000.	70.07	10.40	1.00
491.	0.232	2050.	1.50	2.70	10000.	7.11	10.40	1.00
626.	0.327	2385.	1.50	2.70	10000.	65.69	5.20	1.00

PRESSURE DEPENDENT RESULTS:

OX	P (ATM)/PSI	RØX	TSØX	X*PD	BETAP	BETAF	X*PF	X*AP
	QL	ZAP	ZPF	DNOM1	DNOM2	DNOM3	DNOM4	CNVRG
AP	34.0/ 500.							
1		0.130	897.	1.446	0.542	0.999	11.70	2050.3
AN		-119.8	5.99	0.93	3.032	0.213	3.773	267.284
1		0.036	493.	70.075	0.658	0.950	103.45	497.0
		-56.7	5.78	2.72	9.862	0.237	0.971	0.991
2		0.137	562.	7.108	0.499	0.950	71.41	1907.7
SN		-76.6	5.78	5.56	2.872	0.124	1.681	2.970
1		0.057	831.	65.694	0.542	0.999	54.29	1043.5
		-138.6	5.99	2.92	6.907	0.065	0.964	0.742
AP	68.0/ 1000.							
1		0.286	943.	1.446	0.542	0.999	4.93	1128.3

AN		-129.0	5.99	0.91	1.377	0.126	2.593	125.983	2
1		0.059	517.	70.075	0.658	0.950	62.65	204.2	2
		-63.4	5.05	2.91	5.773	0.134	0.667	0.467	2
2		0.213	589.	7.108	0.499	0.950	44.71	741.4	2
SN		-84.4	5.78	5.42	1.848	0.073	1.155	1.400	2
1		0.082	1026.	65.694	0.542	0.999	26.42	374.8	2
		-189.3	5.99	2.62	4.808	0.039	0.662	0.350	2
AP	136.1/ 2000.								
1		0.600	991.	1.446	0.542	0.999	2.05	592.0	2
AN		-138.7	5.99	0.88	0.656	0.079	1.871	65.854	2
1		0.096	542.	70.075	0.658	0.950	36.25	83.7	2
		-70.8	3.43	3.16	3.577	0.085	0.481	0.244	2
2		0.337	620.	7.108	0.499	0.950	27.75	293.0	2
SN		-93.3	5.77	5.38	1.169	0.046	0.834	0.732	2
1		0.107	1259.	65.694	0.542	0.999	11.84	122.7	2
		-249.8	5.99	2.36	3.672	0.024	0.478	0.183	2

BINDER	RB	TSB	FRB	DELTB	ZP	EXZP	QFUEL	
HTPB	0.0460	922.9	0.05	0.0	0.02	8.	433.0	4
			0.81	51.4	1.07	391.	433.0	
			0.27	17.9	0.16	1158.	433.0	
			0.99	0.0	0.28	0.	433.0	
HTPB	0.0669	1001.3	0.05	0.0	0.01	8.	433.0	4
			0.81	50.9	0.92	464.	433.0	
			0.27	17.3	0.14	1164.	433.0	
			0.99	0.0	0.28	0.	433.0	
HTPB	0.0928	1085.6	0.05	0.0	0.01	9.	433.0	3
			0.81	47.3	0.76	541.	433.0	
			0.27	15.4	0.11	1182.	433.0	
			0.99	0.0	0.31	0.	433.0	

BURN RATE SUMMARY							
PTA	RBAR	N	IT	RB	ROX		
500.	0.0461	0.00	8	0.0460	0.1299	0.0357	0.1371 0.0570
1000.	0.0789	0.73	7	0.0669	0.2859	0.0587	0.2131 0.0819
2000.	0.1267	0.68	7	0.0928	0.5999	0.0963	0.3367 0.1072

0.790 CPU SECONDS USED

13-MAR-89

AN/AP/SN MIXED OXIDIZER TEST CASE

OXIDIZER DEPENDENT VARIABLES:

TYPE	WT %	DIA(MICRONS)	BDSQ	ARATIO	ERATIO	DØXNUM	DELTA	SFE	DEL
AP	1	10.0	5.00						
AN	1	32.0	150.00	3.0896	1.04	5.70 0.100	0.48	0.441	0.1180
	2	32.0	50.00	1.0614	31.11	3.58 0.363	3.72	0.408	0.0304
SN	1	10.0	200.00	1.1843	10.37	10.40 0.363	2.15	0.141	0.0526
				1.0606	41.48	5.20 0.864E-01	4.92	0.011	0.0301

OXIDIZER CONSTANTS:

TYPE	QCOEF	RHOX	AOX	EOX	HINAP	EAP	TMONO	AAP	KAP1
AP	0.200	1.95	3.22E+08	30000.	1.7	15000.	1413.	365.	1.75
		CIGN	TMELT	POWD	TLOSS	FRD	GEOM	HIEAP	TMONOH
		4.32	865.0	1.70	1.00	900.0	0.200	15000.	1413.
AN	0.290	1.72	4.51E+05	12000.	2.0	25000.	1247.	127.	0.528E-01
		CIGN	TMELT	POWD	TLOSS	FRD	GEOM	HIEAP	TMONOH
		0.50	443.0	1.70	1.00	100.0	0.300	25000.	1247.
SN	0.260	2.26	1.15E+02	4500.	2.0	25000.	999.	800.	0.271E-01
		CIGN	TMELT	POWD	TLOSS	FRD	GEOM	HIEAP	TMONOH
		0.10	580.0	1.70	1.00	100.0	0.300	25000.	999.

HTPB BINDER CONSTANTS:

QFUEL	RHOF	AF	EF	CSUBPB	ALFF
433.0	0.90	6.74E+02	10200.	0.43	0.140

CATALYST PROPERTIES:

OX	CONC	ECAT	ACAT	CATK	AAA	CATSSA	XNC1
AN	0.020	10000.	183.6		0.1000	0.1200	1.00
			1)	0.24			
			2)	1.00			

MISC PARAMETERS:

CSUBP	XLAMB	AFH	TZERO	BPI	RHOP	BETMIN	BPMIN	BFDIV
0.30	0.0003	3.00	298.	1.50	1.59	0.30	0.10	0.10

PRIMARY FLAME CONSTANTS:

QPF	KPF	TPF(K)	XNPF	APF	EPF	X*PD	STOIC	FROXM
269.	0.989	1213.	2.00	500.	15000.	1.56	5.70	1.00
288.	0.568E-01	1303.	1.50	2.70	10000.	97.81	10.40	1.00
499.	0.232	2050.	1.50	2.70	10000.	7.11	10.40	1.00
616.	0.327	2385.	1.50	2.70	10000.	64.35	5.20	1.00

PRESSURE DEPENDENT RESULTS:

OX	P(ATM)/PSI	RØX	TSOX	X*PD	BETAP	BETAF	X*PF	X*AP
AP	34.0/ 500.	QL	ZAP	ZPF	DNOM1	DNOM2	DNOM3	DNOM4
AN		0.116	890.	1.555	0.515	0.950	7.81	1825.4
		-118.5	5.72	0.95	3.405	0.138	0.695	9.344
		0.035	493.	97.814	0.631	0.950	88.54	492.9
		-56.6	5.78	2.43	4.997	0.078	0.179	0.035
SN		0.128	558.	7.108	0.499	0.950	66.60	1779.4
		-75.4	5.78	4.87	3.079	0.080	0.310	0.104
		0.055	819.	64.354	0.515	0.950	50.24	1015.3
		-135.6	5.71	2.98	7.099	0.042	0.178	0.026
AP	68.0/ 1000.							
		0.251	935.	1.555	0.515	0.950	3.28	992.5

AN		-127.5	5.71	0.96	1.566	0.082	0.445	3.780	2
1		0.058	516.	97.815	0.631	0.950	54.18	200.5	
		-63.2	4.84	2.70	3.185	0.047	0.115	0.014	2
2		0.198	584.	7.108	0.499	0.950	41.59	689.6	
SN		-83.0	5.78	4.72	1.987	0.047	0.198	0.042	2
1		0.079	1003.	64.354	0.515	0.950	24.27	362.0	
		-183.3	5.71	2.58	4.977	0.025	0.114	0.011	2
AP	136.1/ 2000.								
1		0.514	981.	1.555	0.515	0.950	1.32	507.4	
AN		-136.6	5.72	0.95	0.766	0.051	0.322	1.977	2
1		0.085	536.	97.815	0.631	0.950	28.53	73.8	
		-68.9	2.67	2.67	2.025	0.028	0.083	0.007	2
2		0.315	615.	7.108	0.499	0.950	25.97	274.2	
SN		-91.9	5.78	4.74	1.249	0.030	0.144	0.022	2
1		0.104	1230.	64.354	0.515	0.950	10.97	119.5	
		-242.4	5.71	2.26	3.770	0.016	0.082	0.005	2
BINDER	RB	TSB	FRB		DELTB	ZP	EXZP	QFUEL	
HTPB	0.1337	1194.3	0.17		25.4	0.22	1604.	433.0	3
			0.99		22.4	8.00	0.	433.0	
			0.95		10.2	1.34	237.	433.0	
			0.99		0.5	2.46	4.	433.0	
HTPB	0.2086	1362.6	0.17		26.5	0.12	1778.	433.0	4
			0.99		22.9	8.00	0.	433.0	
			0.95		10.4	1.36	230.	433.0	
			0.99		0.6	2.76	3.	433.0	
HTPB	0.2883	1520.0	0.17		27.0	0.07	1874.	433.0	2
			0.99		22.3	8.00	0.	433.0	
			0.95		10.1	1.11	293.	433.0	
			0.99		0.6	3.06	2.	433.0	
BURN RATE SUMMARY									
PTA	RBAR	N	IT	RB	ROX				
500.	0.0756	0.00	6	0.1337	0.1156	0.0354	0.1279	0.0555	
1000.	0.1281	0.71	6	0.2086	0.2515	0.0576	0.1982	0.0791	
2000.	0.2023	0.66	6	0.2883	0.5142	0.0849	0.3151	0.1044	

0.690 CPU SECONDS USED

```

0, 0, 0, 0
'AN/HTPB' TEST CASE
'AN', 'HTPB'
0.0 , 0.0, 0.0, 0.0, .0 , 0.39, 0.39, 0.0, 0.0, 0.0, 0.0
5., 1.0, 1.0, 20., 1.0, 1.0, 150., 50., 1.0, 200., 1.0, 1.0
298.0, 0.0, 0.0, 0.0, 0.0, 0.12, 0.0, 0.0, 0.0
$NAM1 CATCON(3)=0.01, ALF(3,1)=0.385, ALF(3,2)=0.385,
$NAM1 ATCON(3)=0.02, ALF(3,1)=0.38, ALF(3,2)=0.38
$NAM1 NJOB = 3 $END
$NAM1 NJOB = 3 $END

```

```

000000000111111111222222222233333333334444444455555555556666666666777
123456789012345678901234567890123456789012345678901234567890123456789012

```

13-MAR-89 AN/HTPB TEST CASE

OXIDIZER DEPENDENT VARIABLES:

TYPE	WT %	DIA(MICRONS)
AN 1	39.0	150.00
2	39.0	50.00

TZERO=298.

BURN RATE SUMMARY

PTA	RBAR	N	IT	RB	ROX
500.	0.0263	0.00	9	0.0299	0.0270 0.1108
1000.	0.0456	0.82	9	0.0405	0.0497 0.1862
2000.	0.0814	0.84	8	0.0585	0.0888 0.3100

0.540 CPU SECONDS USED

13-MAR-89 AN/HTPB TEST CASE

OXIDIZER DEPENDENT VARIABLES:

TYPE	WT %	DIA(MICRONS)
AN 1	38.5	150.00
2	38.5	50.00

TZERO=298.

BURN RATE SUMMARY

PTA	RBAR	N	IT	RB	ROX
500.	0.0285	0.00	9	0.0299	0.0322 0.1289
1000.	0.0505	0.80	8	0.0428	0.0559 0.2081
2000.	0.0859	0.77	8	0.0595	0.0970 0.3357

0.370 CPU SECONDS USED

13-MAR-89 AN/HTPB TEST CASE

OXIDIZER DEPENDENT VARIABLES:

TYPE	WT %	DIA(MICRONS)
AN 1	38.0	150.00
2	38.0	50.00

TZERO=298.

BURN RATE SUMMARY

PTA	RBAR	N	IT	RB	ROX
500.	0.0307	0.00	9	0.0307	0.0364 0.1442
1000.	0.0539	0.77	8	0.0441	0.0614 0.2272
2000.	0.0890	0.72	8	0.0598	0.1045 0.3588

0.430 CPU SECONDS USED

APPENDIX B

Composite Propellant Modeling Bibliography

Composite Propellant Modeling Bibliography

1988

Deur, J. M. and Price, E. W., "A Surface Coupled Flamelet Approach to Dynamic Response in Heterogeneous Propellant Combustion", AIAA-88-2938, (1988),
NOTE: Apply the KLLEF model to unstable combustion. A very unrealistic physical model.

1987

Margolis, S. B. and Williams, F. A., "Influences of Two-Phase Flow in the Deflagration of Homogeneous Solids", Combustion and Flame, 67, (1987), pp. 249-258.

Kerstein, A. R., "Percolation Model of Polydisperse Composite Solid Propellant Combustion", Combustion and Flame, 69, (1987), pp. 95-112.

1986

Mitani, T. and Williams, F. A., "A Model for the Deflagration of Nitramines", SAND86-8230, (1986),

Gusachenko, L. K., and Zarko, V. E., "Analysis of Contemporary Models of Steady State Combustion of Composite Solid Fuels", Combustion, Explosions & Shock Waves, Vol. 22, No. 6, (1986), pp. 643-653.

NOTE: Russian review of solid propellant modeling. 64 refs - really quite good.

1985

Gusachenko, L. K., "Use of the Burke-Schumann Diffusion Flame Solution for Description of Combustion of Solids", Combustion, Explosion & Shock Waves, Vol. 21, No. 2, (1985), pp. 41-45.

Cohen, N. S., "A Review of Models and Mechanisms for Pressure Exponent Breaks in Composite Solid Propellants", Report to UTCS, (1985), NOTE: Classical Cohen review. Excellent!

Cohen, N. S. and Flanigan, D. A., "Mechanisms and Models of Solid-Propellant Burn Rate Temperature Sensitivity: A Review", AIAA Journal, Vol. 23, No. 10, (1985),

Blomshield, F. S. and Osborn, J. R., "Effect of Variable Solid Phase Thermal Properties on Propellant Combustion", Acta Astronautica, Vol. 12, No. 12, (1985), pp. 1017-1025.

1982

Price, C. F., Boggs, T. L., Parr, T. P. and Parr, D. M., "A Modified BDP Model Applied to the Self-Deflagration of HMX", 19th JANNAF Combustion Meeting, Vol I, CPIA No. 366, (1982), pp. 299-310.

NOTE: Considers both exothermic and endothermic condensed phase reactions. Compare model with extensive temperature sensitivity data.

Parr, T. P., Parr, D. M., Boggs, T. L. and Price, C. F., "Modeling of the Temperature Sensitivity of HMX Burning Rates Using the Simple BDP Model", 19th JANNAF Combustion Meeting, Vol I, CPIA No. 366, (1982), pp. 289-297.

NOTE: Used original BDP model to try to match HMX data.

Miller, R. R., "A Framework for a Totally Statistical Composite Propellant Combustion Model", 19th JANNAF Combustion Meeting, CPIA Publication 366, Vol. II, (1982),

Eldredge, H. B. , Beckstead, M.W. and White, S.C., "*Solid Propellant Diffusion flame Structure*", 19th JANNAF Combustion Meeting, CPIA No. 366, Vol I, (1982), pp. 99-108.
NOTE: 2-D calculations of diffusion flame shapes.

Cohen, N. S. , and Strand, L.D., "*An Improved Model for the Combustion of AP Composite Propellants*", AIAA J., Vol. 20, No. 12, (1982), pp. 1739-1746.

Beckstead, M. W., "*A Model for Composite Modified Double Base Propellants*", AIAA 20th Aerospace Sciences Conference, AIAA-82-0355, (1982),

Beckstead, M. W. and McCarty, K. P., "*Modeling Calculations for HMX Composite Propellants*", AIAA Journal, Vol. 20, No. 1, (1982), pp. 106-115.

1981

Beckstead, M. W., "*A Model for Solid Propellant Combustion*", 18th Symposium (International) on Combustion, (1981), pp. 175-185.

NOTE: SST model applied to HMX composite propellants.

1980

Cohen, N. S. and Strand, L. D., "*An Improved Model for the Combustion of AP Composite Propellants*", 17th JANNAF Combustion Meeting, CPIA #329, (1980), pp. 53-97.

NOTE: See also AIAA J., Dec 1982.

Cohen, N. S., "*Review of Composite Propellant Burn Rate Modeling*", AIAA Journal, Vol. 18, No. 3, (1980), pp. 277-293.

NOTE: Excellent review of BDP , PEM, Cohen and King models.

BenReuven, M. and Summerfield, M., "*Analysis of Solid Propellant Combustion in a Closed Vessel Including Secondary Reaction*", 17th JANNAF Combustion Meeting, Vol. II, CPIA 329, (1980).

1979

Price, C. F. , Boggs, T.L. and Derr, R.L., "*The Steady-State Combustion Behavior of Ammonium Perchlorate and HMX*", AIAA-79-0164, (1979),

Osborn, J. R. and Renie, J. P., "*An Implicit Flame Interaction Combustion Model*", 15th JANNAF Combustion Meeting, CPIA #297, Vol. II, (1979),

Osborn, J. R. and Renie, J. P., "*Combustion Modeling of Aluminized Propellants*", AIAA/SAE/ASME 15th Joint Propulsion Conference, AIAA-79-1131, (1979),

Kishore, K., "*Comprehensive View of the Combustion Models of Composite Solid Propellants*", AIAA Journal, Vol. 17, No. 11, (1979), pp. 1216-1224.

NOTE: Not a very comprehensive view!

King, M. K., "*A Model of the Effects of Pressure and Crossflow Velocity on Composite Propellant Burning Rate*", AIAA/SAE/ASME 15th Joint Propulsion Conference, AIAA-79-1171, (1979),

Glick, R. L., "*Statistical Analysis of Steady-State Combustion of Composite Solid Propellants*", AIAA/SAE/ASME 15th Joint Propulsion Conference, 79-1130, (1979),

Condon, J. A. , Osborn, J. R. and Renie, J. P., "*Oxidizer Size Distribution Effects on Propellant Combustion*", AIAA Journal, Vol. 17, No. 8, (1979), pp. 877-883.

1978

Price, C. F. , Boggs, T.L. and Derr, R.L., "*Modeling of Solid Monopropellant Deflagration*", AIAA-78-219, (1978), NOTE: Monopropellant model for AP and HMX. Considers 2 parallel reactions and integrates the flame zone numerically.

King, M. K., "*Model for Steady State Combustion of Unimodal Composite Solid Propellants*", AIAA 16th Aerospace Sciences Meeting, AIAA-78-216, (1978),

Condon, J. A. and Osborn, J. R., "*The Effect of Oxidizer Particle Size Distribution on the Steady and Nonsteady Combustion of Composite Propellants*", AFRPL-TR-78-17, (1978).

1977

Condon, J. A. , Osborn, J. R. and Renie, J. P., "*Oxidizer Size Distribution Effects*", 14th JANNAF Combustion Meeting, CPIA #292, (1977), pp. 325.
NOTE: See AIAA J Aug 1979 pp.877-883.

Condon, J. A. and Glick, R. L., "*Statistical Combustion Modeling - The Effect of Additives*", 14th JANNAF Combustion Meeting, CPIA #292, (1977), pp. 341-378.

Cohen, N. S. , Price, C.F. and Strand, L.D., "*Analytical Model of the Combustion of Multicomponent Solid Propellants*", AIAA-77-927, (1977),

Beckstead, M. W., "*A Model for Solid Propellant Combustion*", 14th JANNAF Combustion Meeting, (1977), pp. 281-306.
NOTE: The SST approach and application to aluminized AP composite propellants.

1976

Condon, J. A. , Glick , R. L. and Osborn, J. R., "*Statistical Analysis of Polydisperse, Heterogeneous Propellant Combustion: Nonsteady-State*", 13th JANNAF Combustion Meeting, Vol. II, CPIA #281, (Dec. 1976), pp. 313-345.

Kumar, R. N. , McNamara, R. P., and Strand, L. D., "*Composite Propellant Combustion Modeling with a Porous Plate Burner*", AIAA/SAE 12th Propulsion Conference, AIAA Paper No. 76-669, (1976),

Glick, R. L., "*Distribution Functions for Statistical Analysis of Monodisperse Solid Propellant Combustion*", AIAA J., Vol. 14, (1976), pp. 1631-1633.

Condon, J. A. , Osborn, J. R. and Renie, J. P., "*Temperature Sensitivity of Composite Propellants*", 13th JANNAF Combustion Meeting, Vol. II, CPIA #281, (1976), pp. 367-383.

Beckstead, M. W., "*Combustion Calculations for Composite Solid Propellants*", 13th JANNAF Combustion Meeting, Vol. II, (1976), pp. 299-312.

NOTE: Extends the original BDP model to multimodal propellants, and compares calculations to Miller's data. Makes a priori prediction of the temperature sensitivity of Miller's propellants.

Beckstead, M. W. and McCarty, K. P., "*Calculated Combustion Characteristics of Nitramine Monopropellants*", 13th JANNAF Combustion Meeting, Vol. I, (1976), pp. 57-68.

1975

Ilyukhin, V. S. , Margolin, A. D., Mysov, V. G., and Nonikov, S. S, "*Role of Heterogeneity of Composite Solid Fuels in the Mechanism of Pulsation Burning*", Combustion, Explosion & Shock Waves, Vol. II, No. 3, (1975), pp. 498-501.

Cohen, N. S. and Price, C.F., "*Combustion of Nitramine Propellants*", J. of Spacecraft and Rockets, Vol 12, (1975), pp. 608-612.

1974

Hamann, R. J., "*Three Solid Propellant Combustion Models A Comparison and Some Applications to Non-steady Cases*", Memorandum M-215, (1974), NOTE: Compares Von Elbe's model, the Granular Diffusion Flame Model and the BDP Model.

Glick, R. L., "*On Statistical Analysis of Composite Solid Propellant Combustion*", AIAA J., Vol 12, (1974), pp. 384-385.

1973

Kumar, R. N., "*Condensed Phase Details in the Time-Independent Combustion of AP/Composite Propellants*", Combustion Science and Technology, Vol. 8, (1973), pp. 133-148.

NOTE: Applies a polymer fragmentation type model to AP. Doesn't appear to be very logical.

Glick, R. L., "*Statistical Analysis of Non-Metallized Composite Solid Propellant Combustion*", 10th JANNAF Combustion Meeting, Vol I, CPIA No 243, (1973), pp. 157-184.

1972

Fisher, E. B., Graves, K. W., "*Mathematical Model of Double Base Propellant Ignition and Combustion in the 81 mm Mortar*", CAL Report No. DG-3029-D-1, (1972).

1971

Stamets, L. E. and Weiss, R. R., "*Analytical Models of Solid Propellant Combustion*", Twenty-Second International Astronautical Congress, Brussels, Belgium, (1971),

Coates, R. L., "*An Analysis of a Simplified Laminar Flame Theory for Solid Propellant Combustion*", Combustion Science and Technology, Vol. 4, (1971), pp. 1-8.

Beckstead, M. W. , Derr, R. L. and Price, C. F., "*The Combustion of Solid Monopropellants and Composite Propellants*", Reprinted from 13th Symposium (International) on Combustion, The Combustion Institute, Pittsburgh, PA, (1971), pp. 1047-1056.

Beckstead, M. W. and Cohen, N. S., "*Temperature and Pressure Sensitivity of Composite Propellants*", 7th JANNAF Combustion Conference, Vol. II, CPIA #204, (1971), pp. 85-98.

1970

Beckstead, M. W. , Derr, R. L., and Price, C. F., "*A Model of Composite Solid Propellant Combustion Based on Multiple Flames*", AIAA Journal, Vol. 8, No. 4, (1970), pp. 2200-2207.

NOTE: The classic BDP paper!

1969

Waesche, R. H. W., and Wenograd, J., "*Calculation of Solid Propellant Burning Rates from Condensed-Phase Decomposition Kinetics*", AIAA Seventh Aerospace Science Meeting, AIAA-69-145, (1969),

Merzhanov, A. G., "*The Theory of Stable Homogeneous Combustion of Condensed Substances*", Combustion and Flame, Vol. 13, No. 2, (1969), pp. 143-156.

Chaiken, R. F., "*Implications of a Steady-State Solid Propellant Combustion Model to a Low Pressure Deflagration Limit*", Presented at The Combustion Institute, Western States Section Spring Meeting, WSCI-69-5, (1969).

1968

Fenn, J. B., "*A Phalanx Flame Model for the Combustion of Composite Solid Propellants*", Combustion and Flame, Vol. 12, No. 3, (1968), pp. 201.

Caveny, L. H. and Pittman Jr., C. U., "*Contribution of Solid-Phase Heat Release to AP Composite-Propellant Burning Rate*", AIAA Journal, Vol. 6, No. 8, (1968), pp. 1461-1467.

1967

Hermance, C. E., "*A Detailed Model of the Combustion of Composite Solid Propellants*", Proceedings of the ICRPG/AIAA 2nd Solid Propulsion Conference, (1967), pp. 89.

1966

Hermance, C. E., "*A Physical Model of Composite Solid Propellant Combustion which Includes the Oxidizer Particle Size and Surface Heat Generation*", AIAA 3rd Aerospace Sciences Meeting, AIAA Paper No. 66-112, (1966),

Hermance, C. E., "*A Model of Composite Propellant Combustion Including Surface Heterogeneity and Heat Generation*", AIAA Journal, Vol. 4, No. 3, (1966), pp. 378-388.

1960

Summerfield, M. et al., "*The Burning Mechanism of Ammonium Perchlorate Propellants*", ARS Progress in Astronautics and Rocketry Vol I: Solid Propellant Rocket Research, (1960), pp. 227-249.

NOTE: The granular diffusion flame model.

Chaiken, R. F. and Andersen, W. H., "*The Role of Binder in Composite Propellant Combustion*", ARS Progress in Astronautics and Rocketry Vol I; Solid Propellant Rocket Research, (1960), pp. 141-182.

NOTE: Two temperature model applied to AN composite propellants.

<1960

Chaiken, R. F., "*A Thermal Layer Mechanism of Combustion of Solid Composite Propellants: Application to Ammonium Nitrate Propellants*", Combustion and Flame, 3, (1959), pp. 285-300.

Andersen, W. H., Bills, K. W., Mishuck, E., Moe, G., and Schultz, R. D., "*A Model Describing Combustion of Solid Composite Propellants Containing Ammonium Nitrate*", Combustion and Flame, Vol. 3, (1959), pp. 301-318.

APPENDIX C

Aluminum Combustion References

Aluminum Combustion References

1987

Afanas'eva, E.A., and Levin, V.A., "Aluminum-Particle Ignition and Combustion Behind Shock and Detonation Waves", *Combustion, Explosions & Shock Waves*, Vol. 23, No. 1, (1987), pp 6-11.

Larson, R.S., "Prediction of Aluminum Combustion Efficiency in Solid Propellant Rocket Motors", *AIAA J.*, Vol. 25, No. 1, (1987), pp 82-91.

NOTE: Very comprehensive and complex calculation of efficiency using both 1-D and 2-D gas and particle trajectory analysis. Allows for varying CO₂ and H₂O conc. Unfortunately, he makes the FATAL error of assuming a SINGLE AL PARTICLE SIZE!! (allowing for a log normal distribution about that size.) His final results do not include a particle size, thereby greatly reducing the utility of the results!!

1986

Chozev, Y., Fuhs, A.E., and Kol, J., "Burning Time and Size of Aluminum, Magnesium, Zirconium, Tantalum, and Pyrofuze Particles Burning in Steam", *AIAA-86-1336*, (1986),

NOTE: Qualitative data presented in an awkward format.

Shevchuk, V.G., Bezrodnykh, A.K., Kondrat'ev, E.N., Gradetskii, I.I., and Ivanov, V.N., "Combustion of Airborne Aluminum Particles in Free space", *Combustion, Explosion & Shock Waves*, Vol. 22, No. 5, (1986), pp 531-534.

1985

Babuk, V.A., Belov, V.P., Khodosov, V.V., and Shelkhin, G.G., "Investigation of the Agglomeration of Aluminum Particles During the Combustion of Metallized Composite Condensed Systems", *Combustion, Explosion & Shock Waves*, Vol 21, No. 3, (1985), pp 287-292.

NOTE: Data for 4 AP propellants show agglomeration decreasing and increasing with pressure. Agglomeration appears to be inversely proportional to burn rate.

King, M.K., "Metal Combustion Efficiency Predictions for Low L* Rocket Motors", *J. Spacecraft & Rockets*, 22, 5, (1985), pp 512-513.

NOTE: Some good ideas, but presented in an unintelligible manner. An agglomeration correlation is presented, but there are no results, example or plots.

Lokenbakh, A.K., Zaporina, N.A., Knipele, A.Z., Strod, V.V., and Lepin, L.K., "Effects of Heating Conditions on the Agglomeration of Aluminum Powder in Air", *Combustion, Explosion & Shock Waves*, Vol. 21, No. 1, (1985), pp 69-77.

NOTE: Claim a mechanical cracking of the oxide coating at about 1000 to 1300K for large particles.

Slimak, M.E., "Motor Performance Prediction Methodology", *AFRPL-TR-85-037*, Edwards Air Force Base, (1985),

NOTE: Contains 4 reprints of papers on motor performance and combustion efficiency based on work with SPP.

1984

Brundige, W.N., and Caveny, L.H., "Low Burning Rate Aluminized Propellants in Acceleration Fields", *AIAA J.*, 22, 5, (1984), pp 638-646.

Frederick, R.A. Jr., and Osborn, J.R., "Effect of Acceleration on Propellant.....", *AFRPL-TR-84-073*, Purdue University, (1984),

NOTE: Reviews agglomeration models.

Aluminum Combustion References

Ivanov, G.V., Surkov, V.G., Karmadonov, L.N., and Viktorenko, A.m., "The Role of Condensed-Phase Reactions in the Burning of Mixtures of Fusible Metals with Ammonium Perchlorate", *Combustion, Explosion & Shock Waves*, Vol. 20, No. 2, (1984), pp 161-163.

NOTE: Pb, Sn, Cd, and In were examined. The Pb and Cd apparently react to perchlorates and then form low temperature melting eutectics.

Price, E.W., "Combustion of Metalized Propellants", *Fundamentals of Solid-Propellant Combustion*, Volume 90, *Progress in Astronautics and Aeronautics*, Chapter 14, (1984), pp 479-514.

NOTE: Good Tutorial.

Sambamurthi, J.K., Price, E.W., and Sigman, R.K., "Aluminum Agglomeration in Solid-Propellant Combustion", *AIAA J.*, 22, 8, (1984), pp 1132-1138.

NOTE: Data on both size and fraction of Al agglomerated. Agglomerate size decreases with pressure, and with increasing fine oxidizer size, and with increasing fine fraction. Agglomerate size is maximum for ~15-20 micron Al. Price ignores the Aerojet work.

1983

Cohen, N.S., "A Pocket Model for Aluminum Agglomeration in Composite Propellants", *AIAA J.*, 21, 5, (1983), pp 720-725.

NOTE: Model of AL agglomerate size and concentration based on pocket size, melting of AL (inversely proportional to burn rate), and ignition of AL (compares the fine AP flame temperature to an ignition temperature of 1400K)

Frolov, Yu., V., and Nikolshii, B.E., "Combustion Characteristics of Metallized Compositions", *Combustion, Explosions & Shock Waves*, 19, 5, (1983), pp 101-104.

NOTE: Aluminum, magnesium, sodium nitrate and AP. Emphasizes characteristics for 40-60% metal compositions (air augmented rocket applications?).

Gremyachkin, V.M., "Theory of Ignition of Metallic Particles", *Combustion, Explosion & Shock Waves*, Vol. 19, No. 3, (1983), pp 259-262.

NOTE: Develops a model to calc. ignition temperature as a function of particle diameter and oxygen concentration.

Price, E.W., Sambamurthi, J.K., Sigman, R.K., and Sheshadri, T.S., "Conditions for Inflammation of Accumulated Aluminum in the Propellant Combustion Zone", 20th JANNAF Combustion Meeting, Vol I, (Oct 1983), pp 333.

NOTE: Summary of GIT experiments; Conclusion is there are many contributing factors but oxide melting is probably dominant.

1982

Arkhipov, V.A., Ermakov, V.A., and Razdobreev, A.A., "Dispersity of Condensed Products of Combustion of an Aluminum Drop", *Combustion, Explosion & Shock Waves*, 18, 2, (1982), pp 16-19.

NOTE: Measured size distribution by dropping burning particles onto a glass plate in air at atmospheric pressure. They observed 1) most oxide particles are 1-2 microns, 2) As Do increases the maximum oxide size also increases, 3) Most of the oxide is in the form of hollow spheres, 4) flame location is at a radius of ~3Do.

Davis, D.K., "Effects of Aluminum Level on Solid Rocket Motor Performance", 19th JANNAF Combustion Meeting, II, (1982), pp 17-26.

NOTE: Compares SPP calculations for HTPB and NEPE propellants containing AP, HMX, and Al with motor data.

Aluminum Combustion References

Fedorov, B.N., Plechov, Yu.L., and Timokhin, E.M., "Particle Size of Aluminum Oxide Particles in the Combustion Products of Condensed Substances", *Combustion, Explosion & Shock Waves*, 18, 1, (1982), pp 22-27.

NOTE: Used a small motor and measured the exhaust for AL percentages of 0 to 18% in a propellant at 3.5 and 7.5 MPa. Results show: bimodal distribution of products, 1.5-2 microns peak and a second lower peak at ~6 microns. Higher pressure gives more fine particles.

King, M.K., "Prediction of Metal Combustion Efficiency in Low Port-to-Throat Ratio and Nozzleless Solid Rocket Motors", *AIAA-82-1202*, (1982),

NOTE: Uses empirical agglomeration data from Aerojet, and Al burning rate law ($\text{Dia}^{1.5}$)

Kubota, N., Ichida, M., and Fujisawa, T., "Combustion Processes of Propellants with Embedded Metal Wires", *AIAA J.*, 20, 1, (1982), pp 116-121.

Medvedev, A.E., Fedorov, A.V., and Fomin, V.M., "Mathematical Modeling of Metal Particle Ignition in the High-Temperature Flow Behind a Shock", *Combustion, Explosion & Shock Waves*, Vol. 18, No. 3, (1982), pp 261-265.

NOTE: They conclude that Mg ignites by thermal explosion while Al ignites by a critical ignition temperature 2300K.

Price, E.W., Kraeutle, K.J., Prentice, J.L., Boggs, T.L., Crump, J.E., and Zurn, D.E., "Behavior of Aluminum in Solid Propellant Combustion", *NWC TP6120*, Naval Weapons Center, (1982),

NOTE: Literature review and summary of mechanistic interpretations of AL agglomeration and combustion.

Renie, J.P., Lilley, J.S., Frederick, R.A., and Osborn, J.R., "Aluminum Particle Combustion in Composite Solid Propellants", *AIAA-82-1110*, 18th Joint Propulsion Conference, (1982),

NOTE: Describes current agglomeration models. Describes PEM Al combustion model: no agglomeration and divides Al up proportionally to the pseudo propellant.

1981

Babuk, V.A., Belov, V.P., and Shelukhin, G.G., "Combustion of Aluminum Particles in Composite Condensed Systems Under Low and High Pressures", *Combustion, Explosion & Shock Waves*, 17, 3, (1981), pp 26-31.

NOTE: At low pressure, oxide caps form, inhibiting combustion. At high pressure, oxide caps don't form, leading to faster combustion due to the higher surface area.

Barger, M.E., and George, D., "Metal Particle Size Calculations for Solid Propellant Rocket Motors", 18th JANNAF Combustion Meeting, I, (1981), pp 81-87.

Brundige, W.N., and Kirschner, T.J., "Space Motor Combustion Technology Phase II. Performance Prediction/Verification", Thiokol Elkton Division, *AFRPL-TR-81-68*, (1981),

NOTE: Contains agglomeration data and acceleration data.

Cohen, N.S., Brundige, W.N., and Munson, W.O., "Efficiency of Low-Burn Rate Propellants", 18th JANNAF Combustion Meeting, I, (1981), pp 105-111.

Grigoryev, V.G., Kutsenogii, K.P., and Zarko, V.A., "Model of Aluminum Agglomeration During Combustion of Composite Propellants", *Combustion, Explosion, and Shock Waves*, 17, 4, (1981), pp 9-17.

NOTE: Calculates the size of a pocket.

Kincaid, J.F., and Derr, R.L., "Combustion Efficiency of Highly Aluminized Solid Propellants", 18th JANNAF Combustion Meeting, I, (1981), pp 89-103.

NOTE: Workshop report with emphasis on detonation tendencies.

Price, E.W., Park, C.J., Sigman, R.K., and Sambamurthi, J.K., "The Nature and Combustion of Agglomerates", 18th JANNAF Combustion Meeting, III, (1981), pp 121-145.

NOTE: A detailed description of the qualitative characteristics of agglomerates.

Aluminum Combustion References

Razdobreev, A.A., Skorik, A.I., Frolov, Yu., V., and Ermakov, V.A., "Agglomeration of Aluminum Particles in Conditions of Nonsteady Heating", *Combustion, Explosion, & Shock Waves*, 17, 6, (1981), pp 63-67.

NOTE: Fundamental study looking at the agglomeration of 2 particles at different heating rates, etc. Agglomeration occurs above the metal melting point. Cracks in the oxide allow metal to leak out and bond. Higher heating rate gives faster agglomeration.

Renie, J.P., and Osborn, J.R., "Comments on Aluminum Particle Size, Agglomeration, and Acceleration Effects on Solid Propellant Burning Behavior", 18th JANNAF Combustion Meeting, III, (1981), pp 111-120.

NOTE: Latest PEM. Detailed model of aluminum heating and igniting, but no agglomeration.

Schmidt, W.G., Lovine, R.L., and Poynter, R.C., "Zirconium/Aluminum Combustion", AFRPL-TR-81-19, Final Report, Aerojet Tactical Systems Co., (1981).

NOTE: Excellent source of data. Effect of pressure is more important than that of burn rate on agglomeration. Nitramines increase agglomeration (in HTPB and XLDB). The pocket environment is important to agglomeration, and determines burn rate.

1980

Bakhr, L.P., Levashenko, G.I., and Tamanovich, V.V., "Influence of the Chemical Composition of Metallized Propellants on the Disperse Composition, Optical Characteristics of Oxide Particles, and Flame Emissivity", *Combustion, Explosion & Shock Waves*, Vol. 16, No. 6, (1980), pp 611-616.

NOTE: Measured the particle size of the Al_2O_3 in AP propellants at 40 atm. They see 2 peaks. 22 to 33 % of the oxide is at 0.4μ , and the 2nd peak is between 4 and 7μ . 2 propellants contained the Mg/Al alloy.

Brundige, W.N., and Caveny, L.H., "Combustion of Low Rate HTPB Propellants in an Acceleration Field-- Part II", 17th JANNAF Combustion Meeting, III, (1980), pp 19-42.

Schmidt, W.G., and Poynter, R.C., "Zirconium/Aluminum Combustion", AFRPL-TR-80-8, Interim Report, Aerojet Solid Propulsion Co., (1980).

NOTE: Extends previous work to cover broader range of pressures, nitramines, zirconium, and the pocket environment.

1979

Brundige, W.N., and Caveny, L.H., "Combustion of Low Rate HTPB Propellants in an Acceleration Field", 16th JANNAF Combustion Meeting, III, 343, (1979).

Caveny, L.H., and Gany, A., "Aluminum Combustion Under Rocket Motor Conditions", AGARD Propulsion and Energetics Panel Symposium, Oslo, Norway, (1979).

Caveny, L.H., and Gany, A., "Breakup of Al/Al_2O_3 Agglomerates in Accelerating Flowfields", *AIAA J.*, 17, 12, (1979), pp 1368-1371.

NOTE: Double base propellant with 13% AL. Agglomerates breakup for Weber number ~ greater than 25-30.

Gremyachkin, V.M., Istratov, A.G., and Leipunskii, O.I., "Effect of Immersion in a Flow on Metal-Drop Combustion", *Combustion, Explosion & Shock Waves*, Vol. 15, No. 1, (1979), pp 26-.

NOTE: Account for convective flow around a burning particle.

Homan, H.S., Morris, S.O., and Sirignano, W.A., "Critical Initial Mass of Burning Aluminum Particles for Ignition of Methane/Air Mixtures", WSS Paper 79-27, 1979 WSS/CI Spring Meeting, (1979).

Kraeutle, K.J., Reed, R., Atwood, A.I., and Mathes, H.B., "Effect of Binder Type on Aluminum Combustion and Aluminum Oxide Formation", 16th JANNAF Combustion Meeting, II, (1979), pp 225-236.

NOTE: 3 AP/AL propellants with different binders. Collects residues from pipe and T-burner. Calculated particle damping based on the residue sizes.

Aluminum Combustion References

Kudryavtsev, V.M., Sukhov, A.V., Voronetskii, A.V., and Shapara, A.P., "High-Pressure Combustion of Metals (Three-Zone Model)", *Combustion, Explosion & Shock Waves*, Vol. 15, No. 6, (1979), pp 731-737.

NOTE: Model the reaction of Al + water. They calculate an increasing β to ~350 psi and the very slightly decreasing.

Pai Verneker, D., Seetharamacharyulu, D., and Mallya, R., M., "Combustion of Ammonium Perchlorate-Aluminum Mixtures", *J of Spacecraft and Rockets*, (1979), pp 436.

1978

Babuk, V.A., Belov, V.P., and Shelukhin, G.G., "Completeness of the Combustion of a Metallic Combustible in the Composition of Mixed Condensed Systems", *Combustion, Explosion & Shock Waves*, 14, 3, (1978), pp 145-147.

NOTE: Combustion efficiency; at low pressure they measure low temperature (T^*), at increased pressures they measure higher temperatures, reaching adiabatic flame temperatures at 30-40 atm for 18% Al.

Gany, A., and Caveny, L.H., "Agglomeration and Ignition Mechanism of Aluminum Particles in Solid Propellants", 17th International Symposium on Combustion, (1978).

Gany, A., Caveny, L.H., and Summerfield, M., "Aluminized Solid Propellants Burning in a Rocket Motor Flowfield", *AIAA J.*, 16, 7, (1978), pp 736-739.

NOTE: Nitroplastisol propellant with 13% Al. Doubling the pressure reduces the agglomerate size by one half. Increasing crossflow velocity reduces agglomeration. Large Al reduces agglomeration because the Al does not ignite.

Gurevich, M.A., Ozerov, E.S., and Yurinov, A.A., "Effect of an Oxide Film on the Inflammation Characteristics of Aluminum", *Combustion, Explosion & Shock Waves*, Vol. 14, No. 4, (1978), pp 448-451.

Polishchuk, D.I., Shevchuk, V.G., Velikanova, V.L., Goroshin, S.V., and Nechitailo, I.N., "Critical Ignition Conditions for Conglomerates of Aluminum Particles", *Combustion, Explosion & Shock Waves*, Vol. 14, No. 2, (1978), pp 175-178.

Smelkov, G.I., Aleksandrov, A.A., Pekhotikov, V.A., and Grishin, E.V., "Combustion of Large Aluminum Particles in an Air Flow", *Combustion, Explosion & Shock Waves*, Vol. 14, No. 5, (1978), pp 581-.

1977

Beckstead, M.W., "A Model for Solid Propellant Combustion", 14th JANNAF Combustion Meeting, I, (1977), pp 281-306.

NOTE: Correlation of Aerojet data to account for aluminum agglomeration. First detailed model of ignition and combustion of aluminum within a burn rate model.

Bondarev, V., N., Zolotko, A. N., Klyachko, L. A., et al, "Ignition of Conglomerates of Metallic Particles", *Combustion, Explosion & Shock Waves*, Vol. 13, No. 2, (1977), pp 136-139.

Derevyaga, M.E., Stesik, L.N., and Fedorin, E.A., "Ignition and Combustion of Aluminum and Zinc in Air", *Combustion, Explosion & Shock Waves*, 13, 6, (1977), pp 852-857.

Geisler, R.L., "Summary Report on 1977 JANNAF Aluminum Combustion Workshop", 14th JANNAF Combustion Meeting, I, (1977), pp 181-193.

Gladun, V.D., Frolov, Yu.V., and Kashporov, L.Ya., "Coalescence of Powdered Aluminum Particles on Combustion Surface of Metallized Compositions", *Combustion, Explosion & Shock Waves*, Vol. 13, No. 5, (1977), pp 596-600.

NOTE: "The" paper on NaNO_3 . $\text{NaNO}_3 + \text{LiF}$ reduce the agglomeration time and size!!

King, M.K., "Preliminary Examination of the Validity of the Flame-Sheet Approximation for Aluminum Particle Combustion Modeling", 14th JANNAF Combustion Meeting, I, (1977), pp 221-233.

Aluminum Combustion References

NOTE: Claims that for particles 30-50 microns and smaller, the flame sheet assumption breaks down. Burn times become greater, with the burn rate exponent changing from 2 to 1 with decreasing particle size.

Kraeutle, K.J., and Bradley, H.H., "Combustion of Aluminized Propellants: The Influence of Pressure and Propellant Composition on Formation of Aluminum Combustion Residue", 14th JANNAF Combustion Meeting, I, (1977), pp 209-219.

NOTE: XLDB aluminized propellants; fraction and size of agglomerates decrease as pressure increases.

Merzhanov, A.G., Grigorjev, Yu.M., and Gal'chenko, Yu.A., "Aluminum Ignition", Combustion and Flame, Vol. 29, (1977), pp 1-14.

NOTE: They find that the rate of ignition has an activation energy of 17 Kcal/mole.

Micheli, P., L., and Schmidt, W., G., "Behavior of Aluminum in Solid Rocket Motors", AFRPL-TR-77-29, Vol I, Aerojet Solid Propulsion Co., (1977),

NOTE: Excellent source of data on agglomeration and fraction reacted for HTPB and XLDB propellants.

Micheli, P., L., and Schmidt, W., G., "Behavior of Aluminum in Solid Rocket Motors", AFRPL-TR-77-29, Vol II, Aerojet Solid Propulsion Co., (1977),

NOTE: Metal combustion; Literature review; Excellent summary of work prior to 1977 including Russian literature.

Ozerov, E.S., and Yurinov, A.A., "Combustion of Particles of Aluminum-Magnesium Alloys in Water Vapor", Combustion, Explosion & Shock Waves, Vol 13., No. 6, (1977), pp 778-780.

NOTE: Calculate the effect of Re and P on β . With 105 Mg in an alloy, the particle burns like Mg not Al.

Pressley, H.M., "Survey of Soviet Work in Aluminum Combustion", 14th JANNAF Combustion Meeting, III, (1977), pp 85-104.

NOTE: Overview of Soviet literature with 49 references.

1976

Gladun, V.D., Frolov, Yu.V., Kashporov, L.Ya., and Ostretsov, G.A., "A Model for Detachment of a Condensed Particle from a Combustion Surface", Combustion, Explosion & Shock Waves, Vol. 12, No. 2, (1976), pp 167-172.

NOTE: Calculates agglomerate diameter for Al in NaNO_3 propellants.

Law, C.K., "Models for Metal Particle Combustion with Extended Flame Zones", Combustion Science and Technology, Vol. 12, (1976), pp 113-124.

NOTE: Applies the model to Magnesium.

Price, E.W., and Sigman, R.K., "Behavior of Aluminum in Solid Propellant Combustion", AFOSR TR-77-0050, (1976),

NOTE: Summary of GIT work.

1975

Boreisho, A.S., Ivashchenko, A.V., and Shelukhin, G.G., "Problem of Determining the Sizes of Burning Metal Particles", Combustion, Explosion & Shock Waves, 11, 4, (1975), pp 659-660.

NOTE: Observed size is 1.5 to 4 times larger than actual size with the apparent flame thickness of 15 microns for a 10 micron particle and 30 microns for particles of 30 to 80 microns. Measured at varying pressures but they don't say what pressures or the effect of pressure.

Gremyachkin, V.M., Istratov, A.G., and Leipunskii, O.I., "Model for the Combustion of Metal Droplets", Combustion, Explosion & Shock Waves, Vol. 11, No. 3, (1975), pp 313-318.

NOTE: Take into account O_2 , H_2O and CO_2 in the atmosphere.

Aluminum Combustion References

Kashporov, L.Ya., Frolov, Yu., V., Ostretsov, G., A., and Stepanov, V., N., "Investigation of the Agglomeration of the Condensed Phase with the Combustion of Model Composition with a High Content of Powdered Metal", Combustion Explosion and Shock Waves, 11, 1, (1975), pp 33-43.

NOTE: Summary of Frolov's experimental work.

1974

Churchill, H., Fleming, R.W., and Cohen, N.S., "Aluminum Behavior in Solid Propellant Combustion", AFRPL-TR-74-13, Final Report, Lockheed Propulsion Company, (1974),

NOTE: Excellent data on agglomeration size and fraction for monomodal and bimodal propellants. Basic calculation of pocket size.

Grigor'ev, A.I., and Grigor'eva, I.D., "Ignition of Metal Particles", Combustion, Explosion & Shock Waves, Vol. 12, No. 2, (1974), pp 182-164.

NOTE: Calculate a critical condition based on oxide thickness.

1973

1972

Frolov, Yu.V., Pokhil, P.F., and Logachev, V.S., "Ignition and Combustion of Powdered Aluminum in High-Temperature Gaseous Media and in a Composition of Heterogenous Condensed Systems", Combustion, Explosion & Shock Waves, 8, 2, (1972), pp 168-187.

NOTE: Classic survey paper on the Russian work.

1971

1970

1969

1968